The Role of Tissue Modulus and Cardiac Fibroblast Phenotype in Volume Overload Induced Heart Failure

DISSERTATION

Presented in Partial Fulfillment of the Requirements for the Degree Doctor of Philosophy in the Graduate School of The Ohio State University

By

Rachel Caitlin Childers, M.S.

Graduate Program in Biomedical Engineering

The Ohio State University

2016

Dissertation Committee:

Dr. Keith Gooch, Advisor

Dr. Jun Liu

Dr. Pamela Lucchesi

Dr. Aaron Trask

Abstract

Volume overload (VO) induced heart failure results from an increase in blood volume (preload) to the heart. The heart responds to increases in hemodynamic load through compensative remodeling. VO has a distinct pattern of remodeling compared to pressure overload induced heart failure, which results in fibrosis. VO results in a net decrease in extracellular matrix (ECM). This loss of ECM contributes to the progression of the disease due to the loss of structural integrity.

Since cardiac fibroblasts (CFs) are the main cells responsible for maintaining ECM in the heart, we characterized the in vitro phenotype of CFs isolated from a rat VO model, aortocaval fistula (ACF). Compared to sham operated animals, ACF fibroblasts displayed a phenotype that we described as “hypofibrotic”. ACF CFs secreted relatively less collagen and profibrotic molecules, such as α-smooth muscle actin (αSMA) and connective tissue growth factor (CTGF). Interestingly, ACFs produce approximately twice as much transforming growth factor-β1 (TGF-β), a key profibrotic stimulus, as their sham counterparts. However, there were no changes in the canonical TGF-β pathway that could account for the hypofibrotic phenotype observed in ACF fibroblasts.

Since others have shown that the cytoskeleton and the Rho/ROCK pathway play a role in fibroblast phenotype, we characterized the actin cytoskeleton in sham and ACF

fibroblasts. We found that ACF CFs have significantly less F-actin than sham CFs. We were able to show that it is possible the actin cytoskeleton might account for phenotypic differences in CFs by chemically altering the amounts of F-actin and G-actin. When the cells were treated with a ROCK inhibitor, which allows F-actin to depolymerize into G-actin, CFs displayed a more hypofibrotic phenotype. Conversely, enhancement of F-actin with jasplakinolide treatment forced the CFs to have a profibrotic phenotype.

Numerous studies have linked substrate modulus with effects on the cytoskeleton. Stiff substrates tend to increase cytoskeletal organization and increase F-actin resulting in stress fiber formation in vitro. We wondered if changes in tissue modulus may account for differences in observed phenotype. To know if changes in tissue modulus account for changes in CF phenotype, we first characterized the tissue stiffness changes. We used biaxial tensile testing, which yields a direct measure of tissue modulus, an intrinsic property of the material. Here we show that ACF rats have approximately half the tissue modulus compared to control rats.

Since increased stiffness is positively correlated with CF changes towards a more profibrotic phenotype, we postulated that decreased substrate stiffness may lead to a more hypofibrotic phenotype. Specifically, we hypothesized that sham CFs on softer substrates would have a more hypo-fibrotic phenotype; conversely, CFs from ACF would behave more like normal cells on a higher stiffness. Although the phenotype of sham CFs was shifted to a more hypofibrotic direction on soft substrates, ACF fibroblasts had many indications of a dampened response to stiffness reminiscent of the effect known as "mechanical memory" described by others [1,2].

Dedication

To my parents. For instilling confidence in me, inspiring my intellectual curiosity, imparting the virtue of perseverance, and providing relentless encouragement and support.

Acknowledgments

First, I would like to thank my advisor Keith Gooch. His thoughtful mentorship has had a profound influence on my development as a not only a scientist but also as a person. I have learned many things from him including critical thinking skills, effective communication, and, although he didn't intend to teach this, how to be humble even when you're the smartest person in the room.

I would also like to thank the other members of my committee, who have all gone above and beyond the duties of committee members. I am so grateful to Pamela Lucchesi, my "research mom", for generously welcoming me into her lab and for so much support along the way. This work would have been impossible without her guidance. I thank Aaron Trask for adopting me into his lab, providing mentorship and support. I would also like to share my gratitude to Jun Liu for her collaboration and insightful direction.

Finally, I would like to thank all of those outside of research that have helped me along this journey. I would like to thank my family, and specifically thank my brother, Caleb, who's better grades when we were younger inspired me to overcompensate and get a PhD. I am grateful to all of my friends, especially Jayne and Monica, who provided weekly mental health breaks and camaraderie throughout grad school. Finally, I'd like to

thank my fiancé, Nick, for his love, encouragement, and silly jokes, which made the last two and a half years of grad school even happier.

Vita

2010 .....B.S. Biological Engineering, University of Georgia

2013 .....M.S. Biomedical Engineering, The Ohio State University

2013-2014 .....HHMI Med Into Grad Scholar, The Ohio State University

2014-2016 .....American Heart Association Predoctoral Fellow

Publications

Lucchesi PA, Trask AJ, **Childers RC**, Goodwin RL. Moss & Adams' Heart Disease in Infants, Children, and Adolescents: Development of Myocardial Structure and Function. Wolters Kluwer, 2015.

Joddar B, Firstenberg MS, Reen RK, Varadharaj S, Khan M, **Childers RC**, Zweier JL, Gooch KJ. Arterial levels of oxygen stimulate intimal hyperplasia in human saphenous veins via a ROS-dependent mechanism. PLoS ONE. 2015;10(3):1–16.

Fields of Study

Major Field: Biomedical Engineering

Table of Contents

List of Tables

List of Figures

Chapter 1 : Introduction

1.1) Etiology and biomechanics of heart failure

Altered hemodynamic loads change the stress within the heart walls leading to compensative changes in the heart relative to the duration and types of loads. One common type of altered hemodynamic load is pressure overload (PO). PO results from an increase in afterload, i.e. increasing the end load the heart has to work against to eject blood out of the heart. Common causes of PO include chronic high blood pressure and aortic stenosis. Another type of altered hemodynamic load is volume overload (VO). VO is an increase in preload (i.e. an increase in end-diastolic volume). Physiological VO can occur during pregnancy [3] or high intensity exercise [4]. However, chronic exposure to VO, such as with ventricular septal defects or mitral regurgitation, can lead to maladaptive remodeling in order to compensate for cardiac load changes.

Compensation during heart failure (HF) results in remodeling of the heart to more efficiently pump blood. Following Laplace's Law, the wall stress, or the tension within the heart wall is approximated by:

$$\sigma_{wall} = P\frac{r}{2t} \qquad \text{Eq. (1)}$$

Wall stress (σ_{wall}) is approximated by multiplication of the chamber pressure (P) and the internal radius (r) of the chamber divided by two times the thickness of the left ventricle (LV) wall (t). Compensative remodeling through concentric hypertrophy, occurring in

PO, attempts to decrease wall stress, which is a major determinant of oxygen demand [5–7]. PO remodeling occurs in response to the increase in chamber pressure (P) with an increase in wall thickness (t) by adding sarcomeres in parallel to result in a subsequent decreased wall stress (σ_{wall}).

In VO the heart chamber dilates (increasing r), which is initially beneficial because it maximizes use of the Frank-Starling mechanism. The Frank-Starling mechanism describes an increase in contractility due to increased preload. That is, the heart pumps the volume that it receives, within some limits. Strain from increased preload on cardiomyocytes leads to increased calcium sensitivity, resulting in increased actin-myosin cross bridge formation, and, therefore, increased force output [8]. The increased myocyte force output allows the heart to pump more blood with each heart beat. However, this increase in preload corresponds to increased wall tension, σ_{wall}. Increased wall tension increases myocardial oxygen demand [5]. Chronic increase in chamber volume causes sarcomeres to be added in series to decrease wall tension and ensures sarcomeres are not extended past an optimal length. However, this removes the Frank-Starling advantage and encourages further distension of the chamber and eventually leads to HF.

1.2) Distinct patterns of extracellular matrix remodeling in heart failure

In addition to macroscopic changes in remodeling in the chamber (e.g. wall thickness, chamber dimensions), there is microscopic remodeling leading to changes in extracellular matrix (ECM). In PO there is an increase in ECM production, leading to fibrosis [9]. In VO, there is a net decrease in ECM in the initial and compensative phases of

HF [10]. These changes in ECM content are important in both types of HF. In PO, the increase in ECM and resulting fibrosis have been implicated in diastolic heart failure, where the chamber becomes stiff and relaxation and filling are impeded [9,11]. Fibrosis can also interfere with conductance of the action potential throughout the heart, impeding coordination of contraction and causing arrythmias [9,12]. In VO, where there is too little ECM, this decrease in ECM can be important as it could contribute to myocyte slippage, the inability to transmit force throughout the ventricle, and excess tissue deformation [9,13]. The ECM provides a scaffold for myocytes and other cells within the heart and is an important determinant of structural integrity in the myocardium. Myocytes interact with ECM through integrins and focal adhesion complexes. These integrin/focal adhesion complexes help transmit mechanical force from the myocytes through the ECM allowing coordination in contracting the heart.

1.3) Cardiac fibroblast phenotype

Cardiac fibroblasts (CFs) are the most numerous cell type in the heart and are responsible for ECM maintenance. In healthy hearts, CFs maintain a balance of matrix degradation and deposition. CFs respond to a variety of cues that regulate the balance of ECM ranging from neurohormonal regulation, inflammation, oxidative stress, and mechanical stress [14]. There is also crosstalk from other cells in the heart, such as myocytes, mast cells, and other CFs that send signals to CFs, which secrete new ECM proteins and degrade existing ECM via matrix metalloproteinases (MMPs) [14].

CFs are dynamic cells which display considerable phenotype plasticity. It is well established that fibroblasts, with increased cytoskeletal tension in the presence of

transforming growth factor-β1 (TGF-β), activate into myofibroblasts, a profibrotic phenotype that exhibit a mature cytoskeleton incorporated with α-smooth muscle actin (αSMA) and secrete an abundance of ECM proteins. Previous terminology described fibroblast "differentiation" into myofibroblasts, but the more recent view is that fibroblasts "activate" into myofibroblasts, since "differentiation" implies a terminal phenotype. Myofibroblasts may revert back to a normal, or quiescent, fibroblast phenotype. Results presented in this dissertation suggest that fibroblast phenotype goes beyond the dichotomous fibroblast/myofibroblast phenotype and should be described as more of a spectrum of phenotypes.

In the typical view, fibroblasts are classified as either fibroblast, proto-myofibroblast or myofibroblast (Figure 1.1), especially in the context of diseases in which fibrosis, or excess ECM proteins, are a prevalent. With this method of categorization, "fibroblasts" are basal or quiescent cells representative of fibroblasts in healthy tissue. A "myofibroblast" is an activated profibrotic phenotype characterized by contractile αSMA stress fibers and increased secretion of ECM components and profibrotic factors. Myofibroblasts are usually only activated during wound healing. In the heart, myofibroblasts are rarely seen outside of the valves in healthy tissue and only appear during fibrosis and in infarct areas [15]. A "proto-myofibroblast" is a phenotype between fibroblasts and myofibroblasts in culture that have stress fibers resulting from increased cytoskeletal tension but have not yet transformed into secretory myofibroblasts (until the addition of TGF-β) [16]. However, fibroblasts from hearts in the acute and compensated phases of VO likely do not fit into any of these categories. In VO the LV

has a net decrease in ECM proteins as well as increased MMP and natriuretic protein expression [17] even in the presence of elevated profibrotic factors TGF-β [10] and Angtiotensin-II [18]. If these changes in the tissue are due to changes in CF phenotype, it would suggest that CFs from VO have a more hypofibrotic phenotype compared to normal CFs and are quite opposite of the myofibroblast phenotype.

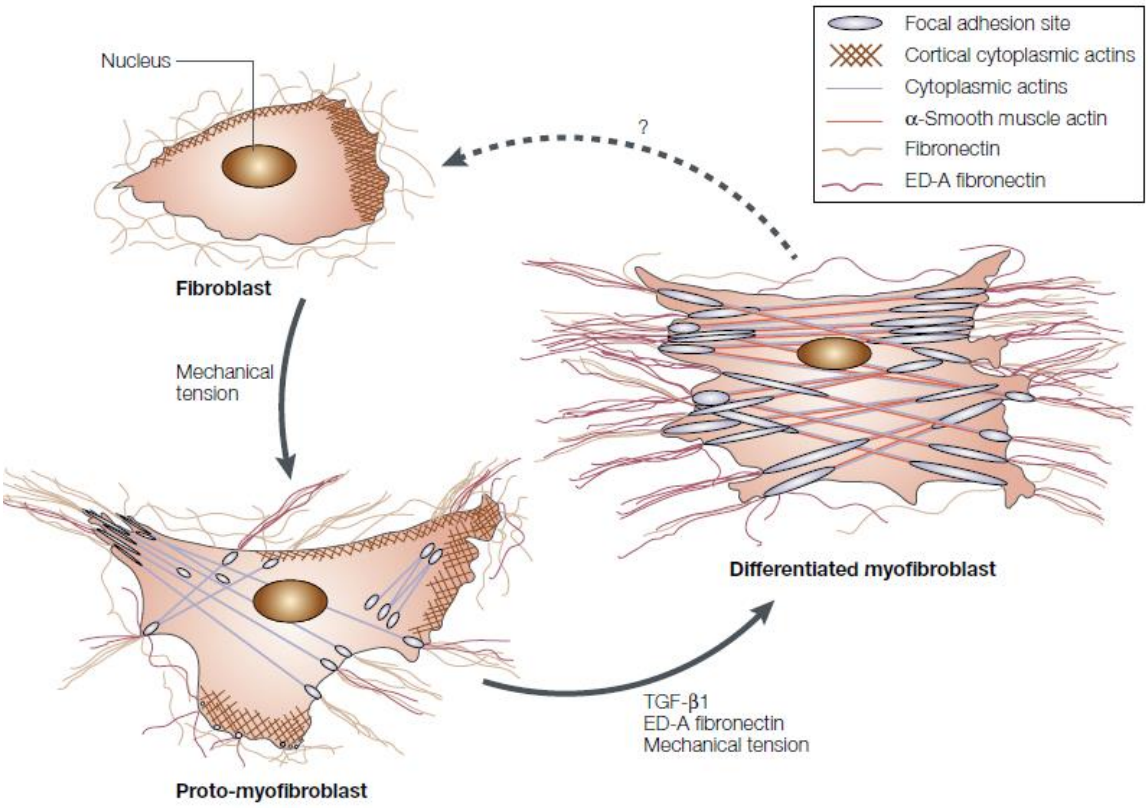

Figure 1.1: Three classifications of fibroblasts.
Image taken from: Tomasek, J. J., Gabbiani, G., Hinz, B., Chaponnier, C. & Brown, R. A. Myofibroblasts and mechano-regulation of connective tissue remodelling. Nat. Rev. Mol. Cell Biol. 3, 349–63 (2002).

To identify the effect of CF phenotype in VO heart failure, one could assess the phenotype of isolated CFs from VO in culture compared to CFs from normal hearts. Several markers are established as being important to distinguish myofibroblast and fibroblasts. The classic indicators of a myofibroblast phenotype are increased αSMA protein, especially when aligned with F-actin stress fibers; increased type-I collagen secretion; fibronectin; and CTGF compared to normal fibroblasts [15,16]. The difficulty in assessing in vitro phenotypes is that in vitro culture conditions, such as the use of growth-factor enriched media, stiff polystyrene culture dishes, and high levels of oxygen tension, contribute to activation of fibroblasts into myofibroblasts [11,19,20]. The longer fibroblasts are in culture, the more myofibroblast population and profibrotic markers tend to increase [2,21]. This can be problematic if one wants to study CFs that are very unlike myofibroblasts. One way to mitigate this issue and to maintain a phenotype closer to the in vivo phenotype is to limit the amount of time in culture. In this work, we only use CFs that are non-passaged for this reason.

Another way researchers attempt to maintain the in vivo phenotype is by mimicking the in vivo environment by providing a substrate with an appropriate elastic modulus. An elastic modulus near physiological or pathological levels of the native tissue in which the specific cell type resides is most appropriate. There is a wide range of tissue moduli throughout the body: the brain is ~0.5 kPa [22], normal lungs are 2-4 kPa [23], and the periodontal ligament connecting teeth is about 10-50 MPa [24]. In comparison, the typical tissue culture polystyrene plastic has an elastic modulus on the order of GPa similar to the elastic modulus of bone and teeth [25]. Normal myocardial tissue modulus is reported to

be in a range of ~10-100 kPa [26,27] and infarct tissue is consistently more stiff than normal tissue due to fibrosis and scar formation [26–28]. To our knowledge, there are not any reports of the tissue stiffness of VO myocardium. Knowing approximate tissue moduli is important because there is growing evidence that cells cultured on substrates outside of their native stiffness change their phenotype in response to those changes in modulus.

1.4) Substrate stiffness regulates fibroblast phenotype

The effect of stiffness on fibroblast phenotype is often studied in diseases where fibrosis and scar formation are an issue; such as wound healing, lung disease, and myocardial infarction. Fibrosis and scar formation are often associated with increased tissue stiffness, and this increased stiffness is suggested to be linked to the persistence of myofibroblasts [2,29,30]. In wounds, fibroblasts migrate to the site of injury and activate into highly contractile and secretory myofibroblasts. The migratory phenotype of fibroblasts is key to arriving at the site of injury, where these cells later use their contractile αSMA reinforced cytoskeleton to help close the wound[31]. During healing, myofibroblasts secrete ECM to replace provisional matrix with granulation tissue. In normal tissue, myofibroblasts undergo apoptosis after a wound is healed; however, in fibrotic tissue, myofibroblast persistence can be detrimental as they contribute to hypertrophic scar formation [31]. Increased mechanical stress leads to increased myofibroblast populations related to hypertrophic scar formation [32] and increased αSMA expression in skin wounds [33]. In gingival and foreskin fibroblasts, the amount of αSMA increases with increasing substrate stiffness [34,35].

In the lung, fibrotic lesions can have a modulus six times that of normal tissue [23]. Lung fibroblasts plated on stiffer gels, reminiscent of fibrotic lung tissue, become activated, and fibroblasts plated on soft gels, similar to healthy tissue compliance, remain quiescent [23]. Activated lung fibroblasts produce excess matrix proteins, have decreased matrix proteolytic gene expression, and are more proliferative. Liu et al. suggest that the fibrotic stiffening of the lung is sufficient to initiate a fibrogenic program to activate fibroblasts and allow feedback amplification of stiffness through matrix synthesis [23].

There is limited research on the effect of stiffness on cardiac fibroblasts, but some think that stiffness may play a role in persistent myofibroblasts in myocardial infarct scars and fibrosis [11,36,37]. In a mixture of neonatal cardiomyocytes and fibroblasts, fibroblast populations dominated over cardiomyocytes on gels of 144 kPa stiffness, a stiffness approximating infarct tissue as measured by AFM; in contrast, on softer gels fibroblasts did not dominate over cardiomyocytes [38]. Additionally, the stiffness-dependence of αSMA iss demonstrated with decreased αSMA in CFs seeded on nanofibrous scaffolds with a decreasing modulus [39]. After activating and replating neonatal CFs on a range of polyacrylamide gels from 0.3-30 kPa, CFs maintained a myofibroblast phenotype but displayed decreasing αSMA expression with decreasing stiffness [40]. Valvular myofibroblasts are deactivated by a phototunable substrate that was reduced from ~32 kPa to ~7 kPa, as indicated by decreased αSMA stress fibers, CTGF expression, and proliferation [30]. These fibroblasts were then reactivated with exogenous TGF-β addition, as evidence by increased expression of αSMA, collagen type I alpha-1, and fibronectin relative to the deactivated fibroblasts without TGF-β. These studies

support the idea that substrate stiffness modulates CF phenotype and their subsequent ability to produce ECM and profibrotic proteins.

1.5) Mechanosensing substrate stiffness and the role of the cytoskeleton

Cells are able to sense stiffness by attaching to and pulling on their surroundings. The actin-myosin cell machinery and cell adhesions are necessary for the transmission of force between a cell and its substrate. Cells attach to their substrates through mechanosensitive adhesion complexes. These adhesion complexes are dynamic protein structures that consist of integrins on the cell surface and other proteins, such as vinculin and talin, that connect at cytoskeleton-associated proteins. Integrins bind to adhesive extracellular proteins, such as collagens, elastins, and fibronectins, creating a link between the cell and its surroundings. Once attached, the cell is able to pull on its substrate by contraction of its cytoskeleton.

Not only do integrins play a role in adhesion, but they also play a role in TGF-β-mediated activation of myofibroblasts. Specifically, integrins αvβ5 and αvβ3 are shown to play a crucial role in activating latent TGF-β [41]. TGF-β is secreted as an inactive complex bound to Latency-Associated Peptide (LAP) and anchored to the ECM via the latent TGF-β-Binding Protein (LTBP) [42]. Integrins αvβ5 and αvβ3 attach to the latent TGF-β complex and enable the cell to pull against the ECM to free and to activate TGF-β [41,42]. Blocking αvβ5 and αvβ3 with peptides or antibodies decreases TGF-β activation and myofibroblast activation [41]. Wipff et al. provide evidence that integrin-mediated fibroblast contraction of compliant ECM substrates is less effective at activating TGF-β when compared to more stiff substrates [43].

Ingber et al. propose a “cell tensegrity” model that states contraction of the cytoskeleton can directly cause changes in gene expression without chemical signals because the cytoskeleton is physically connected to the nuclear structure [44]. The cytoskeletal network directly connects to and rearranges nuclear scaffolds, chromatin and DNA, and, therefore, can alter gene expression. This happens via the linker of nucleoskeleton and cytoskeleton (LINC) [44]. Additionally, tension applied to the nucleus through the actin network can increase nuclear pore size, allowing for increased diffusion through to the nucleus [44].

Cells match external forces from their surroundings with internal tension by altering their cytoskeleton. A network of microtubules that resist compression and microfilaments, which creates tension, work together to create a homeostatic balance against extracellular forces. When cells are on a stiff substrate they increase their cytoskeletal organization by polymerizing globular actin (G-actin) monomers into filamentous actin (F-actin). F-actin acts as struts within the cell to provide structural support. Not only does the actin cytoskeleton provide structural support, but it also plays a part in the mechanism of pulling on the cell’s surroundings. It is reported that cell modulus corresponds to substrate modulus up to ~5 kPa, above 10 kPa they no longer match the modulus of the substrate and begin forming stress fibers [45]. Ghosh et al. report that increased cytoskeleton organization corresponds to an increase in the modulus of dermal fibroblasts on gels of a higher elastic modulus relative to fibroblasts on softer gels [46]. Similarly, Shulze et al. determined that an increased cell modulus of dermal fibroblasts taken from older donors correlated with increased F-actin relative to G-actin [47]. Also, CFs

treated with cytochalasin D, a drug that inhibits the polymerization of actin, have a decreased cell modulus [48].

Rho-kinase (ROCK) phosphorylates myosin and other myosin-related proteins to cause an increase in actin stress fiber formation and contractility of a cell. ROCK plays a role in responding to stiffness because it influences the polymerization of F-actin and the cell's ability to pull on its substrate, and therefore, sense substrate modulus. ROCK is shown to increase the relative ratio of F-actin to G-actin [49,50]. In two different studies, the addition of a ROCK inhibitor to lung fibroblasts caused a decrease in αSMA and F-actin stress fibers, reversing the effect of increased modulus, and decreasing the activation of fibroblasts [23,49]. In addition, the inhibition of ROCK is shown to prevent myofibroblast activation and collagen type-I synthesis in lung and Tenon's fibroblasts [51,52].

1.6) Mechanotransduction of substrate stiffness in fibroblasts

Several transcriptional regulators appear to link alterations in the cytoskeleton associated with a response to substrate stiffness to changes in gene expression. One mechanism that potentially explains the transduction of stiffness to gene expression involves myocardin-related transcription factor A (MRTF-A, also known as megakaryoblastic leukemia 1 protein, MKL1). MRTF-A transduces mechanical stress via the polymerization state of the actin cytoskeleton. MRTF-A is sequestered by G-actin monomers in the cytosol and freed after polymerization into F-actin. Once freed, MRTF-A is able to translocate to the nucleus. In the nucleus, MRTF-A promotes a fibrogenic program including expression of αSMA, transgelin, and calponin by interacting with the serum response factor (SRF) [53]. On stiff (~20 kPa) polyacrylamide gels, human lung

fibroblasts increase F-actin, and have an increase in MRTF-A nuclear translocation, and, in turn, an increase in αSMA compared to soft gels (~0.5 kPa) [49]. However, MRTF-A null fibroblasts did not have increased αSMA in response to increased stiffness [49].

Another mechanotransduction factor is the yes-associated protein (YAP), which translocates to the nucleus when there is increased cytoskeletal tension or changes in cell shape and adhesion [54,55]. YAP nuclear translocation promotes connective tissue growth factor (CTGF) expression and is associated with the myofibroblast activation of mesenchymal stromal cells [56], lung fibroblasts [57], and cancer-associated fibroblasts [58]. One study suggests that the degree of F-actin organization acts as a regulator of YAP transcriptional activity [59]. YAP is suggested to act as a mechanical rheostat that stores information from past mechanical environments to influence cell fate [1]. This type of "mechanical memory" of substrate stiffness also occurs in lung fibroblasts [2]. Lung fibroblasts initially plated on soft substrates and then moved to stiff substrates known to activate fibroblasts into myofibroblasts have a dampened response to the stiff substrates as evidenced by reduced levels of myofibroblasts.

1.7) Summary of dissertation focus

Since CF function impacts VO heart failure, we hypothesize that CFs from VO hearts are less fibrotic than those from control hearts (Chapter 2). In other systems reduced stiffness is shown to reduce fibrotic potential; so we also hypothesized that VO hearts are softer than normal hearts. To test this, we measured the myocardial tissue modulus with biaxial tensile testing (Chapter 3). Additionally, since softer substrates

have been shown to make fibroblasts less fibrotic we hypothesized that reduced stiffness promotes a hypofibrotic phenotype in CFs (Chapter 4).

1.8) Experimental contributions.

This work was substantially improved by its collaborative nature. I performed all of the experimental work presented in this thesis with the exception of: 1) ACF surgeries, echocardiography, and several cardiac fibroblast isolations that were performed by Jean Zhang, 2) osmotic mini pump surgeries and pressure-volume loop data acquisition performed by Aaron Trask, and 3) all of the data within Figures 2.1 and 2.2 which were done by Mary Cismowski and Aaron West.

Chapter 2 : Cardiac Fibroblasts Isolated from Volume Overload Induced Heart Failure Display a Hypofibrotic Phenotype and Alterations in the Cytoskeleton

2.1) Introduction

Cardiac fibroblasts (CFs) are the most abundant cell type in the heart and exhibit considerable plasticity, allowing them to adapt to extracellular cues, such as growth factors, neurohormones, and the mechanical environment. Under normal conditions, CFs regulate a dynamic balance between extracellular matrix (ECM) deposition and degradation to maintain left ventricular (LV) structural and mechanical stability. However, in response to myocardial injury and mechanical stress, CFs undergo phenotypic differentiation to repair and preserve myocardial structural integrity. Under chronic stress, however, these CF changes contribute to adverse LV remodeling and ultimately heart failure (HF).

One form of mechanical stress is volume overload (VO). VO occurs when the heart chronically pumps an increased volume of blood (preload). VO HF is poorly researched compared to HF resulting from pressure overload or post-infarct, which are associated with extensive myocardial interstitial fibrosis. In contrast, we [10,60] and others [61–64] show that VO results in changes in ventricle geometry (dilation and increased eccentricity of LV), mechanics (increased wall stress and decreased chamber stiffness) and, eventually, deleterious changes in function. Structural changes are accompanied by a

net loss of ECM and interstitial collagen [10,18,60]. Intriguingly, this net ECM loss occurs despite increased expression of pro-fibrotic signaling molecules such as angiotensin II [18] and transforming growth factor-β1 (TGF-β) [10].

Cardiac fibroblast phenotype is often described as a dichotomy between normal fibroblasts or myofibroblasts, characterized by increased expression of α-smooth muscle actin (αSMA), collagen I/III, and connective tissue growth factor (CTGF). However, the fibroblast phenotype in VO HF does not fit into that dichotomous system. Here we describe CFs isolated from VO HF as a hypofibrotic phenotype, quite opposite of myofibroblasts, and as producing a net decrease in ECM when compared to control CFs. We investigate the role of the cytoskeleton as a possible factor contributing to the hypofibrotic phenotype observed.

The cytoskeleton is an important component of mechanotransduction of extracellular mechanical stress to indirect modulation of gene expression. Dynamic regulation of the actin cytoskeleton is mediated by RhoA-ROCK signaling and by the balance between actin-polymerizing and de-polymerizing proteins. The actin cytoskeleton in turn, integrates signals from both biochemical (e.g. TGF-β1) and mechanical inputs to indirectly modulate gene expression by controlling the nuclear-cytoplasmic shuttling of transcriptional regulators [65]. One such example is myocardin-related transcription factor A (MRTF-A), [66] also known as Megakaryoblastic leukemia 1 protein (MKL1). Monomeric G-actin binds and sequesters MRTF-A and, upon actin polymerization into F-actin, MRTFA is released and allowed to translocate to the nucleus

where it interacts with serum response factor (SRF) to regulate the increased expression of genes such as αSMA, SM-22, and calponin [53].

Additionally, another transcriptional regulator, yes-associated protein (YAP) is related to fibroblast activation and matrix remodeling [57,58]. YAP is active in the nucleus and nuclear translocation is shown to be dependent upon cytoskeletal tension [54,55]. One study suggests that the degree of F-actin organization acts as a regulator of YAP transcriptional activity [59]. Anseth and co-workers suggested that YAP acts as a mechanical rheostat in mesenchymal stem cells that stores information from past mechanical environments to influence cell fate [1]. This type of mechanical "memory" of substrate stiffness also occurs in lung fibroblasts [2]. Lung fibroblasts initially plated on soft substrates and then moved to stiff substrates, known to activate fibroblasts, have a dampened response to the stiff substrates as evidenced by reduced levels of myofibroblast activation.

We hypothesized that sustained VO results in CFs with a hypofibrotic phenotype. To test this hypothesis, CFs were isolated from rats experiencing aortocaval fistula (ACF) -induced VO and from rats subjected to a sham operation. Markers and mediators of matrix synthesis and degradation where assessed under basal conditions and in the presence of exogenous TGF-β. The role of TGF-β signaling and changes in the actin cytoskeleton in the phenotype observed in vitro is explored.

2.2) Materials and Methods

2.2.1) Animals. Male Sprague Dawley rats (~200 g, Envigo) were housed in IACUC approved housing with 12 hour light/dark cycles and were provided continuous

access to standard chow and water. Age- and weight-matched rats were used for sham and aortocaval fistula (ACF) surgeries. ACF was created under ~2% isoflurane anesthesia. First, we performed blunt dissection to expose the abdominal aorta and inferior vena cava, then an 18-gauge needle was inserted through the shared wall of the vessels and the aorta puncture was sealed with cyanoacrylate glue or sutures. Shunt patency was confirmed visually by mixing of arterial blood in the vena cava. Finally, the abdomen was closed with sutures, and buprenex was given for pain at 24 and 72 hours post-operatively and as needed. Sham surgeries consisted of opening the animal, blunt dissection to expose the aorta and inferior vena cava, and closure of the abdomen with sutures. VO was confirmed via echocardiography at 4 weeks after surgery by a left ventricular end-diastolic diameter of at least 8 mm.

2.2.2) Cell culture. We used an in vitro culture protocol that allows us to characterize cellular phenotypes in adult primary, non-passaged CFs. Briefly, cardiac dissection of 4 week ACF and sham rats was followed by isolation of the left ventricle. The LV was rinsed in Hank's Balanced Salt Solution (HBSS) and cut into small chunks of ~1 mm^2. A series of enzymatic digestions (80U of collagenase type-II, Worthington Biochemicals and 0.1% trypsin) was used to free CFs into solution. The cell solution was neutralized with 10% fetal bovine serum (FBS) DMEM with 4.5 g/L glucose and pelleted in a centrifuge. Cells were filtered through a 100 µM cell strainer (Fisher Scientific) and plated. Non-adherent cells were removed after 45 minutes in culture by replacing media with 10% FBS DMEM with 1.0 g/L glucose. Cells were washed several times with warm PBS 24 hours later, and media was replaced as needed until cells reached ~50-70%

confluence. The use of primary culture avoids the well-known effects of passage on CF phenotype. CFs were growth-arrested in 0.05% FBS-DMEM for 48 hours prior to harvesting or treatment unless otherwise noted.

2.2.3) Drug Treatments. Cells were pretreated with 50 nM of jasplakinolide in DMSO for 1 hour or with DMSO vehicle in serum-free medium. After serum starving for 1 hour, TGF-β treated cells were treated with 3 ng/mL TGF-β1 (R&D systems) for 24 hours in serum-free medium. ROCK inhibitor treatment was done using 10 μM concentration of Y-27632 (Sigma) for 24 hours in serum-free medium after serum starving.

2.2.4) Real-Time quantitative PCR. TRIzol extraction reagent was used to lyse CFs, they were then scraped and sonicated. RNA was extracted with chloroform and centrifuged. The aqueous phase was purified using Qiagen RNeasy Mini Kit (Qiagen), and RNA concentration was determined using a NanoDrop 2000 (Thermo Scientific) spectrophotometer. Reverse transcription was done with the Maxima First Strand cDNA Synthesis Kit (Thermo Scientific). Equivalent amounts of cDNA were amplified in duplicate with Maxima Probe qPCR master mix (Thermo scientific) and Roche Universal Probe and primer pairs for the target genes (see Table 2.1 for primer sequences). 40 amplification cycles were carried out using an Eppendorf MasterCycler-ep Realplex thermocycler. Relative expression was determined by using the $2^{-\Delta\Delta Ct}$method, normalizing data to the housekeeping genes Rpl13a and LDHA.

Table 2.1: PCR primer sequences

Target	Gene	Accession Number	Forward Primer Sequence	Reverse Primer Sequence
α-smooth muscle actin	ACTA2	NM_031004.2	tgccatgtatgtggctattca	accagttgtacgtccagaagc
collagen type-1 α-1	COL1A1	NM_053304	tctggtctccagggtcctc	gtccatctttgccaggagaa
collagen type-3 α-1	COL3A1	NM_032085	tcccctggaatctgtgaatc	tgagtcgaattggggagaat
connective tissue growth factor	CTGF	NM_022266	gctgacctagaggaaaacattaaga	ccggtaggtcttcacactgg
lactate dehydrogenase A	LDHA	NM_017025.1	gatgatggatcttcagcatgg	gcttggagtttgcagtcaca
MMP-13	MMP13	NM_133530	ggacaagcagctccaaagg	ggtccagaccgagggagt
PPAR-γ	Pparg	NM_013124.3	ggtgaaactctgggagatcct	aatggcatctctgtgtcaacc
ribosomal protein L13A	Rpl13a	NM_173340.2	ccctccaccctatgacaaga	ggtacttccacccgacctc
transgelin (SM22)	TAGLN	NM_031549.2	agtgtggccctgatgtgg	tcaccaacttgctcagaatca
TGF-β1	TGFB1	NM_021578	tcagacattcgggaagcagt	acgccaggaattgttgctat

2.2.5) Immunofluorescence staining. After fixation with 4% paraformaldehyde for 30 minutes, CFs were permeabilized with 0.03% Triton X-100 and blocked in BSA and goat serum or fish block (for MRTF-A stained cells, which required an anti-goat secondary antibody) for 1 hour. CFs were incubated overnight at 4°C with gentle agitation with the following primary antibodies: anti-MRTF-A, Santa Cruz sc-21558; anti-YAP, Cell Signaling 14074; anti-αSMA, Sigma a2547. Unbound primary antibody was removed by washing CFs with PBS several times prior to incubation with fluorescent secondary antibodies. CFs were counterstained with DAPI (nuclei), and TRITC conjugated phalloidin (F-actin) (Millipore, FAK100) and/or Alexa Fluor 488-conjugated DNAse-I (Thermo Scientific), to preferentially stain G-actin (Thermo Fisher Scientific). Fluorescent images were taken with an Olympus IX51 microscope or a Zeiss 710 confocal microscope for cytoskeletal protein images. Fluorescence was quantified using ImageJ.

2.2.6) Immunoblot. CFs were scraped in lysis buffer (1% Triton X, 10 μg/ml aprotinin, 0.5 mM PMSF, 500 μM Na_3VO_4) and conditioned media were concentrated

with Amicon Ultra 0.5 mL Centrifugal Filters with a molecular weight cut off of 10,000 Da. Proteins were separated by SDS-PAGE gel and then transferred to PVDF membranes. Immunoblotting was performed using antibodies against :collagen type I (AbCam ab292, 1:2000), αSMA (Abcam ab7817, 1:5000), CTGF (Cell Science CPC100, 1:1000), phospho-SMAD2/3 and SMAD 2/3 (both from Cell Signaling, 3102, 1:1000) ERK1 (Santa Cruz, sc93, 1:5000), and ERK 2 (Santa Cruz, sc154, 1:5000). Relative band densities were quantified using Image Lab and normalized to the sum density of ERK1 and ERK2 proteins.

The ratio of F-actin to G-actin was analyzed using a kit from Cytoskeleton (Denver, CO) and according to the protocol provided. Briefly, cell lysates were scraped and collected with F-actin stabilization lysis buffer provided in the kit. Lysates were briefly sonicated and centrifuged at 350 x g to pellet unbroken cells and debris, and the supernatant was centrifuged at 100,000 x g at 37°C for 1 hour to pellet F-actin. The supernatant contained G-actin, and the F-actin pellet was suspended with F-actin depolymerizing buffer (provided in the kit) in a volume equal to that of the supernatant. The G-actin and F-actin solutions were prepared in SDS loading buffer and separated by a 10% SDS-PAGE in parallel. Proteins were transferred to a PVDF membrane, and incubated with an anti-pan-actin antibody provided in the kit. Ratios were determined by densitometry. Relative total actin was normalized to ERK1/2 and to loading controls between multiple blots.

2.2.7) Proteomics. Proteomic analysis was performed on cell lysates from freshly isolated sham and ACF CFs that had been grown for 24 hours on plastic. Briefly, lysates

(n=3) were separated by SDS-PAGE, separated into 8 fractions and then subjected to in-gel trypsin digestion. Capillary-liquid chromatography-nanospray tandem mass spectrometry was performed by the Ohio State Proteomics Core facility. Label-free quantitation was performed using the spectral counting approach, which relies on the number of peptides identified in a given protein normalized to the total count within the sample [67]. 729 unique proteins were identified by this approach, and 161 proteins were differentially expressed between sham and ACF CFs (n=3, $p<0.05$). We used the DAVID 6.7 Bioinformatics Resource [68] to identify functional classes of proteins overrepresented in the datasets, narrowing our focus to proteins that were: 1) identified in all three replicates at $P<0.05$; 2) had at least 3 spectral hits; and 3) involved actin organization

2.2.8) ELISA. Freshly isolated cardiac fibroblasts from sham treated (n=6) and 4 week ACF (n=5) animals were grown on 60 mm dishes in DMEM+10% FBS to approximately 70% confluence. Cells were then serum starved for 48 hours in DMEM+0.2% FBS. Cells were then placed into DMEM lacking serum for 24 hours and media collected. Media was centrifuged at 1500 x g for 5 min to remove any particulates, and then stored at -80°C prior to analysis. Cells were washed once in PBS, lysed in modified Hunter's buffer, and protein concentration was determined using a bicinchoninic acid protein assay kit (23225, Thermo Scientific, Rockford, IL). Latent TGF-β was activated by incubating conditioned media in 0.17 N HCl for 10 minutes at 25°C, followed by neutralization in 0.17 N NaOH/0.05 M Hepes, pH 8. TGF-β levels were then immediately determined using a mouse/rat/porcine/canine-specific ELISA

assay and protocol (MB100B, R&D Systems, Inc., Minneapolis, MN), and normalized to total cellular protein content.

2.2.9) Statistics. Results are reported as the mean ± standard error of the mean. Two-way analysis of variance was performed followed by post-hoc test to determine statistical difference between conditions. Statistical significance was determined with a $p<0.05$.

2.3) Results

2.3.1) VO-CFs display a basal hypofibrotic phenotype. There was a 50% decrease in both collagen type-I alpha-1 (col1α1) mRNA expression ($p=0.0074$) and collagen type-I secretion into the media ($p<0.001$, Figure 2.1A). Compared to sham, there was a significant decrease in αSMA in both the mRNA (78%, $p=0.0015$) and protein level (55% decrease, $p<0.001$) in ACF (Figure 2.1B). A similar trend was also observed in CTGF, with decreased mRNA and protein in ACFs ($p<0.001$ and $p=0.0022$, respectively) (Figure 2.1C). There was a marked increase in matrix metalloproteinase 13 (MMP13) expression in ACF CFs ($p=0.032$) (Figure 2.1D). Col3α1 decreased in ACF CFs ($p=0.0048$) (Figure 2.1E) but the percent decrease was less than that in Col1α1, leading to a greater Col1α1 to Col3α1 ratio for ACF CFs than sham CF (Figure 2.1F, $p=0.045$). Taken together, these data indicate that CFs isolated from sham and ACF maintain distinct phenotypes in culture and that the phenotype of ACFs is hypofibrotic as evidenced by decreased basal expression of ECM components, αSMA, and CTGF and by increased MMP13.

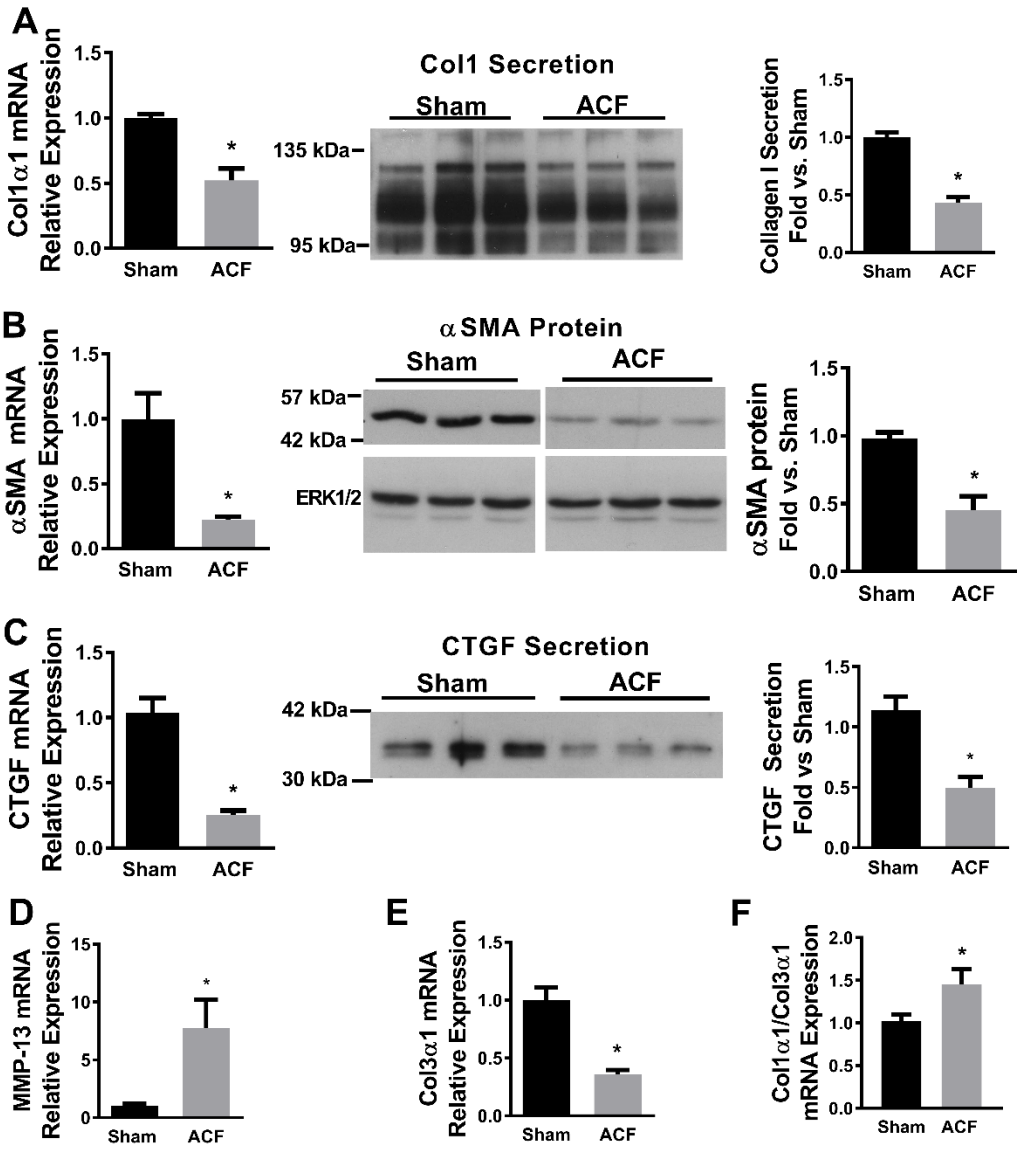

Figure 2.1: Basal CF phenotype description
Left: mRNA expression as determined by qPCR (relative expression normalized to housekeeping gene and sham). Right: cumulative protein expression data (n=4-6). Secreted proteins were normalized to total cellular protein. αSMA was normalized to ERK1/2 (loading control). *p<0.05 compared to sham.

2.3.2) VO-CFs have an intact TGF-β-Smad2/3 pathway despite a hypofibrotic phenotype. TGF-β is a potent regulator of cardiac myofibroblast differentiation and

regulates pro-fibrotic gene transcription through canonical (Smad2/3) and non-canonical (e.g. RhoA) pathways. Although isolated ACF CFs have a clear hypofibrotic phenotype, they exhibit approximately doubled TGF-β mRNA expression and secretion into the conditioned media relative to Sham CFs (**Error! Reference source not found.**A, $p<0.001$ for both). Others have reported that signaling pathways downstream of TGF-β receptor activation can inhibit Smad2/3 phosphorylation [69–71]. For example, ANP-induced cGMP/PKG activation prevents Smad2/3 phosphorylation and nuclear translocation by TGF-β [70,72,73]. However, there was normal TGF-β-mediated Smad2/3 phosphorylation (Figure 2.2**Error! Reference source not found.**B) and nuclear translocation (not shown) in ACF-CFs.

Since ACF CFs have elevated endogenous TGF-β levels and intact SMAD2/3 signaling, we next explored their response to exogenous TGF-β. Compared to Sham CFs, TGF-β failed to stimulate collagen type-I secretion in ACF CFs (Figure 2.2C). TGF-β induced comparable fold increases in CTGF and α-SMA expression in ACF compared to sham (Figure 2.2D-E) but the absolute magnitude of the increase was smaller.

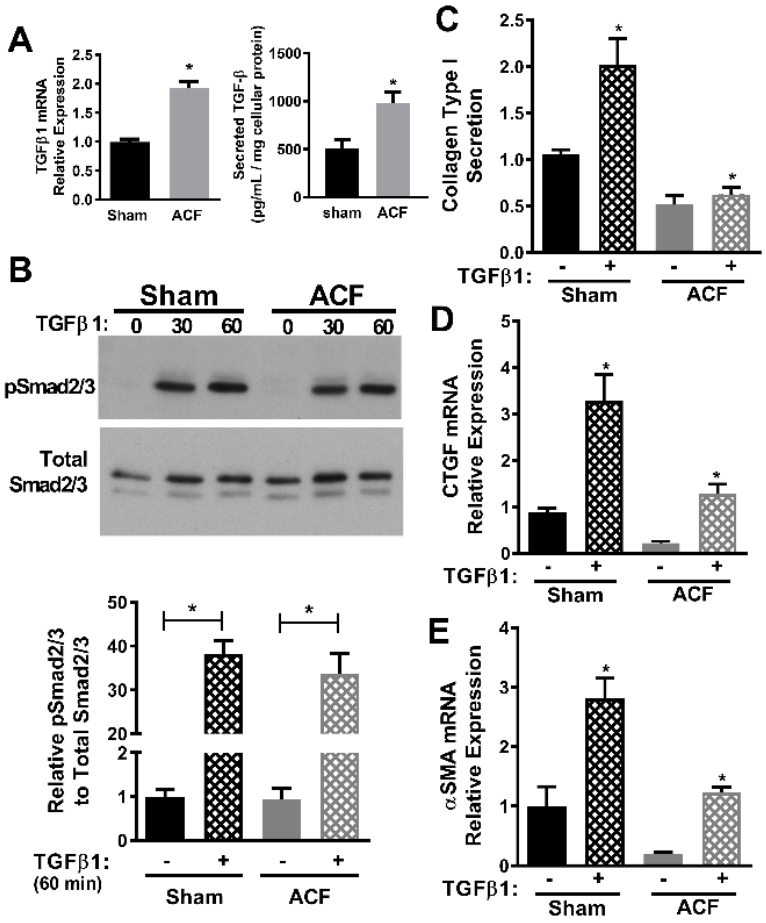

Figure 2.2: ACFs have increased TGF- β and intact TGF-β canonical signaling.
A) TGFβ mRNA and secretion in sham and ACF CFs. B) Immunoblots (top) and cumulative data (right; n=6) showing Smad2/3 phosphorylation folllowing 30 or 60 min treatment with 3 ng/ml TGF-β. C) TGF-β increases collagen secretion in sham but not ACFs. D) TGF-β induces a comparable fold increase but not magnitude increase in CTGF E) TGF-β induces a comparable fold increase but not magnitude increase in αSMA. *indicates $p<0.05$ compared to sham

2.3.3) Distinct patterns of actin cytoskeleton proteins in sham and ACF CF.

Proteomics results indicated differences among several cytoskeletal proteins in sham and ACF CFs (Table 2.2). Both actin binding proteins (enrichment score 7.7) and cytoskeletal proteins (enrichment score 14.7) were over-represented in the ACF data set compared to

sham. Actin regulatory proteins increased in ACF CFs vs. sham CFs, included actin depolymerizing factors (destrin [66], CapZA [59]), and regulators of actin treadmilling and branching (ARP2/3) [74,75]). Actin regulatory proteins decreased in ACF CFs vs. sham CFs included the actin bundling protein, transgelin, and myosin light chain. Immunofluorescence staining indicates decreased amounts of both F-actin (p=0.035) and G-actin (p=0.024) in ACF CFs compared to sham CFs (

Figure 2.3). These data together suggest an instability of the actin structure in ACF-CFs even when grown on rigid plastic, a substrate that should promote the formation of a stable, actomyosin cytoskeleton.

Table 2.2: Proteomics of Cytoskeletal Proteins

Protein	Description/Function	Sham Spectral Counts	ACF Spectral Counts	ACF/ Sham
Destrin	Actin depolymerizing	19.7	27.0	1.40
CapZA	F-actin capping protein, actin depolymerzing	2.7	4.7	1.75
ARP2	Actin treadmilling/branching	1.7	10.0	6.00
ARP3	Actin treadmilling/branching	4.7	10.3	2.20
Transgelin	Actin bundling protein	4.7	0.0	0.00
Myosin light chain	Cytoskeletal component	28.0	18.7	0.67

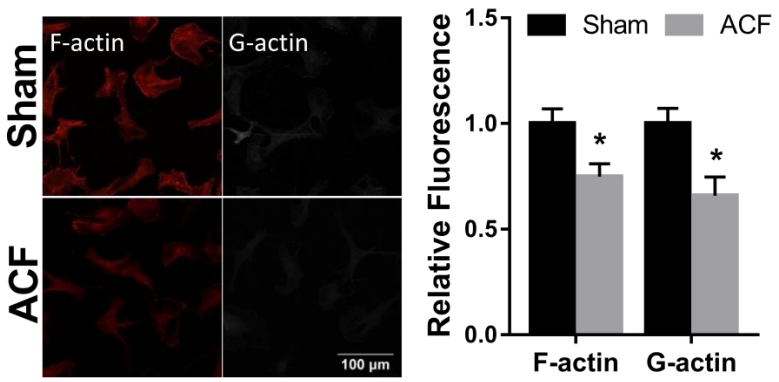

Figure 2.3: Decreased F-actin and G-actin in ACF CFs.
ACF CFs have less F-actin and G-actin as measured by fluorescent staining. * $p<0.05$ compared to sham.

2.3.4) ROCK inhibitor treatment recapitulates the ACF phenotype in Sham CFs.

Since ACFs have less F-actin, we hypothesized that we could recreate the ACF phenotype in sham CFs by allowing actin depolymerization with ROCK inhibitor treatment. After addition of the ROCK inhibitor, Y-27632, the phenotype of sham CFs was much closer to the hypofibrotic ACF phenotype as seen by an increase in MMP13 and a decrease in αSMA and CTGF mRNA expression (Figure 2.4A-C). Sham CFs treated with both the ROCK inhibitor and TGF-β were comparable to ACF CFs treated with TGF-β alone. For instance, control ACF CTGF expression was not statistically different from ROCK inhibitor treated sham CTGF expression ($p=0.16$), and sham CFs treated with both TGF-β and the ROCK inhibitor expressed CTGF at levels similar to ACFs treated with TGF-β ($p=0.22$). Overall, addition of the ROCK inhibitor created a more hypofibrotic phenotype. These data point to the possibility that the cytoskeleton or the Rho-ROCK pathway is involved in the hypofibrotic phenotype of ACFs.

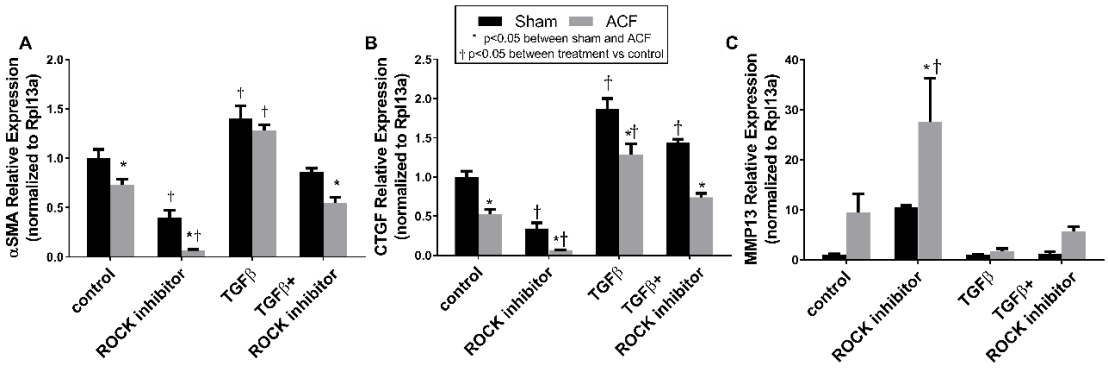

Figure 2.4: ROCK inhibitor induces a more hypofibrotic phenotype.

2.3.5) ACFs had a higher G-actin to F-actin ratio that could be decreased with Jasplakinolide (Jas) treatment. ACF CFs had a higher G/F-actin ratio compared to sham CFs ($p<0.001$, Figure 2.5A). The ratio was decreased after treatment with Jas, which stabilized F-actin, in both sham and ACFs ($p=0.025$ and $p<0.001$, respectively). TGF-β did not significantly affect the G/F-actin ratio in sham and decreased it 28% in ACF ($p=0.64$ and $p=0.019$, respectively). The increased G/F-actin ratio in ACF compared to sham was mostly due to the significantly lower amounts of F-actin (Figure 2.5B) in ACF CFs ($p=0.0051$). Jas caused an increase in F-actin over control in both ACF and sham. The increased F-actin amount in ACF after Jas treatment was not significantly different from basal sham CF levels of F-actin. Jas treatment caused a slight decrease in G-actin amounts but an overall increase in total actin (Figure 2.5CD). Total actin was slightly lower in control ACFs compared to sham ($p=0.051$, Figure 2.5D). However, Jas

treatment caused an increase in total actin compared to basal levels in ACFs to a level that was not statistically different from control sham CFs (p=0.29).

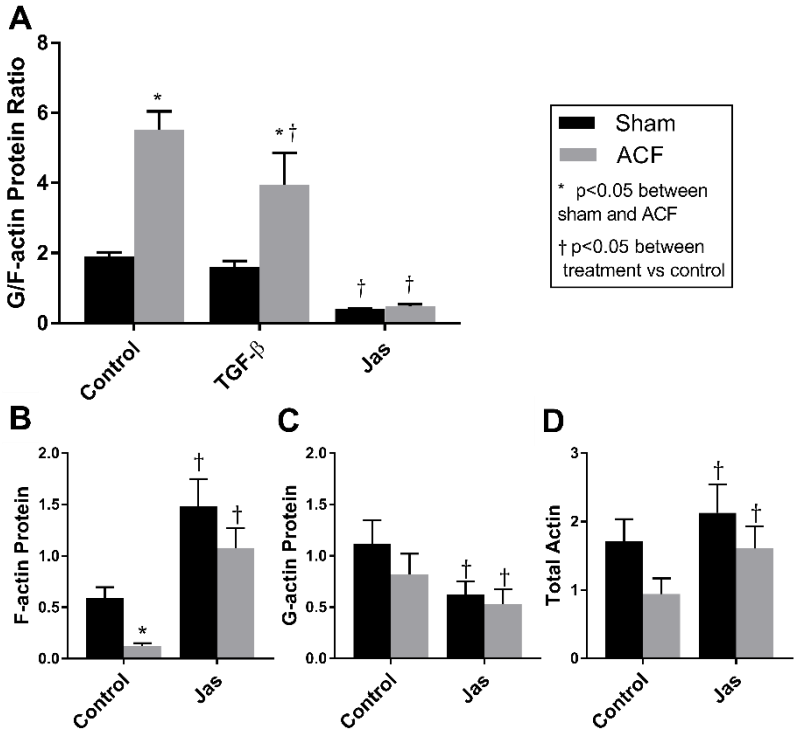

Figure 2.5: Jas treatment increased F-actin. Overall Jas treatment caused the G/F-actin ratio to decrease in both sham and ACF (A). Jas causes a significant increase in F-actin (B) and decrease in G-actin (C) compared to control in both sham and ACF. Jas treatment increased ACF CF's total actin (G-actin plus F-actin) to levels similar to control sham CFs (D).

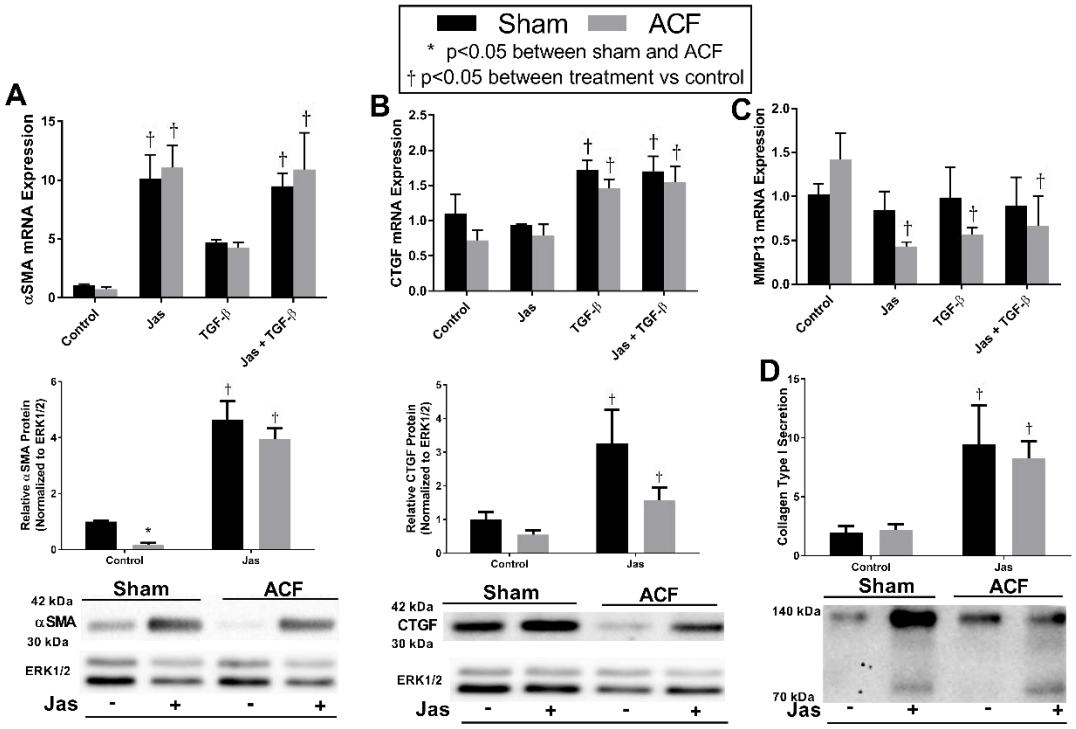

Figure 2.6: Jas treatment increases profibrotic phenotype.

2.3.6) Enhancing F-actin polymerization with Jas causes a more profibrotic phenotype. Overall Jas treatment caused an increase in a pro-fibrotic phenotype as measured by αSMA, CTGF, MMP13, and collagen secretion (Figure 2.6). Jas caused a larger increase in αSMA expression than TGF-β treatment. Jas caused a 10-fold increase in αSMA compared to a 4.5-fold increase with TGF-β treatment in sham and a 15-fold increase with Jas compared to a 5.8-fold increase with TGF-β in ACF (Figure 2.6A). αSMA protein quantitation also confirmed a large increase after Jas treatment ($p<0.001$ for both). While there was no increase in CTGF mRNA with Jas treatment there was a significant increase in measured CTGF protein with Jas treatment (Figure 2.6B). CTGF

protein increased 3.3-fold for sham and 2.9-fold for ACF with Jas treatment ($p=0.034$ and $p=0.023$, respectively). Both Jas and TGF-β treatment decreased the elevated MMP13 mRNA levels seen in basal ACFs (Figure 2.6C). Jas treatment caused an increase in type I collagen secretion into the media of both sham and ACF cultures ($p=0.033$ and $p=0.0040$, respectively, Figure 2.6D). Collectively, these data show that enhancement of F-actin resulted in a more profibrotic phenotype.

2.3.7) Jas causes an increase in nuclear MRTF-A. Since nuclear translocation of the transcription factor MRTF-A is regulated by the actin cytoskeleton, and we see cytoskeletal differences between sham and ACF, we tested whether MRTF-A translocation could account for the differences in ACF and sham phenotype. In addition, we tested whether stabilization of F-actin with Jas treatment or treatment with TGF-β could increase nuclear MRTF-A. We did not see differences in nuclear MRTF-A between non-treated sham and ACF CFs; however, treatment with Jas caused an increase in the MRTF-A fluorescence in the nucleus of both sham and ACF (Figure 2.7A) ($p<0.001$ for both). There was not a significant effect of TGF-β treatment on nuclear MRTF-A ($p=0.12$ for sham and $p=0.89$ for ACF). Although Jas caused a significant increase in the fraction of MRTF-A that was in the nucleus in sham ($p=0.015$), the fraction of nuclear MRTF-A remained constant with treatment in ACFs ($p=0.14$) (Figure 2.7B). That is, for ACFs, the increase in MRTF-A fluorescence in the nucleus is due to an overall increase in MRTF-A. Since αSMA is regulated by MRTF-A, we looked at the relationship between αSMA expression and the amount of MRTF-A in the nucleus (Figure 2.7C). This plot

demonstrated that the decrease in αSMA in ACF CFs was not related to a lack of MRTF-A in the nucleus.

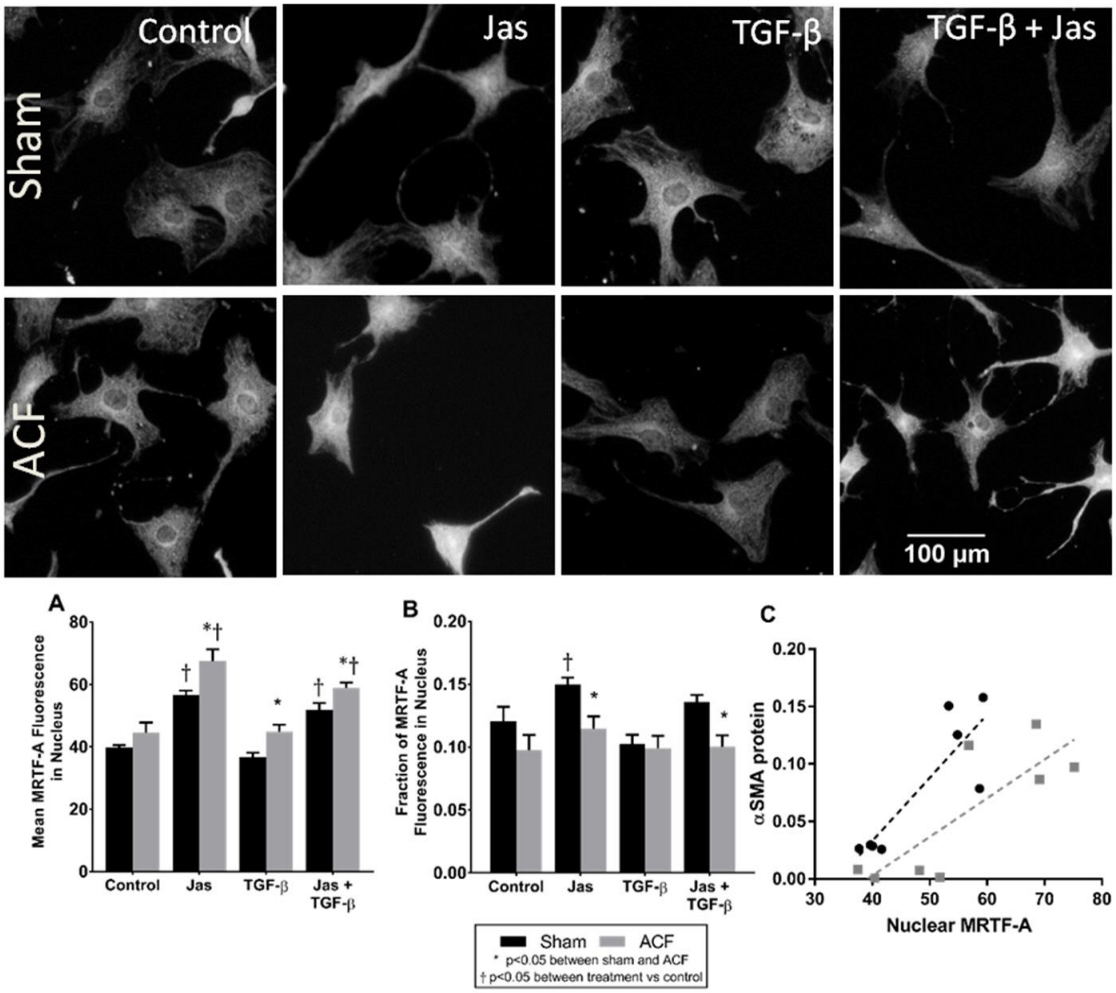

Figure 2.7: Jas treatment increases nuclear MRTF-A.

2.3.8) Jas treatment caused and increase in nuclear YAP. Since YAP is shown to be a mechanosensitve transcription factor that is regulated by the actin cytoskeleton, [76]

we measured cellular YAP localization. Treatment with Jas caused an increase in the amount of YAP fluorescence in the nucleus of both sham and ACF CFs ($p=0.045$ and $p=0.0080$, respectively, Figure 2.8A). There was no significant difference between TGF-β treated CFs compared to control in either sham or ACF ($p=0.97$ and 0.74, respectively). There also were not any significant differences in the amounts of YAP fluorescence in the nucleus between sham or ACF. The fraction of YAP was overall lower in ACF compared to sham and did not change with any treatments (Figure 2.8B), so the increase in YAP fluorescence in the nucleus with Jas treatment was due to an increase in overall YAP fluorescence. Since nuclear YAP promotes transcription of CTGF we looked at the relationship between CTGF protein and the amount of YAP in the nucleus (Figure 2.8C). This demonstrates that the amount of nuclear YAP is not responsible for the decreased amount of CTGF.

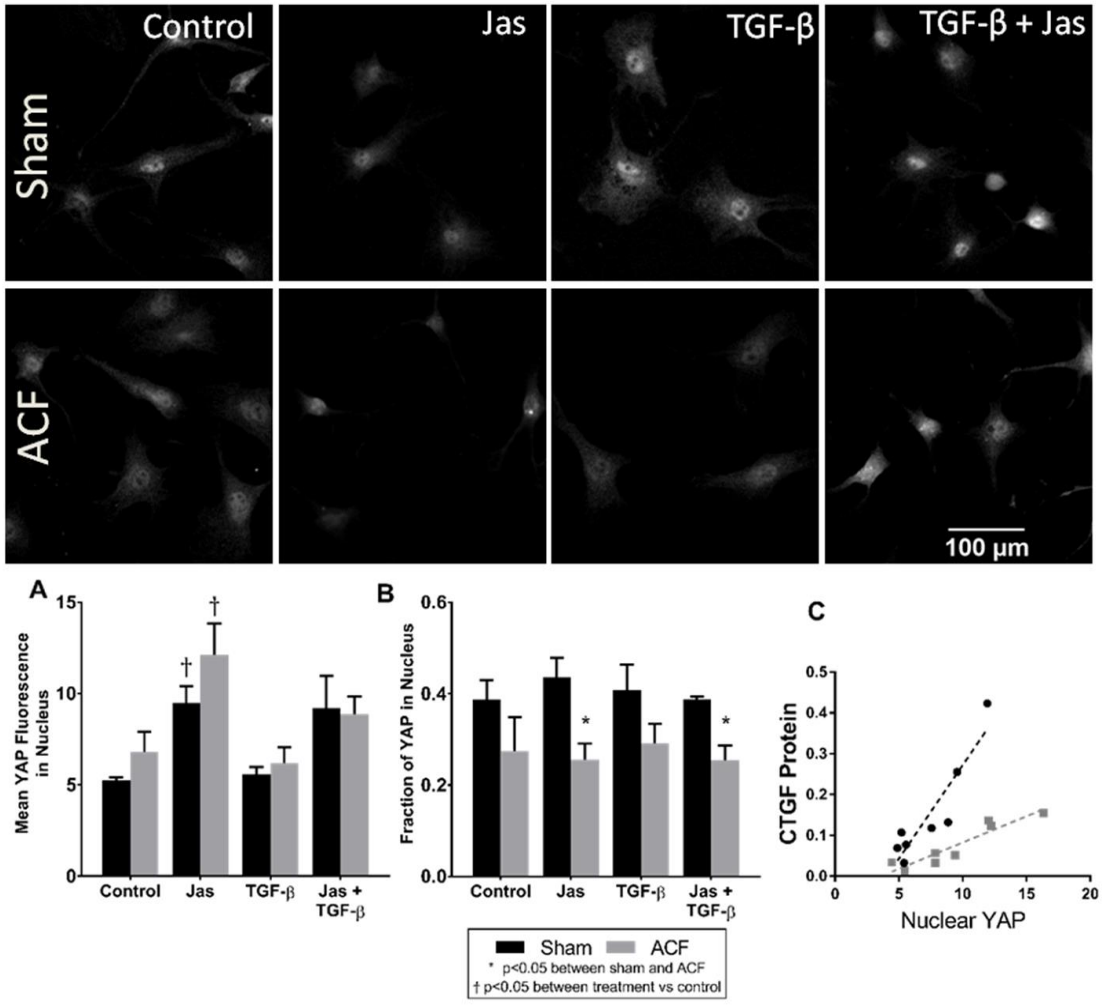

Figure 2.8: Jas treatment increases nuclear localization of YAP.

2.4) Discussion

In this study, we report a hypofibrotic phenotype of CFs isolated from the ACF model of VO HF. We indicated that these cells are different from normal fibroblasts because, given the same environment as CFs isolated from sham animals, they produced less CTGF, αSMA, collagens, and increased MMP13 (Figure 2.1) despite having

increased endogenous TGF-β levels (Figure 2.2). We have previously seen an increase in MMPs, a decrease in collagens, and an increase in TGF-β in ACF tissue compared to sham [17]. Here we report those same changes in the isolated CFs, suggesting that CFs may be responsible for the decrease in ECM in VO HF. This hypofibrotic phenotype is counter to the myofibroblast phenotype found in HF with fibrosis or myocardial infarction.

Since our initial investigation into the TGF-β canonical pathway indicated that this pathway was intact (Figure 2.2), we looked at the role of the cytoskeleton in phenotype modulation. The actin cytoskeleton controls many aspects of cell phenotype, including protein synthesis and signal transduction [51,56,76–78]. We discovered several cytoskeletal differences between sham and ACF CFs. Our proteomic data indicated that there were differences in the profiles of cytoskeletal proteins between sham and ACF (Table 2.2). We also saw that ACFs have overall less cytoskeletal actin with decreased F-actin and G-actin amounts (Figure 2.1 and Figure 2.5). Compared to basal sham CFs, ACFs have approximately half the amount of αSMA protein, a molecular marker important to the phenotype of myofibroblasts and that contributes to the contractility of the cytoskeleton. In addition, we found that, in basal conditions, ACFs have a much higher G-actin to F-actin ratio compared to sham CFs as a result of significantly less F-actin (Figure 2.3). Thus, ACF CFs do indeed have an altered cytoskeleton.

We manipulated the cytoskeleton with two different drugs, Jasplakinolide to enhance F-actin and Y-27632, a ROCK inhibitor, to allow depolymerization of F-actin. We hypothesized that ACF CFs treated with Jas would behave more like sham CFs and

that sham CFs treated with the ROCK inhibitor would behave more like CFs from ACF. The downstream effects of the activation of ROCK includes increased polymerization of F-actin and formation of stress fibers. Others have previously reported that when ROCK is inhibited with Y-27632 the G/F-actin ratio increases [49,50]. Y-27632 is previously shown to decrease αSMA expression [52,79], collagen deposition [52,79], and CTGF [52] in Tenon's fibroblasts, consistent with the decrease in αSMA and CTGF expression seen here (Figure 2.4A-B). Overall, the hypofibrotic phenotype was recapitulated in sham CFs treated with a ROCK inhibitor, suggesting a possible connection between an altered cytoskeleton and the ACF phenotype.

In these non-passaged primary CFs, 50 nM Jas treatment was enough to cause a significant decrease in the G/F-actin ratio and a more profibrotic phenotype in both cell types. Other groups tended to use higher concentrations of Jas to see a significant change in G/F-actin ratios [51,77], but this is likely because they are using passaged cells that already have a somewhat transformed phenotype from being in culture. Treatment of human HFL-1 lung fibroblasts used at passages 3-8 and treated with 50 nM of Jas does not cause a significant change in G/F-actin ratio, αSMA, or collagen-I [51]. However, when these same fibroblasts were treated with a 100 nM Jas, it caused a significant increase in αSMA, collagen-I as well as a decrease in the G/F-actin ratio. It is probable that our CFs are more sensitive to Jas because they are not passaged and, therefore, have not developed extensive stress fiber networks which are known to develop on plastic in culture.

Altering the cytoskeleton with Jas treatment was able to promote nuclear translocation of cytoskeleton dependent transcriptional factors MRTF-A (Figure 2.7) and YAP (Figure 2.8) in ACF CFs. However, for similar amounts of either YAP or MRTF-A in the nucleus, ACF CFs have relatively lower amounts of either CTGF (Figure 2.8C) or αSMA (Figure 2.7C) protein. This suggests, that at least on plastic, the profibrotic response to cytoskeletal alterations due to Jas treatment is not as pronounced in ACF CFs compared to sham CFs. There are likely other factors that promote or maintain a hypofibrotic phenotype in ACF CFs.

Chapter 3 : Pressure-Volume Loops and Biaxial Tensile Testing to Measure Myocardial Tissue Modulus in Volume Overload and Pressure Overload Heart Failure

3.1) Introduction

Heart Failure (HF) develops as a result of chronic hemodynamic stress due to volume overload (aortic or mitral valve regurgitation) and/or in response to pressure overload (hypertension or aortic stenosis). These stresses lead to fundamentally different patterns of left ventricular (LV) remodeling, contractile dysfunction, and ECM remodeling. Chronic pressure overload (PO) is associated with increased LV collagen deposition and concentric myocyte hypertrophy, resulting in a dramatic increase in the LV wall thickness to chamber diameter ratio. In contrast, volume overload (VO) results in a progressive dilatation characterized by a disproportionate decrease in the LV wall thickness to diameter ratio, increased myocardial wall stress, eccentric myocyte hypertrophy, and matrix degradation.[10,80,81]

Changes in the heart's composition and geometry (e.g., size and shape) can influence how much the heart wall deforms due to applied forces. Tissue with a greater stiffness deforms less for a given applied force. LV stiffness can contribute to LV dysfunction. For example, increased myocardial stiffness decreases cardiac pump efficiency by impeding filling and ejection.[6] Analysis of LV pressure volume (PV) loops

can provide several measures of tissue stiffness including the β index, which is calculated from the end-diastolic pressure volume relationship (EDPVR) to assess passive chamber stiffness.

While PV loops can be used to assess changes in the LV chamber stiffness, it is not clear how these changes relate to differences in tissue geometry (e.g., thickening of the heart wall) or in geometry-independent changes in tissue mechanical properties (e.g., due to changes in the ECM or cellular proteins). The ability to account for the effects of geometry is important since recent work indicates that the geometry-independent tissue mechanical property, referred to as "modulus", influences the morphology, migration, proliferation, survival, and differentiation of many cell types.[82] Modulus influences cardiac cell phenotype gene expression, [83] sarcomeric structure, [84] contractility and force generation,[85] cardiac fibroblast activation into myofibroblasts, [41] and ECM regulation.[37] Thus, characterizing tissue modulus changes for hearts experiencing PO and VO may enhance our mechanistic understanding of unique patterns of HF progression in these fundamentally different hemodynamic states.

To obtain a geometry-independent measures of tissue mechanical properties from PV loop data, chamber stiffness is often normalized to wall volume in an attempt to account for differences in size and shape between disease states. Alternatively, more sophisticated equations attempt to calculate modulus from PV loop data and measures of heart geometry. Both approaches rely on simplifying assumptions (e.g., spherical chamber with homogenous mechanical properties) that are known to be inaccurate. There has been a growing appreciation for the contribution of chamber geometry on apparent

stiffness since Mirsky in 1979 [86] and Yin in 1981, [5] to recent patient-specific finite element models using anatomical data from computed tomography.[87] However, PV loops are still commonly used to assess chamber stiffness, despite its known limitations.[88–90] The accuracy of this approach is not clear and has not been experimentally validated against direct measures of myocardial tissue modulus.

Multiple methods for directly measuring tissue modulus exist, such as atomic force microscopy (AFM), micropipette aspiration, uniaxial, or biaxial tensile testing. There is a range of estimates of myocardial modulus that vary widely depending on method and from study to study. For instance, the modulus of myocardial tissue of normal adult rodents ranges from approximately 18 kPa [26] to 109 kPa [27] when measured by AFM in two different studies. For this reason, it may be helpful to compare relative changes in modulus within the same measurement technique and study, as opposed to comparing absolute values. AFM is the most commonly used method to measure elastic modulus because of its relative simplicity compared to other methods. However, AFM and micropipette aspiration are used on the surface of materials and therefore would not measure modulus throughout the thickness of the heart wall. They measure mechanical properties of a roughly micron-sized region and, therefore, are subject to high variability based on what part of the tissue is tested. Tensile testing can be used to measure modulus throughout the whole thickness of a tissue. Tensile testing is able to recreate stresses that are on the appropriate physiological scale for the tissue. Biaxial testing is most appropriate in the case of measuring the myocardium because the heart tissue is

anisotropic (having different properties in different directions) and because the heart is subjected to multidirectional loads during the cardiac cycle.

In this study, we paired PV loop analysis in vivo with biaxial tensile testing ex vivo to: 1) better characterize mechanical changes in PO and VO HF, and 2) examine the ability of PV loops to estimate tissue modulus by comparing results with direct measures of modulus via biaxial mechanical testing. This is the first time, to our knowledge, that there has been a direct comparison of PO and VO using biaxial tensile testing, or a direct comparison of PV loops to biaxial tensile testing.

3.2) Methods

3.2.1) Animals. Sprague-Dawley male rats (~200 g, Envigo, Indianapolis, IN) were housed in a temperature and humidity controlled environment with a 12-hour light/dark cycle. Animals were provided free access to water and standard chow. All studies conformed to the NIH Guide for the Care and Use of Laboratory Animals. The protocol was approved by the IACUC of the Research Institute at Nationwide Children's Hospital. Control rats with no other treatments were age- and weight-matched to their PO and VO counterparts. All animals were sacrificed under 2-4% isoflurane (Baxter, Deerfield, IL) by exsanguination followed by cardiac dissection.

3.2.2) Aortocaval fistula Surgery. VO was induced surgically as described[91,92] 8-weeks before sacrifice. Briefly, rats were anesthetized with 2% isoflurane. An abdominal incision was created, and the abdominal aorta and caudal vena cava were exposed by blunt dissection. An 18-gauge needle was used to create the fistula through the shared wall of the aorta and vena cava. The aortic puncture was sealed with cyanoacrylate glue.

Shunt patency was confirmed visually by the presence of red arterial blood in the vena cava. The abdominal wall and skin were closed using 5-0 suture. Buprenorphine (0.03 mg/kg, Reckitt Benckiser Pharmaceuticals, Hull, England) was given postoperatively and as needed for pain. VO was confirmed at 4- and 8-weeks post-ACF via echocardiography to ensure fistula patency. A threshold of 8.0 mm LV end-diastolic diameter (LVEDD) was used to verify VO.

3.2.3) Angiotensin-II infusion. PO was induced by a pressor dose of angiotensin II (Ang II)(400 ng/kg/min, Bachem, Torrance, CA, http://shop.bachem.com/h-1705.html) infused for 4 weeks subcutaneously via osmotic mini-pumps (2ML4, Alzet, Cupertino, CA, http://www.alzet.com/products/ALZET_Pumps/index.html), according to the manufacturer's instructions. The dose and duration was chosen based on previous studies that demonstrate hypertension, LV concentric hypertrophy and fibrosis.[93]

PV loops. Invasive LV PV loop measurements were performed on a subset of animals (n= 4 or 5 per group), that were also used for biaxial mechanical testing after sacrifice, as described.[92] Rats were anesthetized under 2-4% isoflurane anesthesia and ventilated via tracheotomy using a small animal ventilator (SAR-830; CWE, Ardmore, PA). A combined micro-tip PV catheter (1.9F; SciSense, London, ON, Canada) was inserted into the right common carotid artery and advanced to the LV. PV loops were acquired off-ventilator, as previously described.[92] Baseline LV hemodynamic parameters were acquired; preload was varied by brief occlusion of the vena cava to obtain the LV-*EDPVR*. Data were acquired and analyzed using Labscribe2 software (iWORX, Dover, NH). The β coefficient was estimated by fitting the LV-EDPVR points with the equation:

$$P = A + ce^{\beta V}. \qquad (1)$$

P is chamber pressure and V is chamber volume. β is an index of chamber stiffness with units of inverse volume (mL^{-1}). A and c are constants. A dimensionless index of chamber stiffness, β_w, was calculated by multiplying β by the wall volume, estimated by LV weight divided by tissue density, in an effort to normalize to chamber size, as described by Burkhoff et al.[94] Both β and β_w are common methods to assess chamber stiffness, but they are affected by geometry and pressure within the chamber. Mirsky et al. showed that incremental modulus (E_{inc}) can be estimated from measured pressure, cavity volume, wall volume (V_w), and calculated mid-wall (Eq. 2)[94] or endocardial (Eq. 3)[95,96] radii.

$$E_{incM} = \frac{3}{4} P \frac{V}{V_w} \left(\frac{R_o}{R_m}\right)^3 \mu \qquad (2)$$

$$E_{incE} = \frac{9}{4} V \left(1 + \frac{V}{V_w}\right) \frac{dP}{dV} \qquad (3)$$

These estimated incremental moduli are based off a model assuming a heterogeneous isotropic material with a simplified spherical geometry with a constant wall thickness.

3.2.4) Tissue preparation for mechanical testing. After PV loop assessment and sacrifice, hearts were rinsed, cannulated and subjected to retrograde perfusion in a Langendorf apparatus using 100 mL cold perfusion buffer solution for ~10 minutes. The perfusion buffer contained: 137 mM NaCl, 2.7 mM KCl, 5.5 mM glucose, 12 mM $NaHCO_3$, 1mM $MgCl_2$, 1mM EGTA (Sigma-Aldrich, St. Louis, MO), 0.2 mM NaH_2PO_4, 25 mM 2,3-butanedione monoxime (BDM) (Fisher Scientific, Waltham, MA, https://www.fishersci.com/shop/products/2-3-butanedione-monoxime-98-acros-organics-3/p-4510165), and 1% Triton X-100 (MP Biomedicals, Santa Ana, CA) in distilled water. This solution was similar to calcium-free Tyrode's solution plus EGTA as a calcium

chelator, BDM, which inhibits myocyte contraction, and Triton X-100 detergent to permeabilize and release intracellular stores of calcium similar to the relaxing solution published elsewhere.[80] This solution prevented myocyte terminal contraction, which artificially increases the tissue's passive resistance.

3.2.5) Biaxial mechanical testing. The biaxial testing protocol was adapted from a previously published protocol using the same testing system (ElectroForce Planar Biaxial TestBench, Bose Corp., Eden Prairie, MN).[97] Following perfusion, the LV free wall was cut into approximately a 10 mm x 10 mm square with muscle fibers of the endocardial surface aligned in the longitudinal-axis direction to minimize shear as described by Sommer et al. [98]. Two pairs of size 29 fly fishing hooks (The Orvis Company, Manchester, VT) with 3-0 silk sutures were attached, evenly spaced, to each of the 4 sides of the tissue. Distance between hooks on the opposite side of the tissue was measured with calipers and used as gauge length. Five markers were placed evenly in a quincunx pattern in the center of the tissue square for video strain tracking. The suture loops were then fitted on the pulley to allow free shear. The tissue was floated with a piece of styrofoam to counteract the effect of gravity in relaxing solution (perfusion solution without Triton X-100 or BDM). After the tissue was loaded, a high-frequency ultrasound imaging system (Vevo660, VisualSonics, Toronto, Canada) was used to take longitudinal and circumferential direction tissue cross-sectional images for thickness measurements, following a previously published protocol.[99] The tissue was preloaded at approximately 0.5 g and preconditioned at least 9 times using an equi-biaxial tensile ramp in the a range of 0.5 g to 50 g at 0.5g/s controlled by WinTest 7 software (Bose Corp.,

Eden Prairie, MN). Strains were tracked with a digital video extensometer built into the Bose biaxial testing system. The 10th measurement was used for analysis.

3.2.6) Constitutive Modeling. The stress-strain data from each sample was fit to a reduced Fung type strain energy function (Eq.4), based on the method developed by Sacks[100] and as previously published.[97]

$$W = \frac{C}{2}(e^{A_1E_{11}^2+A_2E_{22}^2+2A_3E_{12}^2} - 1) \qquad (4)$$

$$Sij = \frac{\partial \mathrm{W}}{\partial E_{ij}} \qquad (5)$$

W is the strain energy, or the amount of energy stored in the tissue undergoing the deformation. E_{11} and E_{22} are Green strains in two-orthogonal loading directions, approximating the longitudinal axis direction and circumferential axis direction, respectively. E_{12} is the shear strain. S_{11} and S_{22} are the second Piola-Kirchoff stresses in either direction, and C and A_1, A_2, A_3 are material constants. Lagrangian stresses (T_{ij}) were calculated from the cross-sectional dimensions of the sample and the force output from the load cells. S_{ij} were computed from the measured T_{ij} and the deformation gradient calculated from the Green strains, as previously published.[97] The best fit of parameters was found using an unconstrained non-linear solver algorithm that reproduces experimentally found stress-strain curves based on Eq. 5. Initial guesses for each parameter were varied over several orders of magnitude to verify independence from the initial values.

3.2.7) Histology. N=5 from each experimental group were anesthetized and perfusion fixed with 4% paraformaldehyde with 60 mM KCl. Hearts were paraffin embedded, and 5 μm thick sections were cut, deparaffinized in xylene, serially rehydrated

in ethanol and rinsed in distilled water. Slides were stained with Masson's Trichrome or hematoxylin & eosin staining (Sigma-Aldrich, St. Louis, MO). Low magnification micrographs were acquired using a stereomicroscope (Olympus SZX7, Olympus Corporation, Center Valley, PA) equipped with illumination (ACE 1, SCHOTT, Mainz, Germany) and an Olympus DP71 camera (Olympus Corporation, Center Valley, PA). High magnification images were taken with an Olympus IX51 microscope using a 40X objective (Olympus Corporation, Center Valley, PA).

Cardiomyocyte cross-sectional area and percent collagen coverage were quantified using ImageJ (NIH, Bethesda, MD). Non-overlapping high-power fields (20 fields per rat) from LV free walls were examined for myocyte cross-sectional area and collagen. Myocyte cross-sectional areas were calculated by outlining the perimeters of myocytes cut in cross-section in ImageJ. The percent coverage of collagen for each field was quantified as a percentage (of blue pixels) to the rest of the entire tissue area within the field (with red pixels and nuclei included and white non-stained areas excluded) and were mostly devoid of coronary vessels.

3.2.8) Statistics. Results are reported as mean ± standard deviation (SD), and figures were created with GraphPad Prism version 7.00 for Windows, GraphPad Software, La Jolla California USA, www.graphpad.com. Statistical comparisons across groups were analyzed by one-way analysis of variance (ANOVA). Differences between groups and the control were determined with Dunnett's test for multiple comparisons. Two-way ANOVA with repeated measures was used to compare differences between longitudinal and circumferential stress-strain data and Tukey's post-hoc test was used to

assess differences in the stress-strain data between groups. The statistical threshold was set at 0.05 in all tests.

3.3) Results

3.3.1) Verification and characterization of HF. To assess both PO and VO HF, we measured cardiac structure, function, and blood pressure (BP) as shown in Table 3.1. Compared to control, PO animals exhibited a 14% increase in LV to body weight ratio (p=0.0027), consistent with hypertrophic cardiac remodeling. In addition, PO animals had a relatively unchanged LV- end-diastolic diameter (LVEDD) (4% decrease, p=0.25), but a significantly thicker posterior wall thickness (PWT) (18% increase, p=0.0048) resulting in a decreased LVEDD/PWT ratio (20% decrease, p=0.017), which is characteristic of concentric hypertrophy. The pressor dose of Ang II was confirmed by a 45% and 41% increase in systolic (p<0.001) and diastolic (p<0.001) BP, respectively. Additionally, there was a ~55% increase in end-diastolic pressure (EDP) (p=0.053). The increase in end-systolic pressure (ESP) did not achieve statistical significance (p=0.33) and end-diastolic volume (EDV) was unchanged (p=0.46). VO animals showed an 8% increase in body weight compared to control animals (p=0.027), which was likely due to increased water retention that was visible in some animals after dissection. Compared to control, in VO animals LV weight was increased 75% (p<0.001), LV to body weight ratio increased 62% (p<0.001). LVEDD was increased 42% (p<0.001); PWT was unchanged, yielding a 29% increased LVEDD/PWT ratio (p<0.001), indicative of eccentric remodeling. There was no change in systolic BP (p=0.70) and a modest (20%) decrease in diastolic BP

(*p*=0.0020) in VO rats. VO rats had a 14% decreased ESP (p=0.049) and a non-significant increase in EDV (p=0.12) and EDP (p=0.28).

Table 3.1: Left ventricular remodeling and animal model parameters.

	Control	Volume Overload	Pressure Overload
Body Weight (g)	391 ± 5	423 ± 14*	359 ± 9
LV weight (g)	1.36 ± 0.06	2.17 ± 0.11*	1.37 ± 0.09
LV: Body ratio (g/kg)	3.58 ± 0.07	5.79 ± 0.27*	4.08 ± 0.14*
LV End-Diastolic Diameter (mm)	7.5 ± 0.1	10.6 ± 0.2*	7.1 ± 0.1
Posterior Wall Thickness (mm)	1.7 ± 0.04	1.9 ± 0.07	2.0 ± 0.1*
LVEDD/PWT	4.4 ± 0.1	5.6 ± 0.2*	3.5 ± 0.2*
Systolic Blood Pressure (mm Hg)	121 ± 3	114 ± 7	189 ± 8*
Diastolic Blood Pressure (mm Hg)	87 ± 3	71 ± 2*	132 ± 5*
End-Systolic Pressure (mm Hg)	128 ± 7	110 ± 6*	134 ± 1
End-Diastolic Volume (µL)	259 ± 29	308 ± 43	252 ± 35
End-Diastolic Pressure (mm Hg)	9±1	12±1	14±2

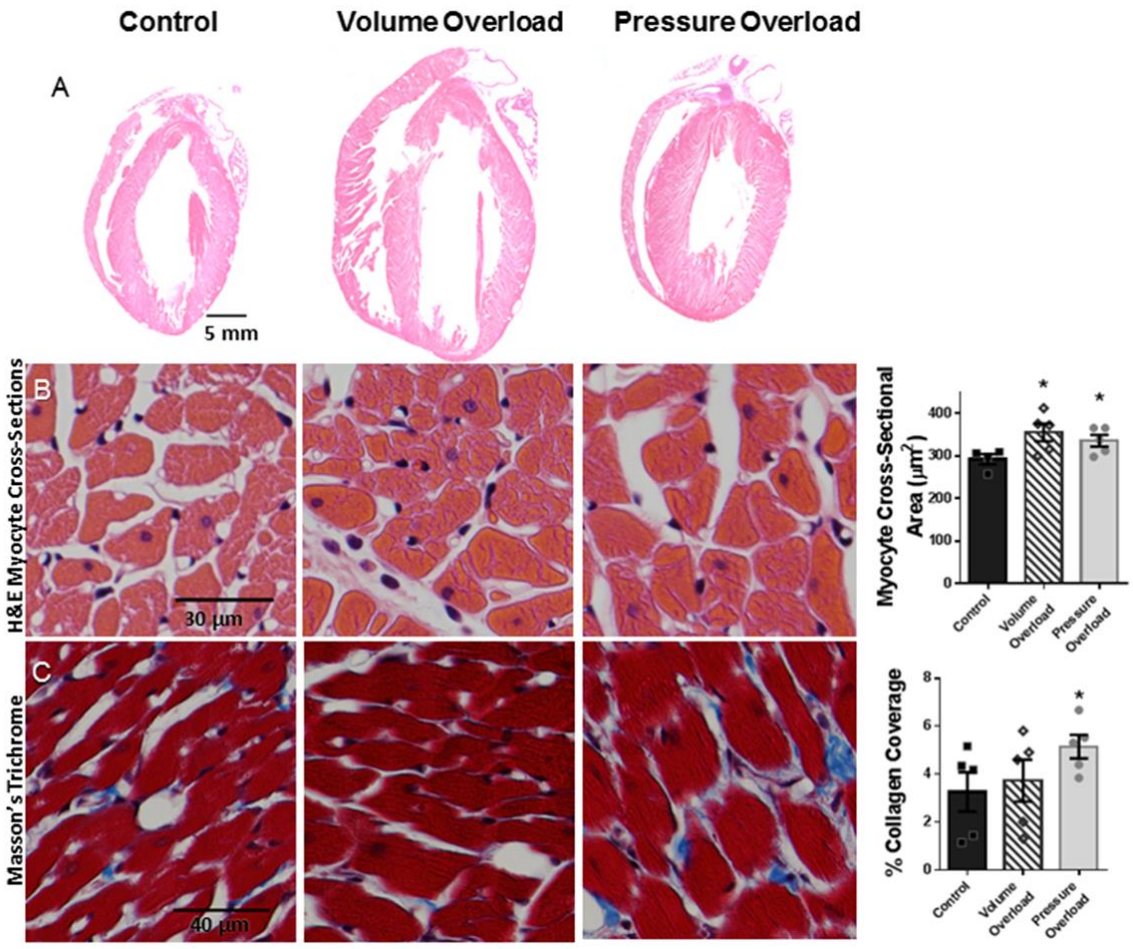

Figure 3.1: Histological assessment of control, VO, and PO hearts
Row A: 5X magnification images show concentric remodeling with thicker ventricle walls in pressure-overload (PO).Volume overload (VO) has increased chamber size and decreased wall thickness to chamber diameter ratio compared to control. Row B: Hematoxylin & eosin staining for measurement of myocyte cross-sectional area. Both VO and PO hearts showed increased cross-sectional area compared to control. Row C: Masson's trichrome staining for quantification of interstitial collagen content. PO had increased percent collagen coverage compared to control. N=5 for each group. * indicates $p<0.05$

3.3.2) Increased myocyte thickness in VO and PO and increased collagen content in PO. Macroscopic remodeling of the LV in PO and VO was visually evident in H&E-

stained tissue sections (Figure 3.1A). Myocyte cross-sectional area increased 47 μm^2 in VO (p=0.024) and 27 μm^2 in PO (p=0.037). Quantification of interstitial fibrosis via Masson's Trichrome (Figure 3.1C-D) staining revealed a 53% increase in interstitial collagen in PO hearts compared to control (p=0.041), while there was no difference between VO and control (p=0.43). Additionally, the ratio of perivascular collagen to the cross-sectional area of the blood vessel wall was increased 40% in PO compared to control (p=0.043), as previously reported in this model[101] (data not shown).

3.3.3) PV Loops suggest increased stiffness in PO and decreased stiffness in VO. The EDPVR of VO was shifted to the right (suggesting decreased apparent stiffness) and the EDPVR of PO was shifted to the left (suggesting increased apparent stiffness) (Figure 3.2A). Relative to control hearts, the β-coefficient was increased 98% in PO (p=0.0058) and decreased 38% for VO (p=0.014) (Figure 3.2B). Moreover, β_w, the index of chamber stiffness, for PO animals was approximately 2-fold over control (p=0.011) but was unchanged in VO (p=0.69)(Figure 3.2C). The calculated incremental modulus from the midwall stresses ($E_{inc\ M}$) did not show any significant differences (Figure 3.2D), and the incremental modulus using calculated endocardial stresses and strains ($E_{inc\ E}$) showed a 75% decrease in VO (p=0.089) and no significant change in PO (p=0.27) compared to control (Figure 3.2E).

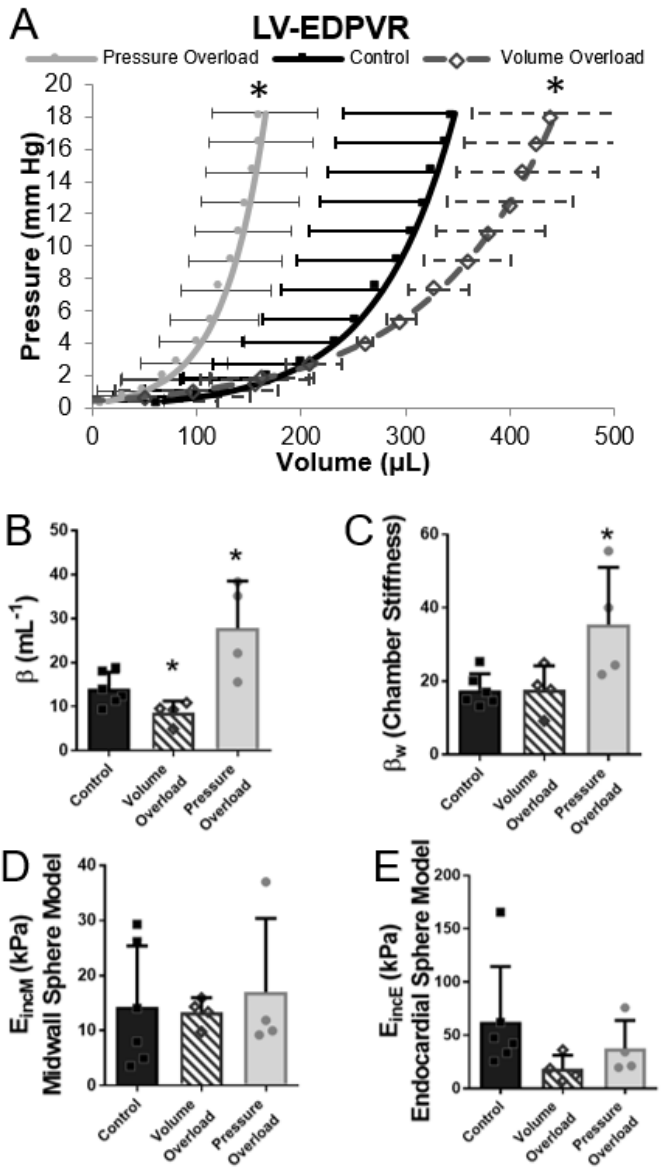

Figure 3.2: Average fits of LV-EDPVR and other estimates of chamber stiffness
A) Average fits of left ventricular end-diastolic pressure-volume relationship (LV-EDPVR) curves for each group. The shift up and to the left demonstrates an increase in pressure-overload (PO) chamber stiffness. The shift of the curve down and to the right shows a decrease in chamber stiffness in volume-overload (VO) chambers. B) β index of chamber stiffness from EDPVR curves. C) β normalized with wall volume. D) Calculated incremental modulus using modeled strains from the midwall and E) modeled strains from the endocardium. N=4 for PO and VO, n=5 for control *p <0.05 compared to control.

3.3.4) Biaxial testing indicates decreased modulus in VO but no change in PO compared to control. The average stress-strain relationship in the control (n=9), PO (n=10), and VO (n=10) groups are shown in Figure 3.3A characteristic J-shaped nonlinear stress-strain relationship was observed in all groups (Figure 3.3). In general, a more horizontal curve corresponds to a material that requires less stress to deform it (i.e., a lower modulus). For all groups, the hearts had a greater modulus in the circumferential direction than the longitudinal direction. For example, the circumferential and longitudinal strains at the same stress level were significantly different from each other in control, PO, and VO ($p<0.001$) groups. Circumferential strains were 83-96% larger in the VO group at the same stress levels (at 3 kPa and above), as compared with the control group ($p=0.020$) (Figure 3.3). The stress-strain responses were not significantly different between the control and PO groups in either longitudinal or circumferential direction. Shear strain was small in all groups (~1% or less maximum shear strain throughout the tests).

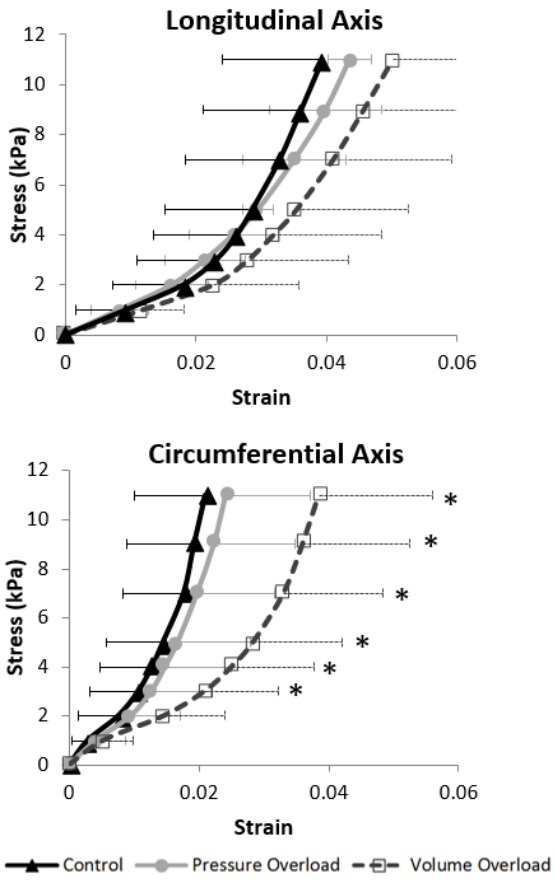

Figure 3.3: Average stress-strain curves from biaxial testing.
N=9 for PO and control, n=10 for VO. * indicates $p<0.05$ compared to control.

Table 3.2: Constitutive model parameters from biaxial tensile stress-strain data.

	C	$A_{1\,(long)}$	$A_{2(circ)}$	$A_{3(shear)}$	$C*A_2 > C*A_1$
Control	0.9 ± 0.22	292 ± 76	556 ± 139	0.35 ± 4.3	p = 0.014
Volume Overload	0.55 ± 0.08	198 ± 35	360 ± 73	-2.48 ± 2.1	p = 0.0034
Pressure Overload	0.76 ± 0.13	197 ± 30	477 ± 119	-4.09 ± 1.03	p = 0.0094
ANOVA	p = 0.27	p = 0.33	p = 0.48	p = 0.51	

3.3.5) Constitutive modeling showed anisotropy in all conditions and decreased modulus in VO. The material constants (Table 3.2) derived from constitutive modeling of the biaxial mechanical data quantitatively confirmed the trends seen in the average stress-strain curves above. For example, the parameter corresponding to the modulus of the heart in the circumferential direction ($C*A_2$, 270 ± 34 kPa) was greater than that for the longitudinal direction ($C*A_1$, 133 ± 14 kPa) for all groups (Table 3.2). This corresponds to the observation that the stress-strain curves for the circumferential direction is to the left of the corresponding curves in the longitudinal direction; both observations indicate that the heart was stiffer in the circumferential direction (Table 3.2). For control hearts, $C*A_2$ was ~90% greater than $C*A_1$. Similarly, for VO hearts $C*A_2$ was ~70% greater than $C*A_1$. For PO hearts, $C*A_2$ was ~140% greater than $C* A_1$, suggesting that the degree of anisotropy increased during PO. VO had smaller moduli, ~ 56% lower in the circumferential direction ($C*A_2$, p=0.016) and 43% lower in the longitudinal direction ($C*A_1$, p=0.0064) compared to control (Figure 3.4). PO moduli were not statistically

different from control animals in either direction (p= 0.073 in longitudinal axis and *p*=0.74 in circumferential axis) (Figure 3.4). A_3, the parameter describing the contribution of shear was small (less than 2% of the magnitude of the parameters in either the circumferential or longitudinal direction), similar to other reports[98]. Removing the parameter from the model had very little effect (<1%) on the values of the remaining parameters. Thus, shear only had a minor contribution to the mechanical properties of the tissue under the conditions tested.

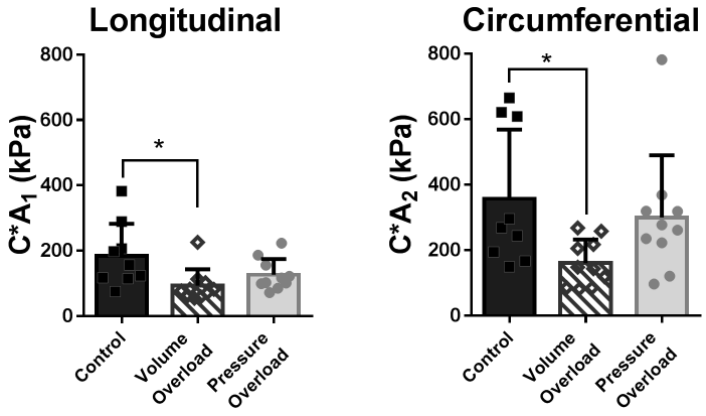

Figure 3.4: VO has decreased and PO has unchanged tissue modulus compared to control.

3.4) Discussion

Our studies extend the results from previous studies by providing, for the first time to our knowledge, 1) direct comparisons of tissue moduli between PO, VO, and normal hearts in one study and 2) side-by-side measurements of mechanical properties of hearts using both in-vivo PV loop data and ex-vivo biaxial data. Our results allowed us to

compare the outcome of the widely used PV-loops with direct mechanical testing on the same tissue to gain further understanding on how the mechanical properties of the heart changes in both PO and VO. Several of the results of this study are similar to those reported by others including: 1) responses in heart structure and hemodynamics in response to Ang II infusion [93,101] and ACF surgery,[10] 2) anisotropic mechanical properties of the myocardium [102], and 3) increased apparent stiffness in PO hearts as calculated from PV loop data.[103,104]

Our results showed that in VO, relative to control hearts, chamber stiffness (from PV data) and tissue modulus (from biaxial testing) both decreased but the magnitude of the decrease differed by ~100%. In PO, relative to control hearts, chamber stiffness doubled but the modulus was unchanged. Thus, changes in tissue stiffness determined from PV loops may not be consistent with the magnitude or direction of change in tissue modulus determined by biaxial mechanical testing. Additionally, the increase in apparent stiffness in PO may likely be due to changes in geometry and compensative remodeling, and not due to an increase in tissue modulus, whereas the decrease in apparent stiffness of VO is due in part to decreased tissue modulus. Reasons for the discrepancies in estimated tissue modulus between the two testing methods may include limitations of the PV-based analysis or limitations of the biaxial-based analysis and are summarized below.

PV loops to evaluate passive mechanics can be difficult due to complex geometries, heterogeneous anisotropic material, and varying pressures and stresses between disease states. It is tempting to use the β index or β_w, which attempt to account for differences in heart size, from straightforward EDPVR analysis as an indication of

tissue modulus. There are inherent limitations to this measurement due to noise from measures of conductance volumes in the catheter and its effect on the exponential fit of the data. Mirsky has highlighted the importance of considering geometrical accuracy and difference in ranges of pressure when interpreting EDPVR. For these reasons, Mirsky derived equations to estimate myocardial modulus (reported here as E_{incM} and E_{incE}) based on PV loop data.[94–96,105] Care must be used, however, when interpreting these calculated moduli since the derivation of the equations make simplifying assumptions not fully consistent with what is known about the heart. Several of the simplifying assumptions include: 1) a simplified geometry such as a spherical LV, 2) the LV has a constant wall thickness, and 3) uniform mechanical properties in all directions Figure 3.1A and Table 3.2 illustrate the inconsistency of these assumptions about chamber geometry, wall thicknesses, and mechanical properties.

Biaxial mechanical testing gives a direct measurement of the passive mechanical properties of the LV wall, but it, too, is not without its limitations. The ex vivo tissue properties are unlikely to be a perfect match to the modulus seen in vivo since the heart is affected by the active mechanics of relaxation and contraction of the chamber and myocytes. Tensile testing's widespread use is greatly limited by the fact that it requires large portions of the heart to be excised. This excised portion is assumed to be typical of the whole LV because it is previously shown that the modulus of the LV wall is similar throughout [106]; however, by excising a section of the LV free wall, the tissue's geometry is altered from its in vivo shape, from convex, to flat. While the biaxial mechanical testing is a step forward from uniaxial testing by applying stresses in multiple directions,

which assesses anisotropy, but this does not perfectly simulate in vivo stresses. In vivo, LV filling pressures cause transmural stresses that are not replicated in biaxial testing. Simpler geometry and analysis is at the expense of altered ex vivo geometry since the mechanical testing is done on tissue of roughly a rectangular shape. In addition, biaxial testing only measures passive tissue properties, whereas in vivo PV loop analysis attempts to focus on the passive mechanics by targeting analysis during the passive filling phase of diastole; PV loops are likely influenced by the active relaxation of the heart.[95]

Since results from PV analysis and biaxial testing analysis do not always agree and both techniques have limitations, an obvious question is, which technique is more accurate? The preferred technique depends on both practical considerations and the particular parameter to be measured. PV loops are routinely performed in clinical settings and provide clinically relevant assessments of heart function, that in most cases is the primary interest. In other cases, one is more interested in the modulus of the heart, especially given the recent studies implicating modulus as an important regulator of cellular function,[82] including cardiac cells[37,41,83–85]. Given that PV loop analysis cannot directly provide modulus, and the equations derived to calculate modulus from PV data apply simplifying assumptions of limited accuracy, we suggest that a method that provides a more direct measure of modulus, such as biaxial mechanical testing, is preferred when tissue biomechanics is the experimental outcome. Multiple methods for determining modulus exist (e.g., AFM, micropipette aspiration, uniaxial, or biaxial testing) and the range of estimates of stiffness varies widely depending on method and from study to study. For instance, the modulus of myocardial tissue of normal adult

rodents ranges from approximately 18 kPa[26] to 109 kPa.[27] For this reason, it may be helpful to compare relative changes in modulus within the same measurement technique and study opposed to focusing on absolute values.

Our data showing that VO hearts have approximately half the modulus of normal myocardium is a new finding. Chaturvedi et al. show that VO tissue was less stiff than PO using human biopsy samples, as measured by uniaxial testing, but did not compare to normal tissue due to lack of sufficient sample numbers[80]. Previously, we noted that there was a net decrease in ECM during acute and compensated VO induced HF which corresponded with decreased chamber stiffness.[10] This led us to hypothesize that the VO tissue had a decreased tissue modulus compared to normal hearts, which we now confirm in this study.

Several studies have shown a correlation between increased collagen amount and chamber stiffness in PO.[107,108] with the assumption that increased collagen translates into an increased modulus. However, we did not observe an increase in 4-week PO LV modulus. It is possible that there is a change in modulus at later time points in the PO HF progression. Relative to control hearts, we observed an ~50% increase in myocardial interstitial collagen content in PO hearts (Figure 3.1) but did not see increased tissue modulus, since the PO LV moduli are equal to, or less than, control tissue measured by biaxial testing (Figure 3.4). These data suggest there is a one-to-one correlation between increased tissue modulus and increased collagen amount. Another consideration is that Masson's Trichrome staining does not distinguish between collagen type I and collagen type III, which display different tensile strength. For example, the ratio of collagen type

III (which is more elastic) to type I ratio, tends to stay constant in PO HF[109] and increases in VO.[10,110] Additionally, there are other factors such as collagen crosslinking or fiber structure that affect the mechanical properties of collagen.[111] Other factors outside of collagen may influence tissue modulus. For instance, titin has been implicated as a contributor to passive mechanics of the hearts tissue,[112] and has been indicated as a possible cause of stiffness changes in HF.[113]

These results are consistent with other studies that concluded that PO tissue has approximately the same modulus as control. Mirsky et al. suggested that PO tissue may have approximately the same modulus as normal tissue when controlling for pressure.[96] This is important since pressure varies among heart disease states and since increasing chamber pressure increases cardiac tissue modulus in vivo. For these reasons, it is difficult to compare the chamber stiffness or tissue modulus across diseases that have distinct chamber remodeling and non-overlapping pressures ranges such as those found in VO and PO. Using a spherical model described above, and reducing pressure to that of controls by administering nifedipine, Mirsky estimated that normal and PO hearts have approximately the same incremental modulus at equal pressures.[96] Therefore, the increase in apparent chamber stiffness in PO hearts is likely due to an increase in overall material, changes in geometry, and/or higher chamber pressures, rather than an increase in the material modulus of the relaxed tissue.

These analyses highlight the differences in remodeling and mechanical properties between PO and VO via two methods of mechanical testing. Based on the combination of the PV loop analysis and measures of modulus via biaxial testing, the increase in

chamber stiffness in PO is likely due to changes in geometry and not changes in material modulus, while the decreases in chamber stiffness in VO is likely a result of a decrease in myocardial modulus as confirmed by biaxial testing. This information may be useful to the design and interpretation of experiments investigating the effect of modulus on cardiac cell behavior and inform further basic research using computational models of the progression of remodeling in HF. In addition, these analyses highlight the difficulty in using PV loop analysis to assess changes in myocardial modulus. We have shown that chamber stiffness measured by PV loops does not necessarily correspond to the tissue modulus measured by biaxial testing.

Chapter 4 : Decreased Substrate Modulus Promotes a Hypofibrotic Phenotype in Cardiac Fibroblasts.

4.1) Introduction

Cardiac fibroblasts (CFs) play a crucial role in the physiological maintenance of extracellular matrix (ECM) and in many pathologies of the heart including myocardial infarction, hypertension, and cardiomyopathy. CFs are often suggested as a target for therapeutic strategies with most studies identifying cardiac myofibroblasts, an activated and profibrotic phenotype of CFs, as the main therapeutic target in many types of heart disease especially when there is fibrosis [11,40,71,114]. Therefore, most studies looking at CFs are framed in the context of the fibroblast to myofibroblast transition and emphasize strategies to make CFs less fibrotic.

However, fibroblasts also play a role in pathologies where there is insufficient ECM such as in emphysema [115], rheumatoid arthritis [116], and, in the heart volume overload (VO) induced heart failure [17]. In VO heart failure, there is a net decrease in extracellular matrix in the LV [10,18,60]. This net decrease in ECM within the tissue is important, because ECM maintains the structural integrity of the chamber, a decrease in ECM likely contributes to disease progression. In a chronic mitral regurgitation model of VO HF, there is a decrease in LV interstitial collagen content, along with increase MMP expression and down regulation of several profibrotic factors and extracellular matrix

genes as well as an increase in several anti-fibrotic factors[117]. In another model of VO HF, aortocaval fistula (ACF), we have reported that there is a decrease in collagen content in the LV[10,17]. CF isolated from ACF VO hearts secrete less connective tissue growth factor (CTGF), have less αSMA, have increased MMP expression, and an increased collagen type-I to type-III ratio (Chapter 2). We refer to these CFs as hypo-fibrotic since they secrete less CTGF and produce a net decrease in ECM proteins compared to CFs from healthy hearts.

Much of what we know regarding the regulation of the fibrotic potential of fibroblasts comes from the study of quiescent fibroblasts transitioning to pro-fibrotic myofibroblasts. In these studies, quiescent fibroblasts become proto-myofibroblasts with increased cytoskeletal tension and then are activated into myofibroblasts with the addition of TGF-β [11,16]. This model is not sufficient to describe CFs isolated from VO HF. Relative to CF from control hearts, CFs from the ACF model produce increased TGF-β, and even when plated on plastic they maintain a more hypofibrotic phenotype than normal CFs, secreting less collagen and CTGF (Chapter 2). In Chapter 2 we suggest that fibroblasts have a spectrum of phenotypes and that CFs in VO HF are on the opposite side of the spectrum of myofibroblasts.

There is growing evidence showing increasing tissue stiffness above normal levels promotes an increase in a profibrotic phenotype. Fibroblasts on substrates of approximately 3 kPa start to become proto-myofibroblasts and fibroblasts on ~20 kPa or higher allow for myofibroblasts activation characterized by αSMA positive stress fibers [118,119]. An in vitro model of cardiac fibrosis consisting of a hydrogel micropatterned to

have areas of soft and stiff substrate rigidity was used to show CFs on stiff regions have increased αSMA, F-actin, and fibronectin, characteristic of myofibroblasts [120]. However, in VO there is a decrease in myocardial tissue modulus and chamber stiffness (Chapter 3). Since increased stiffness causes an increase in profibrotic phenotype the inverse may be true for VO. That is, there may be a potential relationship between the hypo-fibrotic phenotype of CFs in VO and the decreased tissue modulus.

Several transcriptional regulators appear to link alterations in cytoskeletal properties associated with changes in substrate stiffness to changes in gene expression. One mechanism that potentially explains the transduction of stiffness to affect phenotype involves myocardin related transcription factor A (MRTF-A). MRTF-A transduces mechanical stress via the polymerization state of the actin cytoskeleton, where it is sequestered by G-actin and freed by polymerization to F-actin, which allows it to translocate to the nucleus. In the nucleus, MRTF-A promotes a fibrogenic program, including expression of αSMA and transgelin. On stiff (~20 kPa) polyacrylamide gels human lung fibroblasts increased F-actin and displayed an increase in MRTF-a nuclear translocation, and a resulting increase in αSMA compared to soft gels (~0.5 kPa) [49]. Another mechanotransduction factor is the yes-associated protein (YAP), which translocates to the nucleus when there is increased cytoskeletal tension or changes in cell shape and adhesion [54]. YAP nuclear translocation promotes connective tissue growth factor (CTGF) and transgelin expression and has been associated with the myofibroblast activation of mesenchymal stromal cells [56], lung fibroblasts [57], and cancer associated-fibroblasts [58]. In pulmonary fibrosis, stiffness may play a role in regulating fibroblast

phenotype as YAP nuclear translocation on stiff substrates is linked with fibroblast activation [54,57].

Due to the decreased tissue modulus in VO hearts and evidence showing stiffness influences fibroblast phenotype we wondered if the decreased tissue modulus in VO HF may play a role in the hypo-fibrotic phenotype of CFs. We hypothesized that sham CFs on softer substrates would have a more hypo-fibrotic phenotype (with less MRTF-A and YAP in the nucleus and lower profibrotic molecules such as αSMA and CTGF), conversely, CFs from ACF would behave more like normal cells on a higher stiffness.

4.2) Methods

4.2.1) Animals. Male Sprague-Dawley (~200 g, Envigo) were kept in temperature and humidity controlled housing, with free access to standard chow and water, and with a 12 hour light/dark cycle. Age- and weight-matched animals were used for sham and aortocaval fistula (ACF) surgeries. ACF surgeries have been described previously [91,92], briefly, animals were anaesthetized with ~2% isoflurane, an abdominal incision was made, the abdominal aorta and inferior vena cava were exposed with blunt dissection and an 18-gauge needle was inserted into the shared wall of the vessels. The opening on the inferior vena cava was closed with either cyanoacrylate glue or purse string sutures. Arterial mixing in the vena cava was visually confirmed and the abdomen closed up with sutures. The sham surgery is similar where the vessels are exposed by blunt dissection and the abdomen is closed with sutures. Buprenex was given for pain at 24 and 72 hours post-operatively and as needed. VO was confirmed 4 weeks after surgery via

echocardiography, with a left ventricular end diastolic diameter (LVEDD) of at least 8 mm.

4.2.2) Cardiac fibroblasts. We used a protocol to isolated primary adult CFs from rats as described previously in Chapter 3. Briefly, CFs are isolated from LVs of 4 week post ACF or sham rats by enzymatic digestion (80 U collagenase type-2 and 0.1% trypsin) and plated in 10% fetal bovine serum-Dulbecco's modified essential media. The cell solution was plated on polyacrylamide gels (Matrigen) pre-coated with a solution of 10 µg/mL type I rat tail collagen (BD) in 0.02 N acetic acid. Approximately one hour later, media was replaced with 10% FBS DMEM with 1.0 g/L glucose. Cells were gently washed several times with warm PBS 24 hours after isolation and fresh media was replaced until cells reach a confluence of ~60-80%.

4.2.3) Fluorescent Staining. Cells were fixed in 4% paraformaldehyde in PBS solution for a half hour. Fixed cells were then permeabilized with 0.03% Triton-X and blocked in BSA and goat serum or fish block (for MRTF-A staining) for 1 hour. Primary antibodies were incubated overnight at 4°C with gentle agitation (anti-MRTF-A, Santa Cruz sc-21558; anti-YAP, Cell Signaling 14074; anti-PPARγ, Pierce PA3-821A; anti-αSMA, Sigma a2547). Primary antibody was washed with PBS several times prior to incubation with fluorescent secondary antibodies. Counterstains were done with DAPI, to stain nuclei, and TRITC conjugated phalloidin, to stain F-actin (Millipore, FAK100) or Alexa Fluor 488-conjugated DNAse-I (Thermo Scientific), to preferentially stain G-actin (Thermo Fisher Scientific). Fluorescent micrographs were taken with an Olympus IX51

microscope or Zeiss 710 confocal microscope to visual cytoskeletal proteins. Fluorescence was quantified with ImageJ.

4.2.4) Real Time quantitative PCR. CFs were lysed in TRIzol extraction reagent, scraped and sonicated. RNA was extracted with chloroform and centrifuged. The aqueous phase was purified using Qiagen RNeasy Mini Kit (Qiagen) and RNA concentration was determined by a NanoDrop 2000 (Thermo Scientific) spectrophotometer. Maxima First Strand cDNA Synthesis Kit (Thermo Scientific) was used to reverse transcribe RNA. Equivalent amounts of cDNA were amplified in duplicate with Maxima Probe qPCR master mix (Thermo scientific) and Roche Universal Probe and primer pairs for the target genes (See Table 1 for sequences). 40 amplification cycles were carried out using an Eppendorf MasterCylcler-ep Realplex thermocycler. Relative expression was determined by using the $2^{-\Delta Ct}$method, normalizing to the geometric mean of the housekeeping genes Rpl13a and LDHA.

4.2.5) G-actin and F-actin Immunoblot. The ratio of F-actin and G-actin were analyzed using a kit from Cytoskeleton (Denver, CO) and according to the protocol provided. Breifly, cell lysates were scraped and collected with F-actin stabilization lysis buffer provided in the kit. Lysates were briefly sonicated and centrifuged at 350 x g to pellet unbroken cells and debris and the supernatant was centrifuged at 100,000 x g at 37°C for 1 hour to pellet F-actin. The supernatant contained G-actin, and the F-actin pellet was suspended in an equal volume to the supernatant with F-actin depolymerizing buffer provided in the kit. The G-actin and F-actin solutions were prepared in SDS loading buffer and run through an SDS-PAGE gel in parallel. Gels were transferred to a

PVDF membrane, blocked in 5% milk, and incubated with an anti-pan-actin antibody provided in the kit. Ratios were determined by densitometry.

4.2.6) Statistics. Results are reported as mean ± standard error of the mean. Statistical analysis was performed with a two-way analysis of variance and differences between conditions were asses by a post-hoc test. A p-value less than 0.05 is reported as statistically significant.

4.3) Results

4.3.1) Increasing stiffness causes a decrease in the G/F-actin ratios. Both cell spreading and the prominence of F-actin stress fibers increases with increasing substrate stiffness (Figure 4.1A). Stress fiber formation increases with stiffness in sham but does not have a significant effect on ACF CFs (Figure 4.1B, $p<0.001$ and $p=0.31$, between 2 and 50 kPa gels). On 50 kPa gels, F-actin fluorescence was significantly higher in sham CFs compared to ACF CFs ($p=0.041$). Consistent with the increased prominence of stress fibers, the ratio of G-actin to F-actin decreases with increasing stiffness as measured by the fluorescence of DNAse-I and TRITC-conjugated phalloidin in both sham and ACF (Figure 4.1C, $p<0.00.1$). Fluorescent staining technique did not reveal any difference between sham and ACF G/F-actin ratios ($p=0.79$).

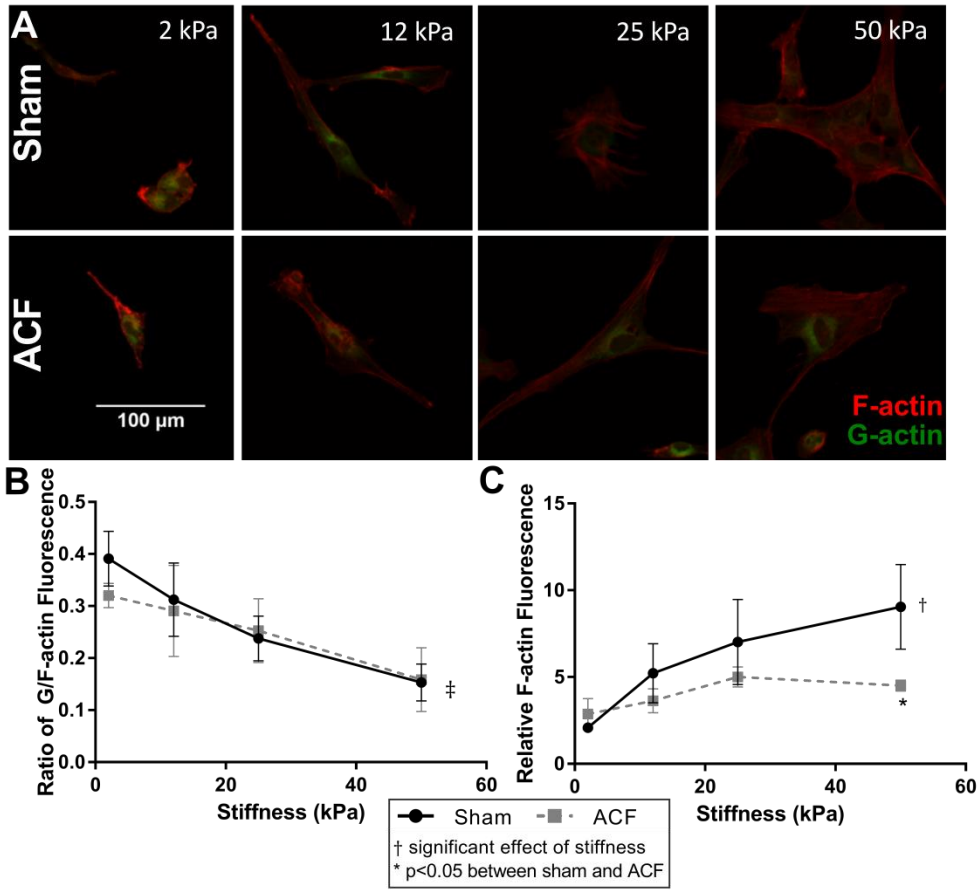

Figure 4.1: Fluorescent staining for G-actin and F-actin.
Increased stiffness decreases the ratio of G-actin and F-actin in both sham and ACF. F-actin increases are smaller in ACF CFs with increasing stiffness.

In general, the G/F-actin ratios determined using immunoblot agreed with the fluorescent technique and showed a decrease in the G/F-actin ratio with increasing stiffness (Figure 4.2A, $p<0.001$). There were consistently smaller G/F-actin ratios in ACFs compared to shams (Figure 4.2A, $p=0.027$) with the largest difference between sham and ACF occurring on 2 kPa gels. Normalizing to housekeeping proteins reveals that the stiffness-induced decrease in G/F-actin ratio in shams is primarily due to a

decrease in G-actin (Figure 4.2B). In addition, the normalized amounts of total G-actin indicate that there may be an increased reservoir of G-actin in the sham CFs compared to ACF (p=0.0069).

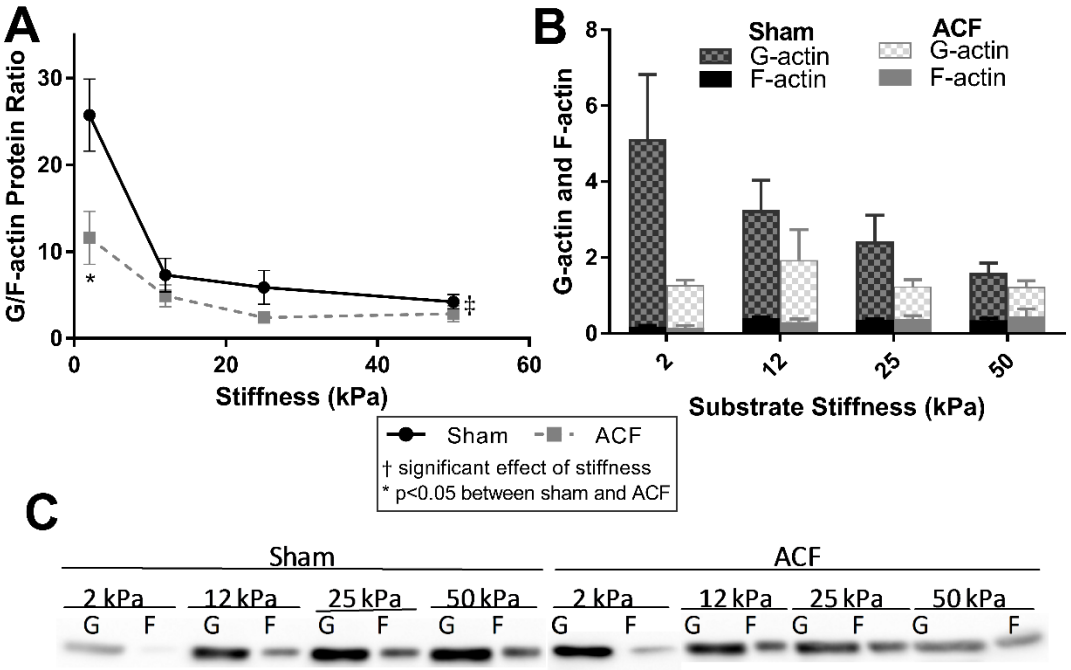

Figure 4.2: Immunoblot quantification of G-actin and F-actin
A) G/F-actin ratio decreases with increasing stiffness in both sham and ACF. B) Normalization of proteins to a housekeeping gene reveals the quantities of F-actin and G-actin. C) Sample blot of supernatant (G-actin) and pellet (F-actin) fractions. This is a non-contiguous blot but all fractions from the same samples are on the same blot.

4.3.2) αSMA is decreased in ACF CFs and on lower stiffness. The amounts of αSMA fluorescence increased similar amounts with stiffness in both sham and ACF CFs (e.g. 64% for sham, p=0.0051, and 65% for ACF CFs, p=0.022, between 2 and 25 kPa)

(Figure 4.3AB). There were no myofibroblasts, as defined by cells with αSMA positive stress fibers in any condition. However, there were proto-myofibroblasts, with increasing F-actin stress fibers with increased stiffness. The effect of stiffness on αSMA fluorescence plateaued at 25 kPa for both sham and ACF CFs. While the difference between sham and ACF did not reach significance using the fluorescent measurements ($p=0.085$) there was a significant 41-65% decrease in ACF mRNA expression of αSMA (Figure 4.3C) compared to sham CFs ($p=0.049$).

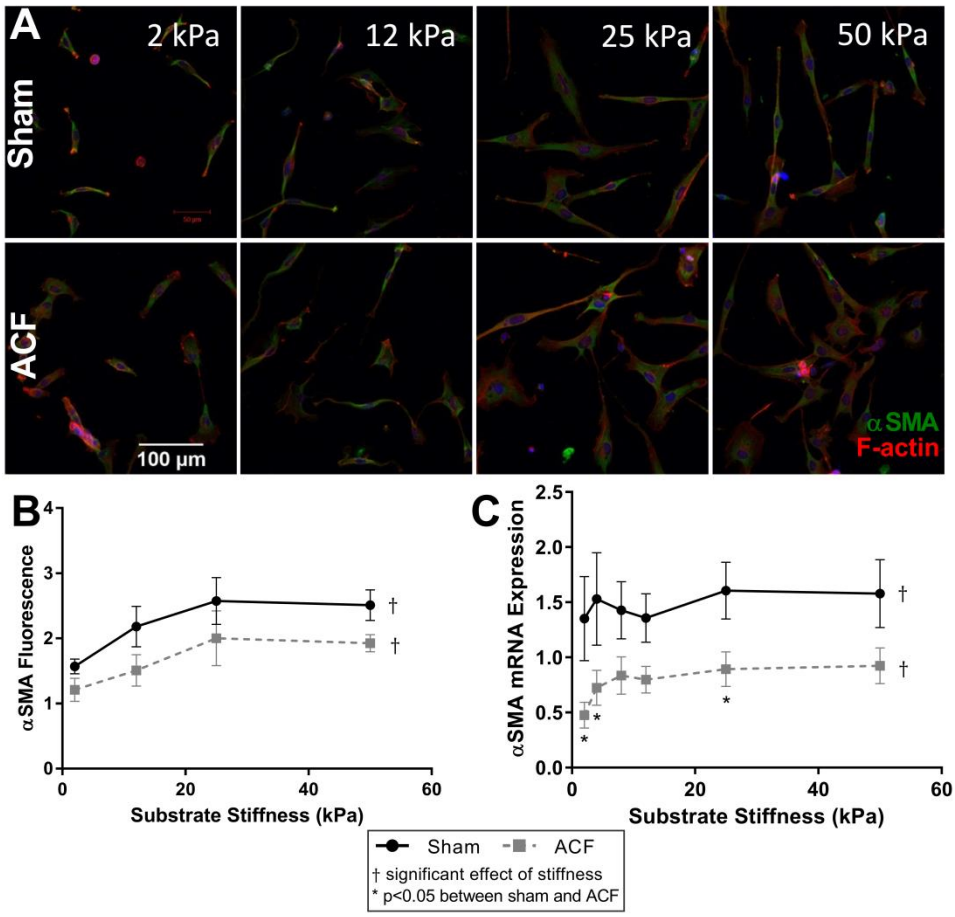

Figure 4.3: αSMA increases with increasting stiffness.
αSMA increases with increasing stiffness in both sham and ACF CFs. However, overall ACF CFs have less αSMA compared to sham CFs.

4.3.3) MRTF-A translocates to the nucleus on higher stiffness. Increasing stiffness causes an increase in translocation of MRTF-A to the nucleus as measured by mean fluorescence of MRTF-A staining in both sham and ACF CFs ($p<0.001$) (Figure 4.4B). There was a larger increase in nuclear MRTF-A fluorescence in sham compared to a more modest increase in ACF (112% increase between 2 kPa and 25 kPa for sham,

$p<0.001$; 36% increase observed in ACF CF, $p=0.0044$). The differences at stiffness values were not statistically different between sham and ACF ($p=0.25$) but the interaction effect, i.e. the observation that sham CFs are more responsive to stiffness, was significant ($p=0.0042$). Since MRTF-A promotes αSMA expression by binding to the SRF promoter region in the nucleus [78], we looked at the relationship between the amount of MRTF-A fluorescence in the nucleus and total αSMA fluorescence and (Figure 4.3C). For CF from both ACF and sham rats, total αSMA levels increased approximately linearly with increasing nuclear MRTF-A levels.

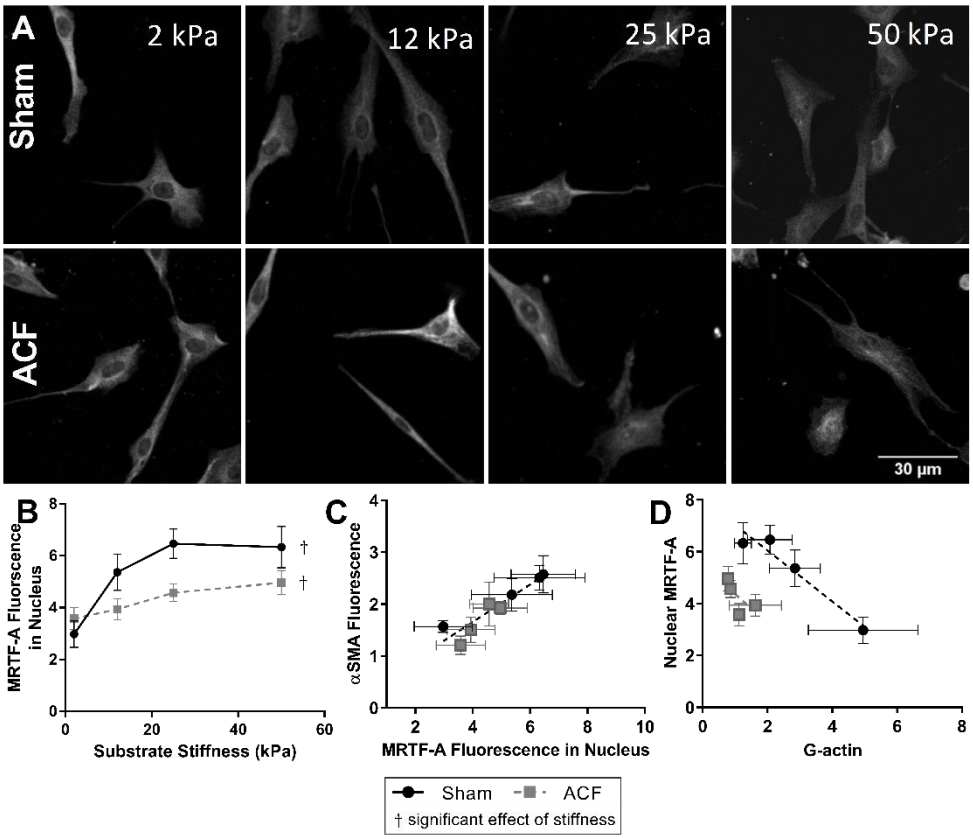

Figure 4.4: MRTF-A nuclear localization is increased with increasing stiffness. A)MRTF-A staining on a range of stiffness. B) Nuclear localization of MRTF-A increases with increasing stiffness in both sham and ACF CFs, however there is a larger increase in sham CFs. Nuclear localization of MRTF-A has a linear relationship with αSMA amounts.

4.3.4) YAP localizes to the nucleus more so in sham CFs than ACF CFs on stiff substrates. Overall, there was a higher amount of YAP fluorescence in the nucleus of sham CFs compared to ACF (37-52% increase compared to ACF, $p=0.022$) (Figure 4.5A). Increasing stiffness increased the amount of nuclear YAP in sham (a 45% increase in YAP nuclear fluorescence from 2 kPa to 25 kPa, $p<0.001$). However, increased

stiffness did not significantly increase the amount of YAP nuclear localization in ACF (Figure 4.5AB).

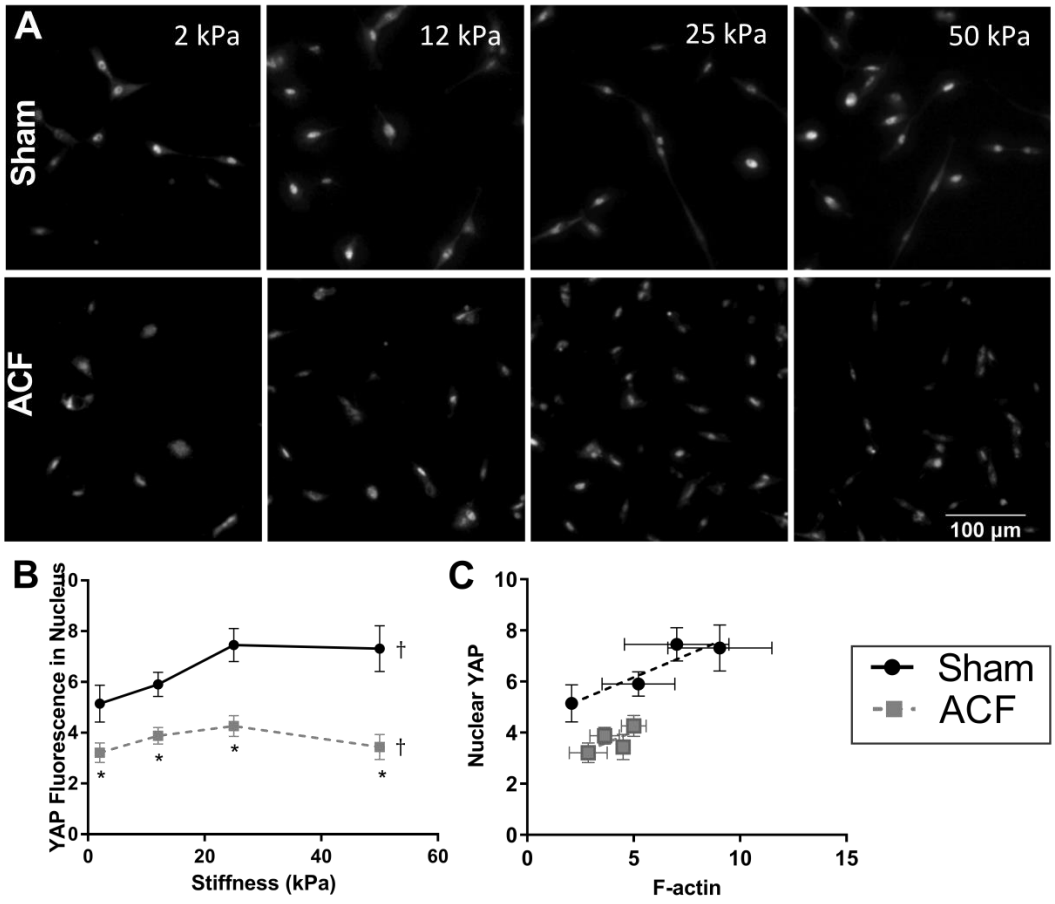

Figure 4.5: YAP nuclear localization increases in sham CFs with stiffness but not ACF.

Nuclear YAP activation directly regulates both CTGF, a profibrotic molecule, and transgelin, an actin bundling protein [121,122]. YAP binds to TEAD and promotes CTGF expression [121]. Overall CTGF expression was lower in ACF CFs compared to sham

($p<0.001$) (Figure 4.6A). Increasing stiffness from 2 kPa to 50 kPa caused a 132% increase in CTGF in sham CFs ($p<0.001$). The effect of stiffness on CTGF expression leveled off around 8 kPa for ACF CFs with an 128% increase between 2 and 50 kPa ($p=0.035$). Since YAP directly affects CTGF expression, the relationship between YAP fluorescence in the nucleus vs CTGF mRNA expression is illustrated in Figure 4.6C. CTGF expression increases approximately linearly with increasing nuclear YAP. ACF points have lower CTGF expression and correlating lower YAP in the nucleus whereas the sham points tend to have higher CTGF expression with correlating higher amounts of YAP in the nucleus.

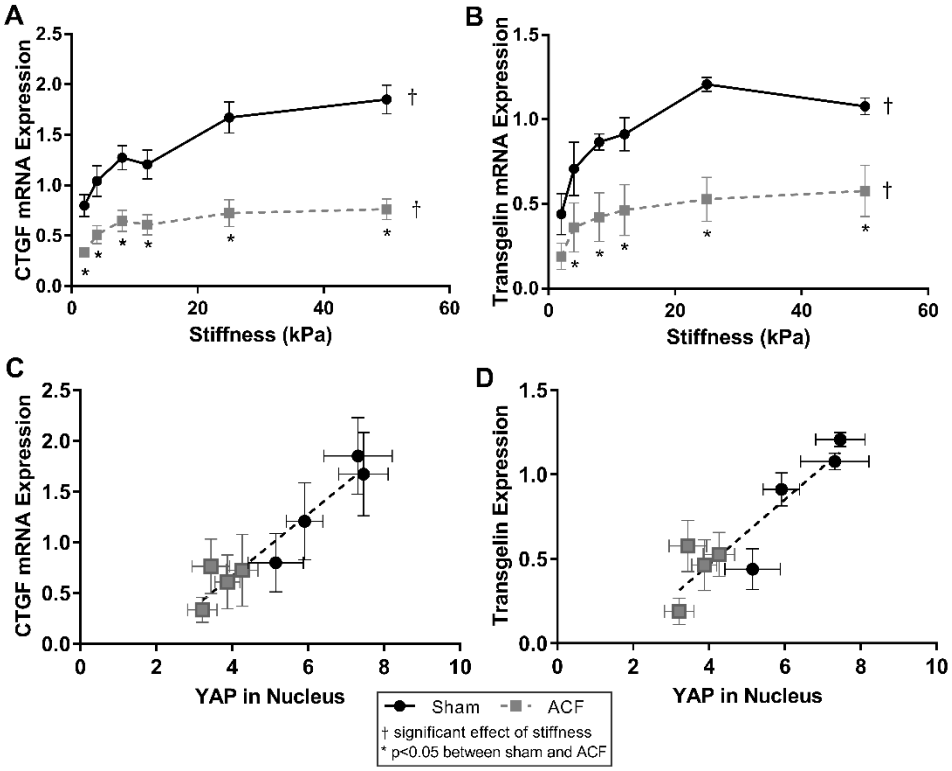

Figure 4.6: Relationship of nuclear YAP with CTGF and transgelin expression.
ACF CFs have less CTGF (A) and transgelin (B) compared to sham CFs on all stiffness levels. The expression levels of both CTGF (C) and transgelin (D) have an approximately linear relationship with nuclear YAP amounts.

A similar pattern as CTGF is observed in transgelin expression between sham and ACF on different stiffness levels. Transgelin's regulation is also dependent on YAP activation [122,123]. For all stiffness values, ACF's transgelin expression was ~50% lower than transgelin expression in sham CFs (Figure 4.6B). Transgelin increased expression in both sham and ACF CFs with increasing stiffness (145% increase in sham and 205% in ACF between 2 and 50 kPa) (Figure 4.6B). There is an approximately linear relationship between the amount of YAP fluorescence in the nucleus relative to transgelin mRNA

expression (Figure 4.6D). This shows that the decreased transgelin expression is related to decreased levels of nuclear YAP.

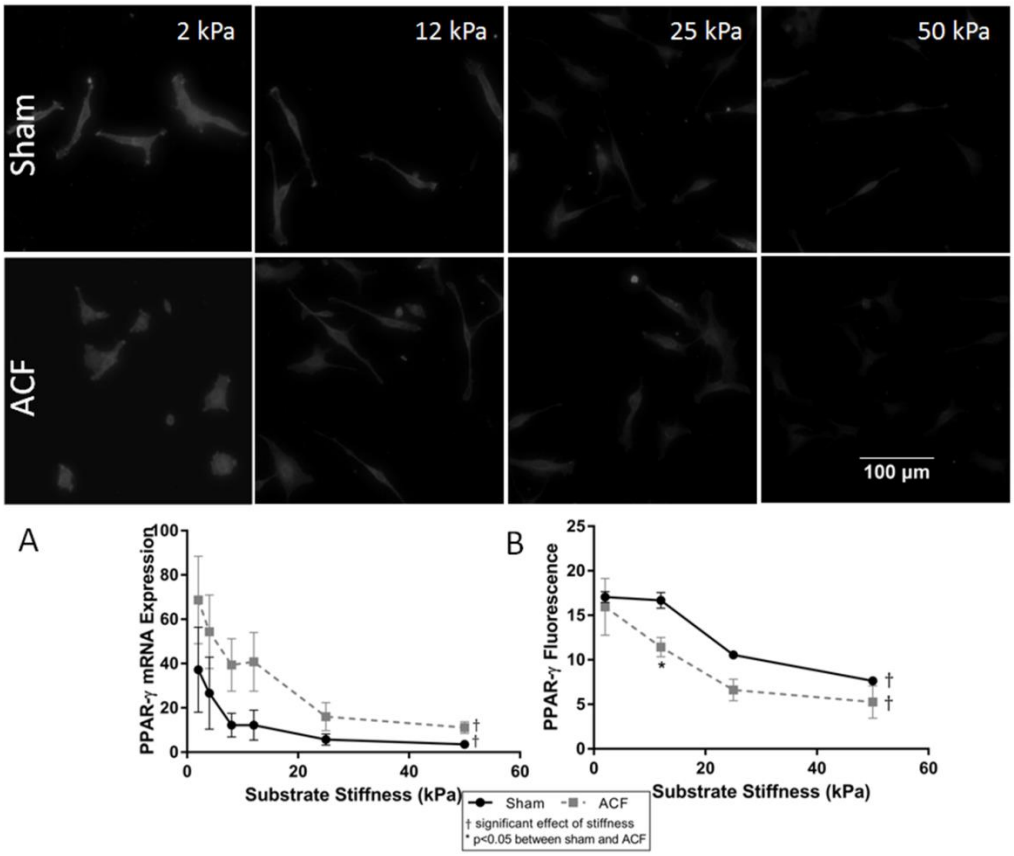

Figure 4.7: PPAR-γ expression decreases with increasing stiffness.
PPAR-γ has the highest fluorescence staining (B) and mRNA expression (A) on the softest gels.

4.3.5) PPAR-γ expression decreases with increased stiffness. The expression of peroxisome proliferator-activated receptor gamma (PPAR-γ), an inhibitor of the TGF-β pathway [124,125], has previously been shown to be influenced by stiffness [1,126] so we looked

at it here. PPAR-γ expression decreases with increasing stiffness in both sham and ACF as measured by mRNA expression (Figure 4.7A) and fluorescent staining of PPAR-γ (Figure 4.7B). In sham CFs there is a 91% decrease in PPAR-γ mRNA ($p=0.0074$) and a 55% decrease in PPAR-γ fluorescence ($p<0.001$) between 2 kPa and 50 kPa gels. In ACF CFs there is an 84% decrease in PPAR-γ mRNA ($p<0.001$) and a 67% decrease in PPAR-γ fluorescence ($p<0.001$) between 2 kPa and 50 kPa gels. There is not a significant difference at most levels of stiffness between sham and ACF CFs in fluorescence and there is not any statistical difference between sham and ACF PPAR-y mRNA expression at any stiffness ($p=0.11$).

4.3.6) Soft stiffness promotes hypofibrotic phenotype. To better characterize the fibrotic potential of the sham and ACF CFs on a range of stiffness, α-1 type I collagen (col1α1) and MMP-13 mRNA targets were measured. Overall col1α1 expression peaks around 12 kPa for both sham and ACF CFs (Figure 4.7A). The expression of col1α1 was ~30% lower in ACF CFs on soft 2 and 8 kPa gels ($p=0.029$ and $p=0.046$, respectively) compared to sham. MMP13 expression had an inverse relationship with stiffness in both sham and ACF CFs (Figure 4.7C). The expression of MMP13 decreased 90% for sham and 84% for ACF CFs between 2 and 50 kPa ($p=0.0011$ and $p=0.0072$, respectively). However, there was no significant difference between sham and ACF expression of MMP13 ($p=0.75$).

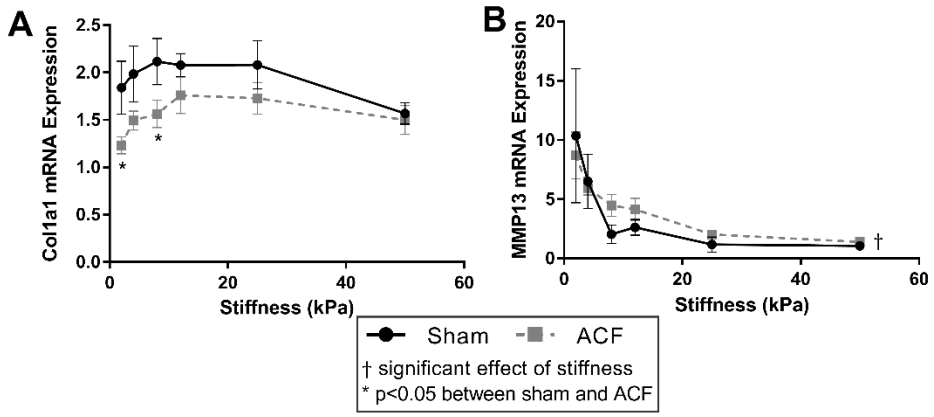

Figure 4.8: Fibrotic potential is decreased on soft substrates.
Overall ACF CFs have lower Col1α1 expression relative to sham (A). The highest MMP-13 expression is on soft gels.

4.4) Discussion

Here we present data that suggests the importance of substrate stiffness on CF phenotype with increased stiffness promoting cytoskeletal protein production, nuclear translocation of transcriptional activators and decreased expression of transcriptional repressors in normal CFs. In addition, CFs from ACF appear to have a dampened response to stiffness compared to sham CFs. Overall, the data suggests the cytoskeleton and mechanotransduction of stiffness to transcriptional factors may account for some aspects of the hypo-fibrotic phenotype of ACFs which come from a softer tissue environment in vivo.

A more hypo-fibrotic phenotype is present in sham CFs on softer gels compared to sham CFs on more stiff gels. On soft gels, sham CFs have a less contractile and less polymerized cytoskeleton evident by a higher G/F-actin ratio (Figure 4.1-2), decreased αSMA (Figure 4.3), and less transgelin (Figure 4.6B). Additionally, on soft gels sham

CFs have a profile of transcriptional factors that would discourage a more profibrotic phenotype. For instance, on the softer gels sham CFs have less MRTF-A and YAP in the nucleus (Figure 4.4 and Figure 4.5, respectively), which means a decrease in transcriptional activators of fibrogenic programs, and increased PPAR-γ (Figure 4.6), a transcriptional repressor of TGF-β. Finally, some of the hallmark targets used to describe CF phenotype indicate that the sham CFs on soft gels are on the hypo-fibrotic side of the spectrum as indicated by decreased CTGF (Figure 4.6A) and increased MMP13 expression (Figure 4.8B). This data together suggests that the decreased stiffness can move normal CFs in the direction of a hypo-fibrotic phenotype such as that of the CFs taken from VO.

Overall, ACF CFs tend to display a more hypofibrotic phenotype compared to sham CFs on the same stiffness. ACFs have less αSMA and CTGF mRNA expression on all stiffness levels (Figure 4.3C and Figure 4.6A). There is a decreased amount of YAP nuclear localization in ACF CFs on all stiffness levels (Figure 4.5B), indicating lower YAP activation. In addition to the decreased αSMA mentioned previously, there is lower transgelin mRNA expression and a decreased reservoir of G-actin, indicating ACFs have a less organized and less contractile cytoskeleton compared to shams. This profile of lower profibrotic molecules and disorganized cytoskeleton is quite opposite of the phenotype for myofibroblasts. Even on the 50 kPa gels, ACFs have less nuclear YAP, less CTGF expression, and similar amounts of transgelin expression as sham CFs on 2 kPa gels. Taken together, this data implies that ACFs retain elements of a hypofibrotic phenotype in culture even on higher stiffness.

In a process called mechanical memory, cells cultured for extended time on substrates of various stiffness are ingrained with aspects of the phenotypic changes brought on by that substrate stiffness even after the cells are moved to a new substrate with a different stiffness. One example of this is that YAP activation of MSCs plated on a stiff substrate and then plated on a softer substrate is dependent on the amount of time spent on the original stiff substrate [1]. A similar phenomena was also observed in lung fibroblasts cultured on soft substrates for 3 weeks displayed a dampened myofibroblast activation when plated on stiff substrates [2]. Our observation that ACF CFs have a hypo-fibrotic phenotype, even when grown on stiff substrates, suggests that these primary CFs retain aspects of their soft in vivo phenotype in culture. Since CFs isolated from ACF are coming from an environment with approximately half the tissue modulus of control hearts (Chapter 3), they are mechanically primed from a soft environment. Taking into account that CFs in soft environments display a more hypofibrotic phenotype, this mechanical memory from the soft environment could explain why ACF CFs are more hypofibrotic compared to sham CFs which come from a more stiff environment.

We are not the first to look at the effect of substrate stiffness on fibroblasts phenotype [40,57,118,119,127,128], but there is only limited data looking at the effect of stiffness on fibroblasts from the heart [30,37–39], and, to our knowledge, there are no reports of non-passaged adult CF's response to substrate stiffness. The effect of passaging in culture on fibroblasts to create a more myofibroblast phenotype is well known [2,21]. Relative to cells in vivo, cell cultures are exposed to altered chemical (e.g. much higher oxygen tension known to promote myofibroblast activation [19,20]), and biochemical environments (e.g.,

exposure to elevated PDGF and TGF-β). In addition, cultured cells are exposed to an altered mechanical environment with the prolonged culture on extremely stiff polystyrene, particularly relevant for studies of cellular responses to stiffness in light of the mechanical memory concept. Passaged lung fibroblasts activate into myofibroblasts around 20 kPa or higher [2,49] and display a low G/F-actin ratio (~1 in lung fibroblasts on 20 kPa gels compared to 2.4-5.9 ratio in CFs on 25 kPa gels here) [49]. Even on the 50 kPa gels, our CFs do not activate to myofibroblasts during ~ 1 week of culture. A transition of fibroblasts towards a myofibroblast phenotype would be a significant issue in our study since we are primarily interested in understanding the behavior of CFs from VO hearts where myofibroblasts are not present, and where the CFs are expressing a hypofibrotic phenotype, which is in contrast to the profibrotic phenotype exhibited by myofibroblasts.

One limitation of this study is the two-dimensional (2D) cell culture systems used. 2D polyacrylamide gels are unlike the three-dimensional (3D) environment in which cells naturally reside. There is growing appreciation for effect on phenotype of culture environments that are more like the native environment consisting of a 3D environment of appropriate stiffness and fibrous architecture [129]. However, 2D cell culture systems, like polyacrylamide gels, are used for simplicity, convenience, and compatibility with a wide range of analytical techniques. Future studies could make use of a more faithful replication of the in vivo environment by using a 3D culture system, with a fibrous architecture, and dynamic strain application.

These results point to the role stiffness plays in modulating CF phenotype. Here we show that normal CFs behave more like a hypofibrotic CFs on soft substrates and that

CFs from ACF have a dampened response to stiffness when compared to sham CFs. Our observations that ACF's have approximately half the tissue modulus as shams (Chapter 3), a more hypofibrotic phenotype results from exposure to decreased substrate modulus in CFs, and that CFs isolated from ACF have a more hypofibrotic phenotype compared to sham CFs (Chapter 2) suggests the reduced stiffness in ACF hearts may cause CFs to adopt a hypofibrotic phenotype. In addition, our previous observations that ACFs are primed in an environment with decreased tissue modulus (Chapter 3) yet retain a hypofibrotic phenotype even in culture on stiff plastic (Chapter 2) coupled with our observations here that ACF CFs have a dampened response to stiffness compared to sham CFs is consistent with the notion of mechanical memory.

Chapter 5 : Discussion and Future Directions

5.1) Summary of major findings.

Results from these studies indicate that the net loss of ECM in VO HF is likely due to a hypofibrotic phenotype in CFs. CFs isolated from ACF-induced HF produced considerably less profibrotic markers such as collagen type-I, αSMA, and CTGF compared to sham CFs, despite increased TGF-β secretions (Chapter 1). An initial investigation into whether there was some dysfunction in the canonical TGF-β pathway did not explain the phenotypic differences between sham and ACF fibroblasts. Normal TGF-β induced Smad2/3 phosphorylation and translocation to the nucleus were present and there were no indications of TGF-β receptor loss.

We turned our focus to the cytoskeleton since it is another known mechanism of fibroblast phenotype control outside of the canonical TGF-β pathway. Proteomics data indicated differences between sham and ACF CFs in several cytoskeletal related proteins. Overall ACF CFs have less cytoskeletal actin including significantly less F-actin, and G-actin. Additionally, ACF had overall less expression of cytoskeletal proteins αSMA and transgelin.

We hypothesized that these differences in the cytoskeleton could account for the hypofibrotic phenotype observed in ACF CFs. To test this hypothesis, we used a ROCK inhibitor to test whether allowing depolymerization of F-actin would make sham CFs

behave more like ACF which have relatively less F-actin. Addition of a ROCK inhibitor to sham CFs shifted the phenotype in the direction of a hypofibrotic phenotype. ROCK inhibitor treatment decreased αSMA and CTGF expression and increased MMP13 expression. Conversely, we tested whether enhancing F-actin with jasplakinolide in ACF CFs could make them behave more like sham CFs which have relatively increased F-actin amounts. Japslakinolide treatment caused an increase is profibrotic markers collagen type-I secretion, αSMA, and CTGF. Taken together we have presented evidence that alterations in the actin cytoskeleton can control CF phenotype.

Due to the known effect of substrate modulus on cytoskeletal organization and growing evidence pointing to the role of stiffness in controlling fibroblast phenotype we characterized the changes in chamber stiffness and myocardial tissue modulus in Chapter 3. Biaxial tensile testing revealed that tissue from ACF has approximately half the modulus as tissue from sham hearts.

The results in Chapter 4 point to the role stiffness plays in modulating CF phenotype. We show that normal CFs behave more like hypofibrotic CFs on soft substrates resulting in a higher G/F-actin ratio, decreased αSMA, transgelin, and CTGF. We also show that CFs from ACF have a dampened response to stiffness compared to sham CFs as indicated by a smaller increase in αSMA, CTGF, and transgelin compared to the larger increase in sham CFs.

Our observations that CFs isolated from ACF have a more hypofibrotic phenotype compared to sham CFs (Chapter 2), that ACF tissue is approximately half the tissue modulus as shams (Chapter 3), and that CFs have a more hypofibrotic phenotype when

exposed to decreased substrate modulus (Chapter 4), suggest that reduced stiffness in ACF hearts may cause CFs to adopt a hypofibrotic phenotype. In addition, our previous observations that ACFs are primed in an environment with decreased tissue modulus (Chapter 3) yet retain a hypofibrotic phenotype even in culture on stiff plastic (Chapter 2) coupled with our observations here that ACF CFs have a dampened response to stiffness with reduced levels of nuclear YAP and MRTF-a is consistent with the idea of mechanical memory.

5.2) Alternative interpretations and limitations.

5.2.1) Importance of cytoskeletal status on CF phenotype. There should be further exploration into which aspects of the cytoskeletal status are most important to the hypofibrotic phenotype. It is still not clear what the most important factors are: overall actin amounts, F-actin amounts, G-actin amounts, or the ratio of G/F-actin. The proteomics data indicates that there are differences between several actin treadmilling and regulatory proteins in ACF CFs relative to sham CFs (Table 2.2). Many proteins with higher spectral hits in ACF CFs promote depolymerization of F-actin into G-actin, which is vulnerable to degradation[130]. It is possible that ACF CFs have higher degradation rates of G-actin compared to sham CFs. This is in part supported by the fact that there are lower levels of G-actin compared to sham CFs (Figure 2.5C and Figure 4.2B).

Since G-actin sequesters MRTF-A in the cytosol, G-actin is important to the regulation of MRTF-A. However, in ACF CFs, where there is less G-actin (Figure 2.5C and Figure 4.2B), it may not have as much of an effect on the control of MRTF-A localization. This may explain the dampened response to stiffness of nuclear MRTF-A in

ACF CFs (Figure 4.4). If there is less G-actin to sequester MRTF-A in the cytosol, then MRTF-A nuclear localization may be less regulated by G-actin, and possibly more dependent on passive diffusion throughout the cell. Whereas, in sham CFs, where there is a more drastic decrease of G-actin with stiffness (Figure 4.2B), MRTF-A could be more closely regulated by G-actin.

5.2.2) Interpretations and limitations of pharmacological manipulations of the cytoskeleton. Although treatment with Jas and Y-27632 are known to alter the cytoskeleton [49,50], off target effects are likely. Using a variety of treatments to achieve similar changes in the actin cytoskeleton to confirm consistent results could help with this limitation. Alternative treatments to test the effect of the cytoskeleton on phenotype include: 1) Cytochalasin D, which is known to inhibit actin polymerization by binding to the growing ends of F-actin filaments, and 2) Latrunculin B, which sequesters G-actin monomers preventing polymerization into F-actin. Not only would these additional treatments help to confirm the importance of the cytoskeleton on phenotype, but it may help pinpoint which factors in cytoskeleton status are important. For example, it is still unclear whether the hypofibrotic phenotype is due to a decrease in overall actin, decrease in F-actin or G-actin alone, or a change in the G/F-actin ratio. Since these drugs act by different mechanisms it could help us pinpoint what aspects of the cytoskeletal status are most important to phenotype. For instance, Cytochalasin D is shown to increase the G/F-actin ratio by increasing the relative amount of G-actin but not changing the amounts of F-actin in mesenchymal cells.[131] Conversely, Latrunculin B is shown to increase G-actin with a concomitant decrease in F-actin [132].

Due to the hypofibrotic phenotype induced by ROCK inhibitor treatment, we can conclude that either the Rho/ROCK pathway or the actin cytoskeleton play a role in creating a hypofibrotic phenotype. To help distinguish whether the hypofibrotic phenotype is due to the Rho/ROCK pathway or due to changes in the cytoskeleton, we could use a RhoA mutant to either overexpress or underexpress RhoA. If we were able to combine a dominant-negative RhoA mutant, which would disrupt the Rho/ROCK pathway, with another treatment that enhanced actin polymerization, such as Jas, it could tell us if the phenotype was due to actin changes rather than the Rho/ROCK pathway. Conversely, we could treat cells overexpressing RhoA with a drug to decrease actin polymerization such as Cytochalasin D or Latrunculin. These experiments would clarify whether the changes were due to the actin cytoskeleton status or due to the Rho/ROCK pathway.

5.2.3) Limitations of aortocaval fistula model. Although the ACF model is the most widely used model of VO it still has several limitations. One major criticism of the ACF models is that it is a biventricular overload, meaning there is increased volume in both the left and right sides of the heart. This is unlike many of the common causes of VO in humans, such as mitral and aortic regurgitation, which result in univentricular overload [133]. Alternative models of valve regurgitations are well established in large animals such as dogs [18], and more recently have been made in rodents as well[134]. These models consist of holes or tears within the valve and replicate VO hemodynamics caused by valve insufficiency in humans.

Another limitation of the ACF model, which is a limitation of many animal models, is the time progression of the disease. In the ACF model, hemodynamics instantly changes after surgery. There is an acute drop in peripheral resistance accompanied by a slight increase in heart rate and cardiac output [135]. Heart failure may occur within a time span of several weeks in the ACF model [17]. However, in humans, valve function declines slowly leading to gradual changes in hemodynamics [136]. In humans, volume overload-induced heart failure progresses over a time span in years rather than weeks.

5.2.4) Confirmation of hypothesized transcriptional regulation mechanisms. We showed that PPAR-γ may play a role in the hypofibrotic phenotype because it is an inhibitor of TGF-β –induced fibrosis and is highly expressed in CFs on very soft substrates. Due to the soft tissue modulus of VO LVs, we speculated that PPAR-γ may be a contributing factor to the hypofibrotic phenotype in CFs isolated from ACF. We have not determined if PPAR-γ is in fact different between ACF and sham in vivo. In order to identify whether PPAR-γ is responsible, we would first need to confirm that there is increased expression of PPAR-γ in vivo in the ACF model relative to sham tissue. This could be confirmed with a western blot or immunohistochemistry on LV tissue. In addition, we could alter the expression of PPAR-γ with siRNA to confirm the role of PPAR-γ in the hypofibrotic phenotype. We would hypothesize that downregulation of PPAR-γ would rescue the ACF phenotype and would have a less hypofibrotic phenotype.

5.3) Future directions.

5.3.1) Investigate myocardial tissue modulus and CF phenotype at multiple time points to better understand progression of HF. A better understanding of the progression of HF could optimize timing of pharmacological and surgical interventions. Lucchesi and coworkers have characterized remodeling and functional changes during ACF induced VO which correlate to the clinical progression of VO HF in humans [10,17,60]. VO HF is described with three phases: acute, compensated which has preserved ejection fraction, and decompensated resulting in pump failure and pulmonary congestion [17]. Remodeling and function vary during these three phases. In the acute stage preload is increased and there is mild dilation [60]. In the compensated stage, there is further dilation, increased compliance, and ECM turnover resulting in net degradation [17]. Decompensated failure results in systolic and diastolic dysfunction and eventually leads to pump failure. During the last stage of heart failure ECM continues to turnover but there is net positive deposition of ECM [17]. The CFs studies done here are from ACFs during the compensated phase of VO because this period of the disease is thought to be highly influenced by the effect of CFs due to drastic changes in ECM. Since the studies presented here are only done in CFs from ~4 weeks post ACF, we are only able to see a snapshot of the phenotype. Experiments to characterize the phenotype throughout the whole progression of the disease could shed light on to which factors are important for influencing CF phenotype at each stage of the disease. If we are able to measure tissue modulus and characterize CF phenotype throughout each stage, we may be able to better understand the relationship between stiffness and CF behavior.

One major strength of the ACF model is that it can be reversed (i.e. the shunt can be closed, changing the hemodynamic load on the heart). ACF reversal is representative of surgical intervention of VO HF. Reversal of the shunt at 4 weeks post ACF allows the heart to rapidly revert back to normal chamber morphology with chamber dimensions and wall thickness similar to sham animals [137]. Surgical intervention is primarily a reduction in hemodynamic load. It would be interesting to see if reduction of hemodynamic load and reversion back to normal morphology also returns myocardial tissue modulus to normal levels. In addition, characterization of the CF phenotype after reversal could lead to insights into the effect of hemodynamic load on CFs and the role of CFs in the heart.

5.3.2) Use magenetic resonance elastography to track changes in VO modulus throughout disease progression. Magnetic resonance elastography (MRE) is a developing technique to measure mechanical properties of soft tissues within the body. Cyclic motions are applied to a tissue while MRI images are taken, providing information about wave propagations through the tissue. These wave propagations can then be analyzed to provide stiffness maps of the tissue. Recently, MRE has been used to assess changes in modulus in a porcine model of heart failure [138]. A major benefit over the mechanical analyses done here is that MRE is noninvasive. This makes it much more agreeable clinically and also makes it more suitable for multiple measurements to track progression throughout the disease. Biaxial testing requires removal of a piece of tissue and can only be done once in rats. PV loops can be done several times in humans but this is not advisable due to the risks associated with the process. In rats PV loops are traumatic enough that it is only done before sacrifice. MRE could be performed as many times as is

practical which would allow for tracking of stiffness changes throughout disease progression. ECM degradation is reported to begin within 1 or 2 days after ACF surgery [17,60]. MRE would allow tracking of stiffness changes directly before and after ACF surgery and answer when stiffness changes occur. Being able to use the same measurement technique in animals and humans is useful because the information learned from animal studies could then be related to clinical data to get the most use from animal studies.

5.3.3) Use histological analysis to characterize CFs in situ. One major limitation of these CF studies is that the cells are in culture which is an environment known to alter CF phenotype. We did these studies on non-passaged cells to limit the effect of culture on phenotype. One step further would be to assess CF phenotype in situ using histological analysis. Histochemistry could be used to corroborate the phenotype of isolated CFs in vitro with the characterization of CFs phenotype in vivo. If we are able to observe differences in the tissue that are similar to the differences we observe in vitro, we can confirm that these are not artifacts of culture. For instance, we could look at YAP and MRTF-A localization in the tissue to see if there are differences in nuclear amounts between sham and ACF.

5.3.4) Characterize adhesion and integrin expression of ACF and sham CFs. Cellular adhesion has a profound impact on cell behavior. Adhesion affects cell locomotion, cytoskeletal organization, cell contraction, and the cell's ability to sense substrate stiffness [65,127,139]. Upregulation of focal adhesion proteins is associated with myofibroblasts [21]. The size of focal adhesions has been related to the cells ability to

create high internal tension and recruit αSMA to stress fibers enhancing their contractility [118]. In addition, there is interplay between substrate stiffness and cell adhesion. On soft substrates adhesions tend to be more diffuse and dynamic while on stiff substrates stable focal adhesions form with increased expression of integrins [82,119,127]. ACF CFs come from tissue that has half the modulus as sham, and since substrate modulus affects adhesions, and adhesions affect CF phenotype this may be one contributing factor for the hypofibrotic phenotype. One could test whether adhesion differs from sham and ACF by using a centrifugation assay to measure adhesion [140]. In addition, one could investigate whether there are differences in known focal adhesions markers such as vinculin, paxillin, and talin.

Not only are integrins essential to adhesion and cell matrix interactions but they also play an important role in cell phenotype control. Integrins are mechanically sensitive elements that transduce signals through the cell. They signal through focal adhesion kinase, small GTPases such as Rho, and regulation of the cytoskeleton components such as talin [141]. Expression of α2β1 integrin is associated with fine cytoskeletal filaments and minimal cytoskeletal tension [35]. Whereas, fibroblasts with increased cytoskeletal tensions replace α2β1 integrins with αvβ3 integrins and develop stress fibers with αSMA [35]. The types and amounts of integrin expression can also affect TGF-β expression, activation (described in more detail below), and TGF-β receptor expression [41,42,141]. Characterization of the types and relative amounts of integrins on ACF CFs could help identify whether they play a role in the CF phenotype of VO HF.

5.3.5) Test whether ACF hypofibrotic phenotype is due to decreased activated TGF-β. Although we observed that there is nearly twice as much TGF-β in ACF compared to sham (Chapter 2), ACF CFs still behave in a hypofibrotic manner. It is possible that although there is an increased amount of TGF-β, it could remain in a latent form and therefore there may not be an increased amount of active TGF-β. TGF-β is secreted as an inactive complex bound to latency-associated pro-peptide and anchored to the ECM via the latent TGF-β-binding protein [42]. Integrins αvβ5 and αvβ3 attach to latent TGF-β complex and enable the cell to pull against the ECM in order to free and activate TGF-β [41,42]. In addition, it has been shown that there is less TGF-β activation on compliant substrates compared to more stiff substrates [43]. Taking into account that ACF hearts have approximately half the tissue modulus as sham hearts, this increase in tissue compliance could hinder the activation of latent TGF-β. Assays to measure the amount of active vs. latent TGF-β are not commercially available; however Hinz et al. have used transformed mink lung reporter cells (TMLCs) that produce luciferase as a function of active TGF-β [43]. TMLCs could be used in co-cultures with either sham or ACF CFs to allow detection of differences in TGF-β activation. This assay could also be performed with sham and ACF CFs on substrates of different stiffness to assess whether the ability of CFs to activate TGF-β is stiffness dependent.

In addition to measuring the relative amounts of active TGF-β, differences in the amount of αvβ5 and αvβ3 integrins present in sham vs. ACF CFs could shed light on the ability of ACF CFs to activate TGF-β. Previously, Hinz et al. have shown that integrins αvβ5 and αvβ3 facilitate the activation of TGF-β by human CF contraction [41]. If there are

significantly less amounts of αvβ5 and αvβ3 integrins on ACF CFs compared to sham CFs this could suggest a decreased ability of ACF CFs to attach to the latency-associated pro-peptide which could impede their ability to activate TGF-β.

5.3.6) Investigate the effect of strain and stiffness in a three dimensional in vitro system to better mimic the in vivo environment. The mechanical environment of CFs is much more complex than 2D culture systems; it has passive (stiffness) and active (strain) mechanical cues in a 3D environment. There is evidence that dimensionality [142], stiffness [38,39], and strain [143–145] all affect fibroblast phenotype individually. The effects of stiffness and cyclic strain in a 3D environment have yet to be determined.

Culture in 2D and 3D systems differentially affect cell function and phenotype [126,142,146]. Given that cell-matrix interactions heavily influence intracellular tension and that there are major differences in fibroblast behavior as a result of different cell-matrix adhesions in 2D vs 3D matrices [139], it is important to perform cells studies in 3D. Previous studies of fibroblasts and stiffness in 3D have explored the effects of apparent stiffness (caused by differences in constrained and free gels) rather than the modulus (an intrinsic property) of the material [36,147]. However, these stiffness changes are not easily quantified or translatable to physiological stiffness changes. Other 3D stiffness studies alter stiffness by changing the concentration of ECM protein, but this changes other variables such as binding site density, pore size, and fiber diameter. Self-assembling peptide hydrogels are a tool that can be used to combine the effects of stiffness and dimensionality without major alteration in pore size and fiber dimension [126,148].

The effect of strain on CF phenotype is not clear; however, in general it appears that strain causes a decrease in a profibrotic phenotype. Application of static strain to 3DTC nylon mesh scaffolds allowed myofibroblasts to revert back to a quiescent fibroblast phenotype [149]. However, static strain applied to neonatal rat CFs via collagen-coated magnetite beads increased αSMA when cells were cultured to express low αSMA levels, but αSMA was reduced when cells were initially coerced into a myofibroblast phenotype [150]. Moreover, static strain is not representative of the in vivo mechanics, because the heart contracts and relaxes, causing cyclic rather than static strain on the cells. Cyclic strain of neonatal rat CFs caused decreased αSMA [143]. Consistent with a deactivation of myofibroblast phenotype, cyclic strain in the presence of serum decreased collagen production [151]. The increase in preload ACF hearts could play a role in the hypofibrotic phenotype and this could be investigated with cyclic strain studies that alter the magnitude of strain with alterations in stiffness to represent either the ACF heart or normal hearts.

References

1. Yang C, Tibbitt MW, Basta L, Anseth KS. Mechanical memory and dosing influence stem cell fate. *Nature materials*. 2014;13(6):645.
2. Balestrini JL, Chaudhry S, Sarrazy V, Koehler A, Hinz B. The mechanical memory of lung myofibroblasts. *Integrative Biology*. 2012;4(4):410.
3. Katz R, Karliner JS, Resnik R. Effects of a natural volume overload state (pregnancy) on left ventricular performance in normal human subjects. *Circulation*. 1978;58(3).
4. O'Keefe JH, Patil HR, Lavie CJ, Magalski A, Vogel RA, McCullough PA. Potential adverse cardiovascular effects from excessive endurance exercise. *Mayo Clinic proceedings*. 2012;87(6):587–95.
5. Yin FCP. BRIEF REVIEWS Ventricular Wall Stress. *Circulation Research OCTOBER Of flvial Journal of the American Heart Association*. 1981;49(4).
6. Lorell BH, Carabello B a. Clinical Cardiology : New Frontiers Left Ventricular Hypertrophy. 2000:470–479.
7. Peterson KL, Tsuji J, Johnson a, DiDonna J, LeWinter M. Diastolic left ventricular pressure-volume and stress-strain relations in patients with valvular aortic stenosis and left ventricular hypertrophy. *Circulation*. 1978;58(1):77–89.
8. Sasayama S. Cardiac hypertrophy as early adjustments to a chronically sustained mechanical overload. *Japanese circulation journal*. 1985;49(2):224–31.
9. Creemers EE, Pinto YM. Molecular mechanisms that control interstitial fibrosis in the pressure-overloaded heart. *Cardiovascular Research*. 2011;89(2).
10. Hutchinson KR, Guggilam A, Cismowski MJ, Galantowicz ML, West TA, Stewart JA, Zhang X, Lord KC, Lucchesi PA. Temporal pattern of left ventricular structural and functional remodeling following reversal of volume overload heart failure. *Journal of Applied Physiology*. 2011;111(6):1778–1788.
11. Van Putten S, Shafieyan Y, Hinz B. Mechanical control of cardiac myofibroblasts. 2016.
12. de Jong S, van Veen TAB, van Rijen HVM, de Bakker JMT. Fibrosis and cardiac arrhythmias. *Journal of cardiovascular pharmacology*. 2011;57(6):630–8.
13. Nadal-Ginard B, Kajstura J, Leri A, Anversa P. Myocyte Death, Growth, and

Regeneration in Cardiac Hypertrophy and Failure. *Circulation Research*. 2003;92(2).

14. Souders CA, Bowers SLK, Baudino TA. Cardiac fibroblast: The renaissance cell. *Circulation Research*. 2009;105(12):1164–1176.

15. Turner NA, Porter KE. Function and fate of myofibroblasts after myocardial infarction. *Fibrogenesis & Tissue Repair*. 2013;6(1):5.

16. Tomasek JJ, Gabbiani G, Hinz B, Chaponnier C, Brown RA. Myofibroblasts and mechano-regulation of connective tissue remodelling. *Nature Reviews. Molecular Cell Biology*. 2002;3(5):349–63.

17. Hutchinson KR, Stewart JA, Lucchesi PA. Extracellular matrix remodeling during the progression of volume overload-induced heart failure. *Journal of Molecular and Cellular Cardiology*. 2010;48(3):564–569.

18. Dell'italia LJ, Balcells E, Meng QC, Su X, Schultz D, Bishop SP, Machida N, Straeter-Knowlen IM, Hankes GH, Dillon R, Cartee RE, Oparil S. Volume-overload cardiac hypertrophy is unaffected by ACE inhibitor treatment in dogs. *The American journal of physiology*. 1997;273(2 Pt 2):H961-70.

19. Sen CK, Roy S. Oxygenation state as a driver of myofibroblast differentiation and wound contraction: hypoxia impairs wound closure. *The Journal of investigative dermatology*. 2010;130(12):2701–3.

20. Modarressi A, Pietramaggiori G, Godbout C, Vigato E, Pittet B, Hinz B. Hypoxia Impairs Skin Myofibroblast Differentiation and Function. *Journal of Investigative Dermatology*. 2010;130(12):2818–2827.

21. Santiago J-J, Dangerfield AL, Rattan SG, Bathe KL, Cunnington RH, Raizman JE, Bedosky KM, Freed DH, Kardami E, Dixon IMC. Cardiac fibroblast to myofibroblast differentiation in vivo and in vitro: Expression of focal adhesion components in neonatal and adult rat ventricular myofibroblasts. *Developmental Dynamics*. 2010;239(6):1573–1584.

22. Flanagan L a, Ju Y-E, Marg B, Osterfield M, Janmey P a. Neurite branching on deformable substrates. *Neuroreport*. 2002;13(18):2411–2415.

23. Liu F, Mih JD, Shea BS, Kho AT, Sharif AS, Tager AM, Tschumperlin DJ. Feedback amplification of fibrosis through matrix stiffening and COX-2 suppression. *Journal of Cell Biology*. 2010;190(4):693–706.

24. Ho SP, Kurylo MP, Fong TK, Lee SSJ, Wagner HD, Ryder MI, Marshall GW. The biomechanical characteristics of the bone-periodontal ligament-cementum complex. *Biomaterials*. 2010;31(25):6635–6646.

25. Ho SP, Marshall SJ, Ryder MI, Marshall GW. The tooth attachment mechanism defined by structure, chemical composition and mechanical properties of collagen fibers in the periodontium. *Biomaterials*. 2007;28(35):5238–5245.

26. Berry MF, Engler AJ, Woo YJ, Pirolli TJ, Bish LT, Jayasankar V, Morine KJ, Gardner TJ, Discher DE, Sweeney HL. Mesenchymal stem cell injection after myocardial infarction improves myocardial compliance. *American Journal of Physiology. Heart and Circulatory Physiology*. 2006;290(6):H2196-203.

27. Hiesinger W, Brukman MJ, McCormick RC, Fitzpatrick JR, Frederick JR, Yang EC, Muenzer JR, Marotta NA, Berry MF, Atluri P, Woo YJ. Myocardial tissue elastic properties determined by atomic force microscopy after stromal cell-derived factor 1α angiogenic therapy for acute myocardial infarction in a murine model. *The Journal of Thoracic and Cardiovascular Surgery*. 2012;143(4):962–6.

28. Zhang S, Sun A, Ma H, Yao K, Zhou N, Shen L, Zhang C, Zou Y, Ge J. Infarcted myocardium-like stiffness contributes to endothelial progenitor lineage commitment of bone marrow mononuclear cells. *Journal of cellular and molecular medicine*. 2011;15(10):2245–61.

29. Quinlan AMT, Billiar KL. Investigating the role of substrate stiffness in the persistence of valvular interstitial cell activation. *Journal of biomedical materials research. Part A*. 2012;100(9):2474–82.

30. Wang H, Haeger SM, Kloxin AM, Leinwand LA, Anseth KS. Redirecting valvular myofibroblasts into dormant fibroblasts through light-mediated reduction in substrate modulus. *PLoS ONE*. 2012;7(7).

31. Hinz B. Formation and Function of the Myofibroblast during Tissue Repair. *Journal of Investigative Dermatology*. 2007;127:526–537.

32. Aarabi S, Bhatt KA, Shi Y, Paterno J, Chang EI, Loh SA, Holmes JW, Longaker MT, Yee H, Gurtner GC. Mechanical load initiates hypertrophic scar formation through decreased cellular apoptosis. *FASEB journal : official publication of the Federation of American Societies for Experimental Biology*. 2007;21(12):3250–61.

33. Hinz B, Mastrangelo D, Iselin CE, Chaponnier C, Gabbiani G. Mechanical Tension Controls Granulation Tissue Contractile Activity and Myofibroblast Differentiation. 2001.

34. Arora PD, Narani N, Mcculloch CAG. The Compliance of Collagen Gels Regulates Transforming Growth Factor-␤ Induction of ␣-Smooth Muscle Actin in Fibroblasts. 1999.

35. Jones C, Ehrlich HP. Fibroblast expression of α-smooth muscle actin, α2β1 integrin and αvβ3 integrin: influence of surface rigidity. *Experimental and molecular pathology*. 2011;91(1):394–9.

36. Galie PA, Westfall M V., Stegemann JP. Reduced serum content and increased matrix stiffness promote the cardiac myofibroblast transition in 3D collagen matrices. *Cardiovascular Pathology*. 2011;20(6):325–333.

37. Xie J, Zhang Q, Zhu T, Zhang Y, Liu B, Xu J, Zhao H. Substrate stiffness-regulated matrix metalloproteinase output in myocardial cells and cardiac

fibroblasts: implications for myocardial fibrosis. *Acta Biomaterialia*. 2014;10(6):2463–72.

38. Bhana B, Iyer RK, Chen WLK, Zhao R, Sider KL, Likhitpanichkul M, Simmons CA, Radisic M. Influence of substrate stiffness on the phenotype of heart cells. *Biotechnology and Bioengineering*. 2010;105(6):1148–1160.

39. Kharaziha M, Nikkhah M, Shin S-R, Annabi N, Masoumi N, Gaharwar AK, Camci-Unal G, Khademhosseini A. PGS:Gelatin nanofibrous scaffolds with tunable mechanical and structural properties for engineering cardiac tissues. *Biomaterials*. 2013;34:6355–6366.

40. Mehta N, Chopra A, Jamney P a., Kresh JY. Transdifferentiation of Cardiac Fibroblasts To Myofibroblast Phenotype and Its Regulation By Extracellular Matrix Composition and Mechanics. *Journal of the American College of Cardiology*. 2014;63(12):A851.

41. Sarrazy V, Koehler A, Chow ML, Zimina E, Li CX, Kato H, Caldarone C a., Hinz B. Integrins αvβ5 and αvβ3 promote latent TGF-β1 activation by human cardiac fibroblast contraction. *Cardiovascular Research*. 2014;102(3):407–417.

42. Worthington JJ, Klementowicz JE, Travis MA. TGFβ: a sleeping giant awoken by integrins. *Trends in Biochemical Sciences*. 2011;36(1):47–54.

43. Wipff PJ, Rifkin DB, Meister JJ, Hinz B. Myofibroblast contraction activates latent TGF-β1 from the extracellular matrix. *Journal of Cell Biology*. 2007;179(6):1311–1323.

44. Wang N, Tytell JD, Ingber DE. Mechanotransduction at a distance: mechanically coupling the extracellular matrix with the nucleus. *Nature reviews. Molecular cell biology*. 2009;10(1):75–82.

45. Rô Me Solon J, Levental I, Sengupta K, Georges PC, Janmey PA. Fibroblast Adaptation and Stiffness Matching to Soft Elastic Substrates.

46. Ghosh K, Pan Z, Guan E, Ge S, Liu Y, Nakamura T, Ren X-D, Rafailovich M, Clark RAF. Cell adaptation to a physiologically relevant ECM mimic with different viscoelastic properties. *Biomaterials*. 2007;28(4):671–679.

47. Schulze C, Wetzel F, Kueper T, Malsen A, Muhr G, Jaspers S, Blatt T, Wittern K-P, Wenck H, Käs JA. Stiffening of human skin fibroblasts with age. *Biophysical journal*. 2010;99(8):2434–42.

48. Shi X, Qin L, Zhang X, He K, Xiong C, Fang J, Fang X, Zhang Y. Elasticity of cardiac cells on the polymer substrates with different stiffness: an atomic force microscopy studyw. *Phys. Chem. Chem. Phys. Phys. Chem. Chem. Phys*. 2011;13(13):7540–7545.

49. Huang X, Yang N, Fiore VF, Barker TH, Sun Y, Morris SW, Ding Q, Thannickal VJ, Zhou Y. Matrix stiffness-induced myofibroblast differentiation is mediated by intrinsic mechanotransduction. *American Journal of Respiratory Cell and*

Molecular Biology. 2012;47(3):340–348.

50. Mcdonald ME, Li C, Bian H, Smith BD, Layne MD, Farmer SR. Myocardin-Related Transcription Factor A Regulates Conversion of Progenitors to Beige Adipocytes. *Cell*. 2015;160:105–118.

51. Ni J, Dong Z, Han W, Kondrikov D, Su Y. The role of RhoA and cytoskeleton in myofibroblast transformation in hyperoxic lung fibrosis. *Free Radical Biology and Medicine*. 2013;61:26–39.

52. Zhang X-H, Sun N-X, Feng Z-H, Wang C, Zhang Y, Wang J-M. Interference of Y-27632 on the signal transduction of transforming growth factor beta type 1 in ocular Tenon capsule fibroblasts. *International journal of ophthalmology*. 2012;5(5):576–81.

53. Small EM, Thatcher JE, Sutherland LB, Kinoshita H, Gerard RD, Richardson JA, DiMaio JM, Sadek H, Kuwahara K, Olson EN. Myocardin-related transcription factor-A controls myofibroblast activation and fibrosis in response to myocardial infarction. *Circulation research*. 2010;107(2):294.

54. Dupont S, Morsut L, Aragona M, Enzo E, Giulitti S, Cordenonsi M, Zanconato F, Le Digabel J, Forcato M, Bicciato S, Elvassore N, Piccolo S. Role of YAP/TAZ in mechanotransduction. *Nature*. 2011;474(7350):179–183.

55. Janmey PA, Wells RG, Assoian RK, McCulloch CA. From tissue mechanics to transcription factors. *Differentiation; research in biological diversity*. 2013;86(3):112.

56. Talele NP, Fradette J, Davies JE, Kapus A, Hinz B. Expression of α-Smooth Muscle Actin Determines the Fate of Mesenchymal Stromal Cells. *Stem Cell Reports*. 2015;4(6):1016–1030.

57. Liu F, Lagares D, Choi KM, Stopfer L, Marinković A, Vrbanac V, Probst CK, Hiemer SE, Sisson TH, Horowitz JC, Rosas IO, Fredenburgh LE, Feghali-Bostwick C, Varelas X, Tager AM, et al. Mechanosignaling through YAP and TAZ drives fibroblast activation and fibrosis. *American journal of physiology. Lung cellular and molecular physiology*. 2015;308(4):L344-57.

58. Calvo F, Ege N, Grande-Garcia A, Hooper S, Jenkins RP, Chaudhry SI, Harrington K, Williamson P, Moeendarbary E, Charras G, Sahai E. Mechanotransduction and YAP-dependent matrix remodelling is required for the generation and maintenance of cancer-associated fibroblasts.

59. Aragona M, Panciera T, Manfrin A, Giulitti S, Michielin F, Elvassore N, Dupont S, Piccolo S. A mechanical checkpoint controls multicellular growth through YAP/TAZ regulation by actin-processing factors. *Cell*. 2013;154(5):1047–59.

60. Ryan TD, Rothstein EC, Aban I, Tallaj JA, Husain A, Lucchesi PA, Dell'Italia LJ. Left Ventricular Eccentric Remodeling and Matrix Loss Are Mediated by Bradykinin and Precede Cardiomyocyte Elongation in Rats With Volume

Overload. *Journal of the American College of Cardiology*. 2007;49(7):811–821.

61. Chen Y -w., Pat B, Gladden JD, Zheng J, Powell P, Wei C-C, Cui X, Husain A, Dell'Italia LJ. Dynamic molecular and histopathological changes in the extracellular matrix and inflammation in the transition to heart failure in isolated volume overload. *American Journal of Physiology. Heart and Circulatory Physiology*. 2011;300(6):H2251–H2260.

62. Oliver-Dussault C, Ascah A, Marcil M, Matas J, Picard S, Pibarot P, Burelle Y, Deschepper CF. Early predictors of cardiac decompensation in experimental volume overload. *Molecular and cellular biochemistry*. 2010;338(1–2):271–82.

63. De Stefano LM, Matsubara LS, Matsubara BB. Myocardial dysfunction with increased ventricular compliance in volume overload hypertrophy. *European Journal of Heart Failure*. 2006;8(8):784–789.

64. Villari B, Hess OM, Kaufmann P, Krogmann ON, Grimm J, Krayenbuehl HP. Effect of aortic valve stenosis (pressure overload) and regurgitation (volume overload) on left ventricular systolic and diastolic function. *The American journal of cardiology*. 1992;69(9):927–34.

65. Schwarz US, Gardel ML. United we stand – integrating the actin cytoskeleton and cell–matrix adhesions in cellular mechanotransduction. *Journal of Cell Science*. 2012;125(13):3051.

66. Miano JM. SRF'ing the actin cytoskeleton with no destrin. *Physiological Genomics*. 2008;34(1):6–8.

67. Nahnsen S, Bielow C, Reinert K, Kohlbacher O. Tools for label-free peptide quantification. *Molecular & cellular proteomics : MCP*. 2013;12(3):549–56.

68. Huang DW, Sherman BT, Lempicki RA. Systematic and integrative analysis of large gene lists using DAVID bioinformatics resources. *Nature protocols*. 2009;4(1):44–57.

69. Lu D, Aroonsakool N, Yokoyama U, Patel HH, Insel PA. Increase in cellular cyclic AMP concentrations reverses the profibrogenic phenotype of cardiac myofibroblasts: a novel therapeutic approach for cardiac fibrosis. *Molecular pharmacology*. 2013;84(6):787–93.

70. Gong K, Xing D, Li P, Hilgers RH, Hage FG, Oparil S, Chen Y-F. cGMP Inhibits TGF-β Signaling by Sequestering Smad3 with Cytosolic β2-Tubulin in Pulmonary Artery Smooth Muscle Cells. *Molecular Endocrinology*. 2011;25(10):1794–1803.

71. Swaney JS, Roth DM, Olson ER, Naugle JE, Meszaros JG, Insel PA. Inhibition of cardiac myofibroblast formation and collagen synthesis by activation and overexpression of adenylyl cyclase. *Proceedings of the National Academy of Sciences*. 2004;102(2):437–442.

72. Li P, Oparil S, Novak L, Cao X, Shi W, Lucas J, Chen Y-F. ANP signaling inhibits TGF-beta-induced Smad2 and Smad3 nuclear translocation and

extracellular matrix expression in rat pulmonary arterial smooth muscle cells. *Journal of Applied Physiology*. 2006;102(1):390–398.

73. Li P, Wang D, Lucas J, Oparil S, Xing D, Cao X, Novak L, Renfrow MB, Chen Y-F. Atrial Natriuretic Peptide Inhibits Transforming Growth Factor -Induced Smad Signaling and Myofibroblast Transformation in Mouse Cardiac Fibroblasts. *Circulation Research*. 2008;102(2):185–192.

74. Koestler SA, Steffen A, Nemethova M, Winterhoff M, Luo N, Holleboom JM, Krupp J, Jacob S, Vinzenz M, Schur F, Schlüter K, Gunning PW, Winkler C, Schmeiser C, Faix J, et al. Arp2/3 complex is essential for actin network treadmilling as well as for targeting of capping protein and cofilin. *Molecular biology of the cell*. 2013;24(18):2861–75.

75. Rouiller I, Xu X-P, Amann KJ, Egile C, Nickell S, Nicastro D, Li R, Pollard TD, Volkmann N, Hanein D. The structural basis of actin filament branching by the Arp2/3 complex. *The Journal of Cell Biology*. 2008;180(5).

76. Reddy P, Deguchi M, Cheng Y, Hsueh AJW. Actin Cytoskeleton Regulates Hippo Signaling. Wanjin H, ed. *PLoS ONE*. 2013;8(9):e73763.

77. Rasmussen I, Pedersen LH, Byg L, Suzuki K, Sumimoto H, Vilhardt F. Effects of F/G-actin ratio and actin turn-over rate on NADPH oxidase activity in microglia. *BMC Immunology*. 2010;11(1):44.

78. Small EM. The Actin–MRTF–SRF Gene Regulatory Axis and Myofibroblast Differentiation. *Journal of Cardiovascular Translational Research*. 2012;5(6):794–804.

79. Honjo M, Tanihara H, Kameda T, Kawaji T, Yoshimura N, Araie M. Potential Role of Rho-Associated Protein Kinase Inhibitor Y-27632 in Glaucoma Filtration Surgery. *Investigative Opthalmology & Visual Science*. 2007;48(12):5549.

80. Chaturvedi RR, Herron T, Simmons R, Shore D, Kumar P, Sethia B, Chua F, Vassiliadis E, Kentish JC. Passive stiffness of myocardium from congenital heart disease and implications for diastole. *Circulation*. 2010;121(8):979–988.

81. Wilson K, Lucchesi PA. Myofilament dysfunction as an emerging mechanism of volume overload heart failure. *Pflügers Archiv : European Journal of Physiology*. 2014;466(6):1065–77.

82. Discher DE, Janmey P, Wang Y-L. Tissue cells feel and respond to the stiffness of their substrate. *Science (New York, N.Y.)*. 2005;310(5751):1139–43.

83. Forte G, Pagliari S, Ebara M, Uto K, Tam JK Van, Romanazzo S, Escobedo-Lucea C, Romano E, Di Nardo P, Traversa E, Aoyagi T. Substrate stiffness modulates gene expression and phenotype in neonatal cardiomyocytes in vitro. *Tissue Engineering. Part A*. 2012;18(17–18):1837–48.

84. Galie PA, Khalid N, Carnahan KE, Westfall M V, Stegemann JP. Substrate stiffness affects sarcomere and costamere structure and electrophysiological

function of isolated adult cardiomyocytes. *Cardiovascular Pathology*. 2013;22(3):219–27.

85. Jacot JG, McCulloch AD, Omens JH. Substrate stiffness affects the functional maturation of neonatal rat ventricular myocytes. *Biophysical Journal*. 2008;95(7):3479–87.

86. Mirsky I, Rankin J. The effects of geometry, elasticity, and external pressures on the diastolic pressure-volume and stiffness-stress relations. How important is the pericardium? *Circ Res*. 1979;44(1965):601–11.

87. Lee LC, Ge L, Zhang Z, Pease M, Nikolic SD, Mishra R, Ratcliffe MB, Guccione JM. Patient-specific finite element modeling of the Cardiokinetix Parachute(®) device: effects on left ventricular wall stress and function. *Medical & biological engineering & computing*. 2014;52(6):557–66.

88. Esfandiari S, Fuchs F, Wainstein R V., Chelvanathan A, Mitoff P, Sasson Z, Mak S. Heart Rate–Dependent Left Ventricular Diastolic Function in Patients With and Without Heart Failure. *Journal of Cardiac Failure*. 2015;21(1):68–75.

89. Hutchinson KR, Saripalli C, Chung CS, Granzier H. Increased myocardial stiffness due to cardiac titin isoform switching in a mouse model of volume overload limits eccentric remodeling. *Journal of Molecular and Cellular Cardiology*. 2015;79:104–114.

90. Diakos NA, Pozios I, Katsaros L, Vakrou S, Sventzouri S, Michelinakis N, Tseliou E, Bonios M, Malliaras K, Papalois A, Anastasiou-Nana M, Terrovitis J V. Afterload-induced left ventricular diastolic dysfunction during myocardial ischaemia and reperfusion. *Experimental physiology*. 2015;100(3):288–301.

91. Garcia R, Diebold S. Simple, rapid, and effective method of producing aortocaval shunts in the rat. *Cardiovascular Research*. 1990;24(5):430–2.

92. Guggilam A, Hutchinson KR, West TA, Kelly AP, Galantowicz ML, Davidoff AJ, Sadayappan S, Lucchesi PA. In vivo and in vitro cardiac responses to beta-adrenergic stimulation in volume-overload heart failure. *Journal of Molecular and Cellular Cardiology*. 2013;57:47–58.

93. McCollum LT, Gallagher PE, Tallant A. Angiotensin-(1-7) attenuates angiotensin II-induced cardiac remodeling associated with upregulation of dual-specificity phosphatase 1. *American Journal of Physiology. Heart and Circulatory Physiology*. 2012;302(3):801–810.

94. Burkhoff D, Mirsky I, Suga H. Assessment of systolic and diastolic ventricular properties via pressure-volume analysis: a guide for clinical, translational, and basic researchers. *American Journal of Physiology. Heart and Circulatory Physiology*. 2005;289(2):H501–H512.

95. Mirsky I, Pasipoularides A. Clinical assessment of diastolic function. *Progress in Cardiovascular Diseases*. 1990;32(4):291–318.

96. Mirsky I. Assessment of diastolic function: suggested methods and future considerations. *Circulation*. 1984;69(4):836–841.

97. Cruz Perez B, Tang J, Morris HJ, Palko JR, Pan X, Hart RT, Liu J. Biaxial mechanical testing of posterior sclera using high-resolution ultrasound speckle tracking for strain measurements. *Journal of Biomechanics*. 2014;47(5):1151–1156.

98. Sommer G, Haspinger DC, Andra M, Sacherer M, Viertler C, Regitnig P, Holzapfel G a. Quantification of Shear Deformations and Corresponding Stresses in the Biaxially Tested Human Myocardium. *Annals of Biomedical Engineering*. 2015;43(10):2334–2348.

99. Palko JR, Pan X, Liu J. Dynamic testing of regional viscoelastic behavior of canine sclera. *Experimental Eye Research*. 2011;93(6):825–32.

100. Sacks MS. A Method for Planar Biaxial Mechanical Testing That Includes In-Plane Shear. *Journal of Biomechanical Engineering*. 1999;121(5):551.

101. Neves MF, Amiri F, Virdis A, Diep QN, Schiffrin EL, Neves MF, Amiri F, Virdis a, Diep QN, Schiffrin EL. Role of aldosterone in angiotensin II-induced cardiac and aortic inflammation, fibrosis, and hypertrophy. *Can. J. Physiol. Pharmacol*. 2005;83(18):999–1006.

102. Olsen CO, Glower DD, Lee KL, McHale P a, Rankin JS. Diastolic anisotropic properties of the left ventricle in the conscious dog. *Circ. Res.* 1991;69(3):765–778.

103. Nakamura T, Nakajima T, Suzuki N, Arai S, Suwa N. Left ventricular stiffness and chamber geometry in the pressure-overloaded hypertrophied heart. *The Tohoku Journal of Experimental Medicine*. 1976;119(3):245–56.

104. Grossman W, McLaurin LP, Stefadouros MA. Left Ventricular Stiffness Associated with Chronic Pressure and Volume Overloads in Man. *Circulation Research*. 1974;35(5):793–800.

105. Mirsky I, Parmley WW. Assessment of passive elastic stiffness for isolated heart muscle and the intact heart. *Circulation Research*. 1973;33(2):233–243.

106. Javani S, Gordon M, Azadani AN. Biomechanical Properties and Microstructure of Heart Chambers: A Paired Comparison Study in an Ovine Model. *Annals of biomedical engineering*. 2016.

107. Diez J. Losartan-Dependent Regression of Myocardial Fibrosis Is Associated With Reduction of Left Ventricular Chamber Stiffness in Hypertensive Patients. *Circulation*. 2002;105(21):2512–2517.

108. Brilla CG, Matsubara L, Weber KT. Advanced Hypertensive Heart Disease in Spontaneously Hypertensive Rats: Lisinopril-Mediated Regression of Myocardial Fibrosis. *Hypertension*. 1996;28(2):269–275.

109. Soufen HN, Salemi VMC, Aneas IMS, Ramires FJA, Benício AMD, Benvenuti LA, Krieger JE, Mady C. Collagen content, but not the ratios of collagen type III/I mRNAs, differs among hypertensive, alcoholic, and idiopathic dilated cardiomyopathy. *Brazilian Journal of Medical and Biological Research*. 2008;41(12):1098–1104.

110. Ruzicka M, Keeley FW, Leenen FH. The renin-angiotensin system and volume overload-induced changes in cardiac collagen and elastin. *Circulation*. 1994;90(4):1989–96.

111. Fomovsky GM, Thomopoulos S, Holmes JW. Contribution of extracellular matrix to the mechanical properties of the heart. *Journal of molecular and cellular cardiology*. 2010;48(3):490–6.

112. Granzier HL, Irving TC. Passive tension in cardiac muscle: contribution of collagen, titin, microtubules, and intermediate filaments. *Biophysical Journal*. 1995;68(3):1027–44.

113. LeWinter MM, Granzier HL. Cardiac titin and heart disease. *Journal of Cardiovascular Pharmacology*. 2014;63(3):207–12.

114. van den Borne SWM, Diez J, Blankesteijn WM, Verjans J, Hofstra L, Narula J. Myocardial remodeling after infarction: the role of myofibroblasts. *Nature reviews. Cardiology*. 2010;7(1):30–7.

115. Ohnishi K, Takagi M, Kurokawa Y, Satomi S, Konttinen YT. Matrix metalloproteinase-mediated extracellular matrix protein degradation in human pulmonary emphysema. *Laboratory investigation; a journal of technical methods and pathology*. 1998;78(9):1077–87.

116. Huber LC, Distler O, Tarner I, Gay RE, Gay S, Pap T. Synovial fibroblasts: key players in rheumatoid arthritis. *Rheumatology (Oxford, England)*. 2006;45(6):669–75.

117. Zheng J, Chen Y, Pat B, Dell'Italia LA, Tillson M, Dillon AR, Powell PC, Shi K, Shah N, Denney T, Husain A, Dell'Italia LJ. Microarray Identifies Extensive Downregulation of Noncollagen Extracellular Matrix and Profibrotic Growth Factor Genes in Chronic Isolated Mitral Regurgitation in the Dog. *Circulation*. 2009;119(15).

118. Goffin JM, Pittet P, Csucs G, Lussi JW, Meister J-J, Hinz B. Focal adhesion size controls tension-dependent recruitment of α-smooth muscle actin to stress fibers. *The Journal of Cell Biology*. 2006;172(2).

119. Yeung T, Georges PC, Flanagan L a., Marg B, Ortiz M, Funaki M, Zahir N, Ming W, Weaver V, Janmey P a. Effects of substrate stiffness on cell morphology, cytoskeletal structure, and adhesion. *Cell Motility and the Cytoskeleton*. 2005;60(1):24–34.

120. Zhao H, Li X, Zhao S, Zeng Y, Zhao L, Ding H, Sun W, Du Y. Microengineered

in vitro model of cardiac fibrosis through modulating myofibroblast mechanotransduction. *Biofabrication*. 2014;6(4):45009.

121. Zhao B, Ye X, Yu J, Li L, Li W, Li S, Yu J, Lin JD, Wang C-Y, Chinnaiyan AM, Lai Z-C, Guan K-L. TEAD mediates YAP-dependent gene induction and growth control. *Genes & development*. 2008;22(14):1962–71.

122. Ota M, Sasaki H. Mammalian Tead proteins regulate cell proliferation and contact inhibition as transcriptional mediators of Hippo signaling. *Development*. 2008;135(24).

123. Yu F-X, Zhao B, Panupinthu N, Jewell JL, Lian I, Wang LH, Zhao J, Yuan H, Tumaneng K, Li H, Fu X-D, Mills GB, Guan K-L. Regulation of the Hippo-YAP pathway by G-protein-coupled receptor signaling. *Cell*. 2012;150(4):780–91.

124. Burgess HA, Daugherty LE, Thatcher TH, Lakatos HF, Ray DM, Redonnet M, Phipps RP, Sime PJ. PPARγ agonists inhibit TGF-β induced pulmonary myofibroblast differentiation and collagen production: implications for therapy of lung fibrosis. *American Journal of Physiology - Lung Cellular and Molecular Physiology*. 2005;288(6).

125. SUN K, WANG Q, HUANG X. PPAR gamma inhibits growth of rat hepatic stellate cells and TGF beta-induced connective tissue growth factor expression1. *Acta Pharmacologica Sinica*. 2006;27(6):715–723.

126. Hogrebe NJ, Gooch KJ. Direct influence of culture dimensionality on human mesenchymal stem cell differentiation at various matrix stiffnesses using a fibrous self-assembling peptide hydrogel. *Journal of Biomedical Materials Research - Part A*. 2016;104(9):2356–2368.

127. Pelham RJ, Wang Y-L. Cell locomotion and focal adhesions are regulated by substrate flexibility. *Proc. Natl. Acad. Sci.* 1997;94(December):13661–13665.

128. Li Z, Dranoff JA, Chan EP, Uemura M, Sévigny J, Wells RG. Transforming growth factor-β and substrate stiffness regulate portal fibroblast activation in culture. *Hepatology*. 2007;46(4):1246–1256.

129. Hogrebe NJ, Reinhardt JW, Gooch KJ. Biomaterial microarchitecture: A potent regulator of individual cell behavior and multicellular organization. *Journal of Biomedical Materials Research Part A*. 2016.

130. Terman JR, Kashina A. Post-translational modification and regulation of actin. *Current opinion in cell biology*. 2013;25(1):30–8.

131. Kim M, Song K, Jin E-J, Sonn J. Staurosporine and cytochalasin D induce chondrogenesis by regulation of actin dynamics in different way. *Experimental & Molecular Medicine*. 2012;44(9):521.

132. Higashida C, Suetsugu S, Tsuji T, Monypenny J, Narumiya S, Watanabe N. G-actin regulates rapid induction of actin nucleation by mDia1 to restore cellular actin polymers. *Journal of Cell Science*. 2008;121(20).

133. Belin RJ, Sumandea MP, Sievert GA, Harvey LA, Geenen DL, Solaro RJ, de Tombe PP. Interventricular differences in myofilament function in experimental congestive heart failure. *Pflügers Archiv - European Journal of Physiology*. 2011;462(6):795–809.

134. Kim K-H, Kim Y-J, Ohn J-H, Yang J, Lee S-E, Lee S-W, Kim H-K, Seo J-W, Sohn D-W. Long-Term Effects of Sildenafil in a Rat Model of Chronic Mitral RegurgitationClinical Perspective. *Circulation*. 2012;125(11).

135. Huang M, Hester RL, Guyton AC. Hemodynamic changes in rats after opening an arteriovenous fistula. *American Journal of Physiology - Heart and Circulatory Physiology*. 1992;262(3).

136. Roman MJ, Devereux RB, Niles NW, Hochreiter C, Kligfield P, Sato N, Spitzer MC, Borer JS. Aortic root dilatation as a cause of isolated, severe aortic regurgitation. Prevalence, clinical and echocardiographic patterns, and relation to left ventricular hypertrophy and function. *Annals of internal medicine*. 1987;106(6):800–7.

137. Wilson K, Guggilam A, West TA, Zhang X, Trask AJ, Cismowski MJ, de Tombe P, Sadayappan S, Lucchesi PA. Effects of a myofilament calcium sensitizer on left ventricular systolic and diastolic function in rats with volume overload heart failure. *American Journal of Physiology. Heart and Circulatory Physiology*. 2014;307(11):H1605-17.

138. Mazumder R, Schroeder S, Clymer BD, White RD, Kolipaka A. Quantification of myocardial stiffness in heart failure with preserved ejection fraction porcine model using magnetic resonance elastography. *Journal of Cardiovascular Magnetic Resonance*. 2016;18(Suppl 1):P29.

139. Cukierman E, Pankov R, Stevens DR, Yamada KM. Taking Cell-Matrix Adhesions to the Third Dimension. *Science*. 2001;294(5547).

140. Guo W-H, Frey MT, Burnham NA, Wang Y-L. Substrate Rigidity Regulates the Formation and Maintenance of Tissues. *Biophysical Journal*. 90:2213–2220.

141. Manso AM, Kang S, Ross RS. Integrins, Focal Adhesions and Cardiac Fibroblasts. *J Investig Med*. 2009;57(8):856–860.

142. Pedersen JA, Swartz MA. Mechanobiology in the Third Dimension. *Annals of Biomedical Engineering*. 2005;33(11):1469–1490.

143. Galie PA, Russell MW, Westfall M V., Stegemann JP. Interstitial fluid flow and cyclic strain differentially regulate cardiac fibroblast activation via AT1R and TGF-β1. *Experimental Cell Research*. 2012;318(1):75–84.

144. Wang J, Chen H, Seth a, McCulloch C a. Mechanical force regulation of myofibroblast differentiation in cardiac fibroblasts. *American journal of physiology. Heart and circulatory physiology*. 2003;285(5):H1871–H1881.

145. Watson CJ, Phelan D, Xu M, Collier P, Neary R, Smolenski A, Ledwidge M,

McDonald K, Baugh J. Mechanical stretch up-regulates the B-type natriuretic peptide system in human cardiac fibroblasts: a possible defense against transforming growth factor-β mediated fibrosis. *Fibrogenesis Tissue Repair*. 2012;5(1):9.

146. Byfield FJ, Reen RK, Shentu T-P, Levitan I, Gooch KJ. Endothelial actin and cell stiffness is modulated by substrate stiffness in 2D and 3D. *Journal of Biomechanics*. 2009;42(8):1114–1119.

147. Baxter SC, Morales MO, Goldsmith EC. Adaptive changes in cardiac fibroblast morphology and collagen organization as a result of mechanical environment. *Cell Biochemistry and Biophysics*. 2008;51(1):33–44.

148. Stevenson MD, Piristine H, Hogrebe NJ, Nocera TM, Boehm MW, Reen RK, Koelling KW, Agarwal G, Sarang-Sieminski AL, Gooch KJ. A self-assembling peptide matrix used to control stiffness and binding site density supports the formation of microvascular networks in three dimensions. *Acta Biomaterialia*. 2013;9(8):7651–7661.

149. Poobalarahi F, Baicu CF, Bradshaw AD. Cardiac myofibroblasts differentiated in 3D culture exhibit distinct changes in collagen I production, processing, and matrix deposition. *American journal of physiology. Heart and circulatory physiology*. 2006;291(6):H2924-32.

150. Wang J, Seth A, McCulloch CAG. Force regulates smooth muscle actin in cardiac fibroblasts. *American Journal of Physiology - Heart and Circulatory Physiology*. 2000;279(6).

151. Husse B, Briest W, Homagk L, Isenberg G, Gekle M. Cyclical mechanical stretch modulates expression of collagen I and collagen III by PKC and tyrosine kinase in cardiac fibroblasts. *American journal of physiology. Regulatory, integrative and comparative physiology*. 2007;293(5):R1898-907.